Interner Bericht
DESY F41-75/3
March 1975

Soft X-Ray Excitation of Core Electrons in Metals and Alloys

by

C. Kunz

SOFT X-RAY EXCITATION OF CORE ELECTRONS IN METALS AND ALLOYS

by

C. KUNZ

Deutsches Elektronen-Synchrotron DESY,
2000 Hamburg 52, Notkestieg 1, W.-Germany

To be published as a chapter of:

Optical Properties of Solids - New Developments

B.O. Seraphin Editor (North-Holland, Amsterdam 1975)

CONTENTS

1. Introduction

This chapter deals primarily with absorption behavior of metals and alloys. The term "soft x-ray region" in the title needs further explanation since terminology is not very precise in this field. Historically the spectral region between the visible and the x-ray regions was attacked from both the high and the low energy sides, "soft x-ray" being the region below about 6 keV photon energy, where x-rays become too "soft" to penetrate macroscopic distances in air, while the region above 6 eV photon energy, where air begins to absorb heavily, is known as the "vacuum ultraviolet". We shall be mainly concerned with the energy region 20 - 500 eV. This is the energy range in which core levels become excited which are only minimally affected by crystal field or life-time broadening (generally less than 0.1 eV). This makes spectroscopy in this region in principle an excellent probe for empty final states. Normal incidence reflectivity measurements do not furnish useful information at energies higher than about 35 eV and are therefore treated only marginally in this review. We also exclude Drude and plasma behavior although with the light metals it may determine the low energy end of this spectral region. Our main concern are the core electron excitations.

Investigations in the vacuum ultraviolet and soft x-ray regions have gained tremendous impact through the use of synchrotron radiation. This development began after 1960 although synchrotron radiation is available since 1946. Before, it was a difficult task to investigate optical properties in this spectral range since classical sources like x-ray tubes and gas discharges are weak, and spark and gas discharges

moreover emit a spectrum with plenty of line structure. Nevertheless some pieces of excellent work have been carried out before the advent of synchrotron radiation, especially in the laboratories of D.H. Tomboulian at Cornell and A.P. Lukirskii at Leningrad. Some of this older work on metals has been reviewed by TOMBOULIAN [1957] and by PARRATT [1959] . Also the proceedings of the conference on optical properties of metals in Paris (ABELES [1966]) deserve mentioning.

This report is mainly based on measurements performed using synchrotron radiation. After about ten years of more or less systematic investigations on metals and some alloys a first resumée can be given on optical behavior in this range. The recent progress in this field has only been touched before in a few review papers, e.g. those by FANO and COOPER [1968 , 1969] and BROWN [1974] . A closed theoretical understanding is still not reached. Theory is now at the level that an à posteriori explanation of many features in the spectra can be given. In the more complicated cases it is, however, not possible to quantitatively calculate details in the spectra.

There are many connections between absorption measurements and other methods investigating core levels and unoccupied states in metals and alloys. We only mention soft x-ray fluorescence emission, photoelectron spectroscopy, appearance potential spectroscopy, isochromate spectrocopy. We should also not forget to stress the importance of absorption data for calculating optical constants which are among other applications, needed to design better instruments in this spectral range.

Section 2 is a historical and tutorial introduction to the field. A short survey on the main experimental techniques, especially on synchrotron radiation is given in section 3. Section 4 deals with the phenomenological optical properties, as optical constants and sum rules. The general theory of absorption in the soft x-ray region is outlined in section 5 while the corresponding experimental results are discussed in section 6. This section is divided into subsections for simple metals, noble and heavy metals, rare earths, transition metals, and the respective alloys. Section 7 is devoted to the edge shape in simple metals both to the theoretical and experimental aspects.

2. Basic concepts, history

2.1. One-electron band picture

The one-electron picture of core electron absorption (and fluorescence emission) is best described by fig. 1. Whenever the photon energy $h\nu$ reaches a value equal to the separation between a core electron binding energy and the Fermi level a sudden increase in the absorption coefficient will occur. At higher energies this step will be followed by structures which are an image of the unoccupied density of states right above the Fermi edge. Since core states are available with different atomic symmetry characters (s, p, d, f ...) also information on the symmetry character of the empty band states (including matrix elements) will be extracted, e.g. transitions from an s like core level will depict the p-projected density of states. Extensive investigations of unoccupied states were planned in the mid-sixties, when four synchrotron radiation groups started out to investigate the properties of metals (and other materials) in this spectral range at the NBS (Washington), at Frascati, at Tokyo and at Hamburg. A chart of expected edge positions as shown in fig. 2 helps to recall the hopes of those days to map the symmetry-projected density of unoccupied states from absorption measurements in this region.

2.2. Matrix elements - local effects

Figure 3 displays the absorption spectrum of Au over a wide energy range. This spectrum is composed from different experimental results (JAEGLE and MISSONI [1966], HAENSEL et al. [1968], GUDAT et al. [1972]). The energy positions where edges should occur are marked. With the exception of faint structures at the positions of the $N_{6,7}$ edges, however, no edges

are observed. Even the $N_{6,7}$ edges were missed in the first experiments and could be observed only with sensitive techniques in a later measurement (GUDAT et al. [1974]).

The reason for the absence of these edges is now well understood on the basis of atomic calculations (see FANO and COOPER [1968 , 1969]). The atomic dipole matrix element is proportional to

$$M \propto \int P_i(r) r P_f(r) dr \qquad (1)$$

where i and f denote initial and final states, r is the distance from the nucleus and the functions P(r)/r are radial wavefunctions. The function $P_i(r)$ is a core function well concentrated inside the atom while the final state function $P_f(r)$ has small amplitude inside the atom at threshold energy. Only at energies high above threshold the final state wavefunction is capable of penetrating into the atom yielding appreciable values of M in eq. (1). The fact that the atom is embedded in a solid does not alter very much this behavior. As a matter of fact $P_f(r)$ in the region where it contributes to the integral in eq. (1) is determined almost completely by the atomic potential and the angular momentum of the final state. As will be explained in detail in section 5 the interplay between the attractive Coulomb force and the repulsive angular momentum force causes the shift of 'oscillator strength' away from the edge to higher energies. This becomes more pronounced when the final state's angular momentum gets larger. For example in fig. 3 the rising absorption coefficient from 140 eV on is due to the $N_{6,7}$ transitions into g symmetric states. This shift of oscillator strength to higher energies also accounts for the dominance of the Au $N_{6,7}$ lines in XPS (x-ray photo-)

electron spectroscopy) where these electrons are ejected by e.g. 1.5 keV photons. This is relevant as well for other excitations in other materials. In cases, however, where the final state has the symmetry of incompletely filled shells (like d-shells in transition metals or the 4f shell in rare earths) $P_f(r)$ has a large amplitude near the atom and M in eq. (1) attains large values at threshold. This gives rise to further complications as we are going to show in the following section.

2.3. Multiplet splitting

Figure 4 shows the spectrum of 4d excitations in Pr. This spectrum was first obtained with classical sources by FOMICHEV et al. [1967] and ZIMKINA et al. [1967] and later confirmed by HAENSEL et al. [1970c] by means of synchrotron radiation. The Pr^{+++} ion, as contained in the metal (BREWER [1971]), has the ground state configuration $...4s^2 4p^6 \underline{4d}^{10} 5s^2 5p^6 \underline{4f}^2$ (WYBOURNE [1965]), where we have underlined the states which are mainly involved in the spectrum of fig. 4. Instead of observing a single band (or a few closely spaced bands) which would be due to transitions into the unoccupied part of the 4f states we observe a large number of lines including two broad peaks at higher energies. The whole feature extends over an energy range of more than 50 eV.

The explanation of this behavior again comes from an atomic picture (DEHMER et al. [1971], STARACE [1972], SUGAR [1972]). In this case the wavefunction $P_f(r)$ in eq. (1) is that of a bound state and therefore there is a considerable overlap with $P_i(r)$ yielding large values of M. In addition the configuration of the excited Pr^{+++} (the other electrons are the metal electrons) namely: $4d^9 5s^2 5p^6 4f^3$ is split into a series of lines, mainly by the 4d-4f exchange interaction term. Both the d and f

electrons involved belong to a shell with the same principal quantum number. This is the reason why the exchange interaction is so strong and why the lines are spread over so large an energy range. The uppermost lines are pushed into the ionization continuum. Therefore they are broadened and smeared out. Figure 4 gives also the theoretical position of lines as obtained from the atomic calculation and shows the good agreement between theory and experiment.

Similar effects have been observed in the XPS-spectra of rare earth metals by FADLEY and SHIRLEY [1970] . The energy of the escaping electron reflects the respective final state configuration left behind. A configuration with one electron less than for absorption spectra has to be considered.

2.4. Electron-hole attraction

It was always argued in the early days of absorption spectroscopy of metals and especially with respect to the complementary process of soft x-ray fluorescence (see fig. 1) that the hole in a good metal is completely shielded from its environment because of the high conductivity of metals. Therefore, no bound electron hole states (excitons) should occur. However, we have just realized when looking at the example of Pr that the shielding is obviously completely ineffective in the region where the 4f electrons are located, otherwise the atomic model would not have given the shape of the spectrum. Let us look at a simple metal like Na where the $L_{2,3}$ transitions should not be subject to any of the complications mentioned in section 2.2 and 2.3.

Figure 5 shows the 2p absorption spectrum of Na metal as measured by HAENSEL et al. [1969a, 1970a]. There is indeed a peak right at the spin orbit split edges as shown in the inset. No one-electron band model of sodium can account for a density of states peak at this position. Indeed, the peak reminds one of an exciton with zero binding energy. As will be explained in detail in section 7 this is too simple a picture.

The main reason of complication is the following: There is a small (about 1 Å wide) potential well due to the hole. This well is not strong enough to bind an electron but it is capable of scattering electrons. Now the main point is that it will not only scatter the one excited electron but also all the other metal electrons predominantly those right at the Fermi level. The sudden creation of the hole is accompanied by an excitation of an infinite number of electrons. The excited electron is equivalent to all these electrons and therefore we deal with a many-body problem, not any more a two-body problem (hole and excited electron), nor a two-body problem in a relaxing medium. The relevant many body theory explaining this 'spike' at the edge is due to MAHAN [1967] and in its more rigorous form to NOZIERES and De DOMINICIS [1969]. We shall come back to this theory in section 7 and also to the objections which DOW [1974a] has raised against applying this theory in the interpretation of the spectra of certain metals, especially Li.

2.5. Density of states structures in alloy spectra

Three major complications of the one-electron picture have been introduced by now and some minor complications will be mentioned in the special sections of this chapter. Nevertheless, there are examples which show in

a convincing way that the density of states plays its role in these spectra. Ordered alloys of Al with other metals display structures above the edge which can be correlated with density of states calculations. Figure 6 shows indeed a very good agreement between a measurement of the ordered alloy AlNi by HAGEMANN et al. [1974a] and a density of states calculation by CONNOLLY and JOHNSON [1971] . Of course, it is obvious that if a sharp onset at the Fermi edge is observed in the spectra, as it is the case at the Al $L_{2,3}$ edge in this alloy, then we should also observe such a drastic increase in the density of state as it occurs in AlNi a few eV above the Fermi level. In section 6.2 and 6.6 this and also other aspects of alloy spectra will be discussed in detail.

3. Experimental methods

3.1. The source - synchrotron radiation

Different kinds of classical laboratory sources are used in the vacuum ultraviolet but all of them are inferior to synchrotron radiation in quality and intensity of the emitted radiation. The one important complication of synchrotron radiation sources is, however, that, while the laboratory sources are small appendices to the monochromators, in a synchrotron radiation set-up the measuring device becomes a small appendix to the light source. It is therefore recommendable to make use of synchrotron radiation only when its advantages are really needed. Since information on this subject is now readily available we shall give only a brief survey on this topic in the following. SAMSON [1967] has written a useful monograph mainly on laboratory sources and techniques. Reviewson synchrotron radiation have been published by SOKOLOV and TERNOV [1968] , MADDEN and CODLING [1967] , HAENSEL and KUNZ [1967] , GODWIN 1969 , CODLING 1973 , MADDEN [1974] , BROWN [1974] , KUNZ 1974 . In addition useful information is contained in the proceedings of three recent meetings (WATSON and PERLMAN [1973] , MARR and MUNRO [1973] , KOCH et al. [1974]) and a bibliography (MARR et al. [1972 , 1974]).

Hydrogen or deuterium lamps provide a relatively weak continuum to about 7 eV and a many-line structure up to about 12 eV photon energy. Helium discharge lamps provide a continuum up to 20 eV. Likewise several other rare gas continua are available in intermediate regions. At higher energies the uranium rod spark discharge source (BRV source) provides a useful continuum with superimposed lines up to at least 250 eV (see DAMANY et al. [1974] for recent developments). Spark sources give short pulses of light

with repetition times of several seconds. The bremsstrahlung tail of x-ray tubes has been used with success by Lukirskii and coworkers from 50 eV on, but serious problems arise from anode contamination and low intensities.

Synchrotron radiation is emitted by electrons and positrons in circular accelerators and storage rings when the velocity of the particles approaches the speed of light. Energies of the particles above 100 MeV are required in order to obtain intensity beyond the visible. Synchrotron radiation is a by-product of the development of modern particle accelerators for high energy physics. Figure 7 shows the emission characteristics of synchrotron radiation. The radiation is well collimated in the momentaneous direction of flight of the particles. The main properties of synchrotron radiation are listed as follows, they are illustrated in several figures:

(1) collimation (figs. 7 and 8),

(2) linear and circular polarization (fig. 8),

(3) time structure (typically pulses of 0.1-1 nsec length at a repetition rate of 1 MHz to 500 MHz),

(4) continuous spectrum (fig. 9),

(5) calculability in terms of absolute intensity (fig. 9),

(6) emission in a clean vacuum, no gas or sputtered materials.

As for examples in drawing the figures the laboratories at the DESY synchrotron and at the DORIS storage rings in Hamburg were taken, there the experiments are located at a distance of 40 m from the source point. A higher flux can be accepted by a monochromator when the distance

from the source point is reduced. This is possible at smaller machines. We shall not discuss here in detail the individual properties of synchrotron radiation and its applications, but refer to the literature given above. Synchrotron radiation has wide applicability not only to the investigation of metals but also to semiconductors, insulators, atoms, organic compounds, and living organisms. Especially structure investigations of organic materials by means of the x-ray part of the spectrum deserves mentioning. For the purpose of this article it is sufficient to recognize the continuous spectrum and the high intensity. Figure 10 gives a comparison between measurements of the Cr 3p absorption spectrum with synchrotron radiation and with classical sources. The line structure of classical sources and an underestimate of experimental errors has mislead many investigators in assigning structures to spectra like this in which no structures exist.

In comparing different accelerators and storage rings there are two important parameters: the characteristic photon energy ε_c above which the spectrum begins to fall off rapidly (see fig. 9). This is determined by the energy E of the orbiting electrons and the radius of bending in the magnets R through

$$\varepsilon_c(\mathrm{eV}) = 2.22 \cdot 10^3 \left(\mathrm{E(GeV)}\right)^3 \left(\mathrm{R(m)}\right)^{-1} \qquad (2)$$

The other important parameter is the current of orbiting particles which determines the intensity of synchrotron radiation. The intensity is only weakly dependend on R. Table 1 gives a list of most of the synchrotrons and storage rings which are either used as light sources or which are of interest as light sources.

3.2. Monochromatization

Most of the measurements we are going to discuss in this context are performed with grazing incidence grating monochromators. The monochromator type most widely used is the Rowland monochromator in which arrangement entrance slit, grating, and exit slit all lie on the Rowland circle (see SAMSON [1967]). Figure 11 shows an arrangement of this type. Since the exit slit has to move precisely along the Rowland circle it is difficult to attach heavy equipment to it. Usually samples and sample handling devices are situated in front of the monochromator. After penetrating the sample synchrotron radiation is focussed onto the entrance slit by a concave mirror at grazing incidence. Thus radiation coming into a window of typically 5x20 mm^2 is accommodated by the monochromator.

With 10 μm wide slits, a grating of 2 m radius of curvature, ruled with 1200 lines/mm a resolution (constant in wavelength) of $\Delta\lambda = 0.05$ Å is achievable. Since in solid state physics mostly resolution in energy ΔE matters, we give as an example $\Delta E = 0.05$ eV at 100 eV and $\Delta E = 1$ eV at 500 eV photon energy. The Rowland monochromator is capable of achieving the highest resolution of all grazing incidence instruments. This, however, is obtained at the cost of flexibility, since it produces a moving exit beam. Moreover, once it is used with a given angle of incidence the spectrum is only free from unwanted higher order background radiation in a region from the highest transmitted photon energy to half that energy. At lower photon energies the unfiltered radiation can be swamped with higher order contributions. The ratio of wanted to unwanted radiation depends mainly on the characteristics of the grating. It further changes when the films under investigation are inserted. Filters, mainly of

aluminum, are used in order to reject second and higher order radiation in certain spectral regions. The pertinent problems are treated in general by SAMSON [1967] and the special problems involved with synchrotron radiation are dealt with by KUNZ [1973a].

Several attempts have been made to overcome the moving exit beam and the higher order problems of the conventional Rowland arrangement. KUNZ [1973a] has summarized eight different arrangements invented for this purpose. Some of these arrangements are designed around a Rowland core and have a fixed exit beam by adding additional reflections from moving mirrors, other arrangements strive for simplicity in the motion of the optical components thereby sacrificing either resolution, or higher order rejection, or directional stability of the emerging beam.

Figure 12 shows a monochromator arrangement designed by DIETRICH and KUNZ [1972] which is used quite successfully at DESY now for several years. It has a moving and rotating first mirror M always illuminating the plane grating G. The rotation of the grating is coupled to the motion of the first mirror. A section of a rotational paraboloid F brings the monochromatized radiation to a stigmatic focus at the position of a 100 μm wide exit slit. The exit beam is fixed, higher orders are efficiently rejected in the range 20 - 280 eV and the resolution is a constant fraction of the photon energy and is in the order of 1:500. The instrument is equipped with an UHV sample chamber which incorporates the exit slit giving good access to the narrow beam of monochromatic radiation.

3.3. Absorption spectroscopy

Absorption measurements are performed by a sample-in sample-out technique. Since samples are either supported by screens of high but limited transparency (∿75 % is achievable) or by supporting substrate films of carbon, aluminum, collodion etc. one spectrum ($I(\omega)$), is taken with the substrate plus sample and another one ($I_o(\omega)$) with a possibly identical substrate film. Afterwards the linear absorption coefficient $\mu(\omega)$ is extracted according to $I(\omega) = I_o(\omega)e^{-\mu(\omega)d}$ where $\hbar\omega$ is the photon energy and d the film thickness. (This procedure is valid if the reflectivity can be neglected, if not, a more complicated evaluation has to be applied, see section 4.1.) Since errors arise due to stray light and higher order light, especially when $e^{-\mu(\omega)d}$ becomes very small, it is necessary to prepare films with different thicknesses d when large variations of $\mu(\omega)$ occur in the range of investigation. Moreover, from plotting $I(\omega)$ versus d at a fixed photon energy stray light and higher order radiation can be corrected for as described e.g. by HAENSEL et al. [1968] . Errors in the relative variation of μ in the order of less than 5 % can be achieved by this method. Absolute errors in μ are mainly determined by the error in measuring the film thickness d and are usually not less than 20 %. With many materials the density of thin evaporated films is less than that of the bulk material. Rather than using direct determination of the thickness like the optical Tolanski method a weighing method (oscillating quartz monitor) is used determining the mass of material per cm^2. Several authors prefer to give their result in terms of the mass absorption coefficient $\mu' = \mu/\rho$ where ρ is the density of the material, others give the result in terms of an atomic absorption cross section $\sigma = (\mu \cdot A)/(\rho \cdot L_A)$ where A is the atomic weight and L_A is Avogadro's number.

A two beam densitometer which improves the accuracy in the grazing incidence region was described by GUDAT et al. [1974] . It is shown in fig. 13. The monochromatic beam hits either one of two mirrors M_1 or M_2 depending on the position of the rotating mirror segment holding M_1. This rotation is synchronized with the pulse frequency (50 Hz) of the synchrotron alternatively sending a light pulse into beam 1 or beam 2. The two beams transmit sample film S_1 respectively reference film S_2 (e.g. a substrate) and are detected with open photomultipliers D_1 and D_2. Small structures in the 10^{-3} range could be resolved with this technique. Moreover differential measurements comparing two different samples are possible (see section 6.2).

Recently BALZAROTTI et al. [1974] have built a set-up in which the samples are rotating synchronously with the synchrotron pulses measuring alternatively two samples with a single beam and with a single detector. They give an accuracy of 0.2 % for the ratio of transmissivities.

3.4. Yield spectroscopy

LUKIRSKII et al. [1966] using the bremsstrahlung continuum have measured absorption and photoelectric yield as a function of photon energy for several materials and could show a great similarity in both types of spectra. GUDAT and KUNZ [1972b] demonstrated the great potentiality of yield spectroscopy when using synchrotron radiation as a method of obtaining absorption structures from bulk samples. In the mean time GUDAT and KUNZ [1975] , and GUDAT [1974] could demonstrate with more than 20 different materials (metals, semiconductors and insulators) that the photoelectric yield spectra show the same structures as absorption spectra in the region of core excitations. Figure 14 shows as an example the spectra of Al as obtained by

both methods. Because of the surface sensitivity of photoelectronic emission sample cleanliness is essential for yield spectroscopy and metal samples have to be prepared under UHV conditions. Figure 15 shows the simple experimental set-up for yield spectroscopy. After the light beam is reflected by a grazing incidence mirror (the photoelectrons emitted from its surface provide a reference signal to account for intensity fluctuations) it hits the sample. The photoelectrons are pulled by an electric field into an open photomultiplier near to the sample. The set-up allows for evaporation, heat treatment, and scratching of the materials under investigation.

The close correspondence between yield and absorption spectra can be explained in the following way (GUDAT and KUNZ [1972b]). Assume that there is a fixed escape depth L for the photoelectrons. Then the yield Y will be proportional to the number of photons absorbed in a depth L from the surface or $Y \propto 1-e^{-\mu L} \approx \mu L$ when $\mu L << 1$. All the power of absorbed radiation goes into excited electrons, be it primary ionization or autoionization from bound states, or Auger decay. Electrons, however, especially in a metal have a short mean free path (about 4 Å at 100 eV kinetic energy) for electron-electron scattering (see e.g. LINDAU and SPICER [1974]). By means of electron-electron scattering they cascade down in energy and undergo multiplication. Eventually the electrons will reach energies just above the vacuum level ($\sim$4.5 eV for Al), where they obtain their largest mean free path (e.g. about 40 Å in Al). A certain fraction of these electrons escape into the vacuum. It can be demonstrated in energy distribution measurement that electrons having energies a few eV above the vacuum level furnish the main component of the total yield.

Thus L is essentially determined by the mean free path of these electrons. The number of electrons will further be roughly proportional to the photon energy $\hbar\omega$ due to multiplication. Thus we obtain

$$Y(\omega) \propto \hbar\omega \cdot \mu(\omega) \cdot L \qquad (3)$$

Since $\hbar\omega$ is a slowly varying factor the yield Y is essentially an image of $\mu(\omega)$. In the following we shall use $Y(\omega)$ and $\mu(\omega)$ equivalently when discussing absorption structures. $Y(\omega)$ is usually not obtained in terms of absolute numbers since the photon flux hitting the samples is not known. The photocurrent from the sample is usually divided by a reference signal which has a flat spectral dependence. Reflectivity losses of radiation from samples at normal incidence and up to angles of incidence of about 45^o are negligible in the spectral range discussed here and do not cause any problems.

3.5. Electron energy loss spectroscopy

Measurement of the energy loss of electrons in the range up to 300 keV serves as an additional means of obtaining optical constants. The method is reviewed by DANIELS et al. [1970] and is based on the following equation

$$P_1(\Delta E, \underset{\sim}{q})\, d\Delta E\, d\Omega = \left(\frac{e}{\pi\hbar v_o}\right)^2 d \cdot \frac{1}{\theta^2+\theta_o^2} \cdot \mathrm{Im}\left(-\frac{1}{\varepsilon(\omega, \underset{\sim}{q})}\right) d\Delta E\, d\Omega \qquad (4)$$

$P_1(\Delta E, \underset{\sim}{q})$ is the probability for a fast electron to loose in a distinct inelastic process an energy ΔE and to experience momentum transfer $\hbar q$ with $\underset{\sim}{q} = \underset{\sim}{q}_\perp + \underset{\sim}{q}_\parallel$ ($\underset{\sim}{q}_\perp$ normal and $\underset{\sim}{q}_\parallel$ parallel components to the direction of the incoming electron). Momentum transfer $\hbar q$ is defined in the experiment by the scattering angle through the relation

$$\underset{\sim}{q}^2 = \underset{\sim}{q}_\parallel^2 + \underset{\sim}{q}_\perp^2 = q_o^2\,(\theta^2 + \theta_o^2) \qquad (5)$$

with $\theta_o = \Delta E/2E_o$ and $v_o, \hbar q_o$, E_o being velocity, momentum and energy of the incoming electrons, respectively, $d\Delta E$ is an energy interval around the energy ΔE, $d\Omega$ a solid angle interval around the direction given by θ, d the film thickness and $\mathrm{Im}(-1/\varepsilon(\omega,\underset{\sim}{q}))$ the imaginary part of the reciprocal dielectric constant, the so called energy loss function. Through this function optical and energy loss measurements are related.

While optical measurements measure the transverse dielectric constant $\varepsilon_t(\hbar\omega,q)$ which is in principle also a function of the wave vector $\underset{\sim}{q}$, energy loss spectroscopy is determined by a longitudinal dielectric constant $\varepsilon_\ell(\Delta E,\underset{\sim}{q})$. In the limit of $\underset{\sim}{q} = 0$

$$\varepsilon_t(\hbar\omega,0) = \varepsilon_\ell(h\omega,0) = \varepsilon(\omega) \qquad (6)$$

(see PINES [1963]). It is this limit in which energy loss measurements are treated as an equivalent method for determining optical constants. In optical measurements $\underset{\sim}{q}$ is linked to $\hbar\omega$ through $\omega/|\underset{\sim}{q}| = c$ (velocity of light). Energy loss measurements, however, allow for an independent variation of ΔE and $\underset{\sim}{q}$. Changes of the spectrum occur when $\underset{\sim}{q}$ becomes larger than about 1/5 of the Brillouin zone radius. In the context of this paper we shall not deal with these special aspects of '$\underset{\sim}{q}$-spectroscopy' (with the exception of section 7.4.3).

One of the main problems in determining $\mathrm{Im}(-1/\varepsilon(\omega))$ from energy loss spectroscopy is the presence of electrons in the spectra which have experienced more than one energy loss process while penetrating the film. These electrons create a large, sometimes even structured background which has to be substracted in a complicated procedure before an $\mathrm{Im}(-1/\varepsilon(\omega))$ spectrum is

obtained. Two remedies against this background have been tried. They are based on the fact that the multiple-loss probability is proportional to d^2/v_o^4 when the single-loss probabilities are small (see eq. (4)). One methode is to keep d small. There is, however, a limitation of about d = 100 Å for unbacked films and it is impossible with many materials to make such films. The other method which was recently realized by RITSKO et al. [1974b] is to increase v_o. They have built a 300 keV energy loss instrument with 80 meV resolution. With such an instrument core excitations in the 100 eV range can be measured without any real background problems.

Other additional structures in energy loss spectra, like those originating from surface losses and excitation of Cerenkov radiation are eliminated much easier. After having obtained $\mathrm{Im}(-1/\varepsilon(\omega))$ a Kramers-Kronig analysis is applied to obtain $\mathrm{Re}(1/\varepsilon(\omega))$. The two functions give complete information on $\varepsilon(\omega)$. For detailed information the reader is referred to the review by DANIELS et al. [1970] .

4. Optical constants and sum rules

4.1. Kramers-Kronig analysis

Once the complex dielectric function $\varepsilon(\omega) = \varepsilon_1(\omega)+i\varepsilon_2(\omega)$ is obtained all the relevant information necessary in linear optics is available. Instead of ε_1 and ε_2 other pairs of independent optical quantities like $n(\omega)+ik(\omega) = \sqrt{\varepsilon(\omega)}$ the optical constants may serve the same purpose. Because of causality being involved in optical response and other restrictions, real and imaginary parts of such functions and others involving reflectivity and absorption are connected by integral relationships the so called Kramers-Kronig relations (see e.g. PHILIPP and EHRENREICH [1964], ALTARELLI et al. [1972], TOLL [1956]). For the determination of one of these quantities a complete knowledge of the other one from the infrared to the x-ray region is required. The measurements below 30 eV, however, are usually reflectivity measurements at normal incidence while those at higher energies are absorption measurements. In order to combine information from both regions an iterative Kramers-Kronig analysis of both reflectivity and absorption measurements is necessary. Joining reflectivity and absorption measurements in the region around 30 eV is usually not without problems. In order to obtain a smooth transition the reflectivity has to be increased and the absorption coefficient must be lowered in this region according to a quite general experience.

The relation most useful for evaluating reflectance measurements in the low energy region connects the phase angle $\Theta_R(\omega_o)$ with an integral over the reflectance $R(\omega)$

$$\Theta_R(\omega_o) = -\frac{\omega_o}{\pi} P \int_0^\infty d\omega \, \frac{\ln R(\omega)}{\omega^2-\omega_o^2} \qquad (7)$$

where P denotes the Cauchy principal value of the integral. If the polarization and the incident angle of the radiation are known the dielectric functions can be calculated elementarily from equations given e.g. by BORN and WOLF [1959] .

As long as the reflectivity of the samples used is small (more accurately GREENAWAY and HARBEKE [1968] : $R << 1$, $k^2 << n^2$) the absorption coefficient μ can simply be calculated from the transmittance T and the thickness d of the sample by applying:

$$\mu(\omega_o) = -\frac{1}{d} \ln T(\omega_o) = \frac{2\omega_o}{c} k(\omega_o), \qquad (8)$$

The real part n of the complex refractive index $\hat{n} = n+ik$ is obtained by the Kramers-Kronig relation

$$n(\omega_o) = 1 + \frac{c}{\pi} P \int_0^\infty d\omega \frac{\mu(\omega)}{\omega^2-\omega_o^2} \qquad (9)$$

If the transmittance of a thin foil is measured in a region where reflectance is still important, the relation

$$\Theta_T(\omega_o) = -\frac{\omega_o}{\pi} P \int_0^\infty d\omega \frac{\ln T(\omega)}{\omega^2-\omega_o^2} + \frac{\omega_o}{c} d \qquad (10)$$

holds (NILSSON [1968] , the sign convention used here is different from that in the reference). $\hat{n}$ is determined from T and Θ_T by the iterative solution of an implicit system of equations (ABELES and THEYE [1966]):

$$T_{EX} - T(n,k) = 0$$

$$\Theta_T - \Theta(n,k) = 0$$

with (see HEAVENS [1964]):

$$T(n,k) = 16 \cdot \frac{n^2+k^2}{C^2+D^2} \,,$$

$$\Theta(n,k) = \arctan\left(\frac{kC+nd}{kD-nC}\right) \,, \qquad (11)$$

$$C = e^{M}\{((n+1)^2+k^2)\cos N + 2k(n+1)\sin N\}$$
$$-e^{-M}\{((n-1)^2-k^2)\cos N - 2k(n-1)\sin N\} \,,$$

$$D = d^{M}\{((n+1)^2-k^2)\sin N - 2k(n+1)\cos N\}$$
$$+e^{-M}\{((n-1)^2-k^2)\sin N + 2k(n+1)\cos N\},$$

$$M = \frac{\omega}{c}\cdot k\cdot d \,, \quad N = \frac{\omega}{c}\cdot n\cdot d \,,$$

T_{EX} is the experimentally determined transmittance and c the speed of light. The Kramers-Kronig relations (7), (9) and (10) are valid for insulators as well as for metals (ALTARELLI et al. [1972]).

In order to obtain a complete set of optical constants for the entire energy range the following procedures were applied by HAGEMANN et al. [1974b]:

If the directly measured absorption coefficient could be matched to μ-values which were available from other experiments in the low energy region, Kramers-Kronig analysis was performed with the total absorption spectrum (eq. (9)).

If in the infrared, the visible- and near UV-regionsonly measured reflectivities were available, first the Kramers-Kronig relation eq. (7) was used with these data extrapolated to higher energies. Together with the measured absorption in the high energy region a total absorption spectrum was constructed with some interpolations.

If the reflectance is high - as for Au and Ag in the intermediate range between 13 eV and 50 eV - a total transmittance spectrum was constructed and the Kramers-Kronig relation eq. (10) was applied. In this case an alternative method was tested which did not make use of eq. (10). In the first step μ_o and k_o is calculated from the measured transmittance T_{EX} (eq. (8)) neglecting the reflectance[+)]. Then n_o was calculated from eq. (9) and the transmittance $T(n_o,k_o)$ of a thin absorbing and reflecting layer (see HEAVENS [1964] , HODGSON [1954]) was determined according to eq. (11). A better approximation of the absorption coefficient is then given by

$$\mu_1 = 2\mu_o + \frac{1}{d} \ln T(n_o,k_o) \qquad (12)$$

This procedure was repeated until T_{EX} and the calculated T(n,k) coincided. In all cases this was achieved with sufficient accuracy by the first corrected μ and the n was determined from it by eq. (9).

The analysis of optical data on Mg, Al, Cu, Ag, Au, Bi, C and Al_2O_3 reported by HAGEMANN et al. [1974b] was carried through by using the interactive

---

[+)] Note that the simple minded idea that the transmittance of a film in a region where small reflection and large absorption occurs is always less than the transmittance calculated from $T = \exp(-\mu d)$ is not right! This is to be seen e.g. from working out eq. (2.21) in GREENAWAY and HARBEKE [1968] .

on-line data processing system at DESY documented in several stages of evolution by NIELSEN [1973] , KLUCKER and NIELSEN [1973] , HAGEMANN et al. [1973] . It consists of a PDP 8e as an intelligent terminal with several convenient input-output and storing features connected to an IBM-computer 360/75, which opens the opportunity to try out variations of the input data with considerable ease and speed.

4.2. Sum rules

The optical constants of materials in the region of linear response fulfil various sum rules. ALTARELLI et al. [1972] have given a systematic derivation of these sum rules. Some of them are very useful to check on the accuracy and consistency of the optical functions as determined by the procedures outlines in the previous section:

$$B \int_0^{\omega_o} \omega \, \varepsilon_2(\omega) d\omega = n_{eff1}(\omega_o), \tag{13}$$

$$c \cdot B \int_0^{\omega_o} \mu(\omega) d\omega = n_{eff2}(\omega_o), \tag{14}$$

$$-B \int_0^{\omega_o} \omega \, \mathrm{Im}\left(\hat{\varepsilon}^{-1}(\omega)\right) d\omega = n_{eff3}(\omega_o), \tag{15}$$

$$\lim_{\omega_o \to \infty} cB \int_0^{\omega_o} \mu(\omega) \left(n(\omega)-1\right) d\omega = 0, \tag{16}$$

$$\lim_{\omega_o \to \infty} \int_0^{\omega_o} \left(n(\omega)-1\right) d\omega = 0, \tag{17}$$

$$B = \frac{m}{2\pi^2 e^2} \, \frac{A}{\rho \cdot L_A} ,$$

with $n_{eff}(\omega_o)$ the effective number of electrons per atom (molecule) contributing to the optical transitions in the frequency range up to ω_o, m the electron mass, e the electron charge, L_A Avogadro's number, A the atomic weight of the substance and ρ its density.

Table 2 gives the three n_{eff} values from eqs. (13-15) and the deviation from the total number of electrons Z as obtained by HAGEMANN et al. [1974b] for their optical functions of several metals. In addition the contributions of the conduction electrons Δn_{cond} and that of the K shell electrons Δn_K is given. The agreement with what is expected is very satisfactory. The fact that Δn_K is considerably smaller than 2 is understood as shift of oscillator strength from one to another shell (see e.g. COOPER [1962]). Partial sum rules for one atomic shell have to be considered with precautions. Only the overall sum rule is strictly valid. Tests of the sum rules as a function of ω_o according to eqs. (13-17) will be shown for Ag in the next section.

4.3. Optical properties of Ag from 1 to 1000 eV

The first attempt to obtain a complete set of optical functions for one material was made in the pioneering paper by PHILIPP and EHRENREICH [1964]. Their sum rule test for Al, yielding $n_{eff1}=n_{eff3}=8.2$ instead of 13, revealed a serious lack of oscillator strength. This was due to an interpolation in the region of the $L_{2,3}$ transitions. Later FOMICHEV [1967] and HAENSEL et al. [1969b] corrected these values and found good agreement with the expected n_{eff}. Recently HAGEMANN et al. [1974b] have determined Kramers-Kronig consistent optical functions based on own experiments and those of other authors with the methods outlined in section 4.1. A complete set of optical functions of Ag between 1 and 1000 eV may serve as an example. The

tabulated values between 10^{-2} eV and $5 \cdot 10^{5}$ eV are available in the original paper.

Figures 16 - 19 show the normal incidence reflectivity R, absorption coefficient μ, ε_1 and ε_2, n and k, and the energy loss function $\mathrm{Im}(-1/\varepsilon)$. The construction of the absorption spectrum from which the other optical functions were derived was made as follows:
From 10^{-3} eV to 0.5 eV the Drude parameters and from 0.5 eV to 3.5 eV the k values from JOHNSON and CHRISTY [1972] were taken. From 3.5 eV to 11 eV the k values obtained from Kramers-Kronig transformed reflectivity measurements under UHV conditions by IRANI et al. [1971] were used. Between 11 eV and 16 eV a segment was interpolated with the help of results by CANFIELD and HASS [1965] and EHRENREICH and PHILIPP [1962]. From 16 eV to 110 eV original results on μ by HAGEMANN et al. [1974b] calculated by the method given in eqs. (10) and (11) were used. The original μ was modified by subtracting 0.7×10^{-5} cm^{-1}. From 110 eV to 300 eV the values by HAENSEL et al. [1968] were used and above 300 eV the data were taken from the compilation by HUBBEL [1971]. Original data from several references are shown in the respective figures together with the Kramers-Kronig consistent curves.

A display of the n_{eff} sum rule integrals as a function of the upper limit of integration in fig. 20 reveals in which energy range the oscillator strength for the different functions ε_2, μ and $\mathrm{Im}-1/\varepsilon$ is located. Figure 21 shows the behavior of the integrals eq. (16) and (17) as a function of the upper limit of integration. The integration over (n-1) (eq. (16)) is

approaching zero within the limit of accuracy of the computer. The rapid oscillations at the high energy end in fig. 21 of the integral over n-1 are an artifact of the integration routine used on the computer. The general trend, however, is clearly recognized and satisfactory.

5. Theory

5.1. One-electron band theory

The one-electron optical properties of a crystalline solid are best described in terms of the imaginary part of the dielectric function (see e.g. HODGSON [1970]):

$$\varepsilon_2(\omega) = \frac{\hbar^2 e^2}{\pi m^2 \omega^2} \int dk \; |\underset{\sim}{e}\cdot\underset{\sim}{M}_{vc}|^2 \; \delta\,(E_c - E_v - \hbar\omega) \qquad (18)$$

where $\underset{\sim}{k}$ is the Bloch wave-vector, $\underset{\sim}{e}$ is the unit vector in the direction of polarization of the incoming radiation, E_v and E_c are energies of occupied valence (or core) and empty conduction states respectively. The integration is carried out over the first Brillouin zone. The dipole matrix element $\underset{\sim}{e}\cdot\underset{\sim}{M}_{vc}$ is given by

$$\underset{\sim}{e}\cdot\underset{\sim}{M}_{vc} = \int d\underset{\sim}{r}\; \psi_c^*(\underset{\sim}{k}_c,\underset{\sim}{r})\; e^{i\underset{\sim}{K}\cdot\underset{\sim}{r}}\; \underset{\sim}{e}\cdot\underset{\sim}{\nabla}\; \psi_v(\underset{\sim}{k}_v,\underset{\sim}{r}) \qquad (19)$$

where ψ_c and ψ_v are Bloch functions and the integration extends over unit volume. $|\underset{\sim}{K}| = \frac{2\pi}{\lambda}$ is the wave vector of the incoming light wave with wavelength λ.

An immediate consequence of (18) is the $\underset{\sim}{k}$-selection rule namely $\underset{\sim}{k}_c = \underset{\sim}{k}_v + \underset{\sim}{K} + \underset{\sim}{g}$ where g is a reciprocal lattice vector. For long wavelength radiation namely $\underset{\sim}{K} \approx 0$ and $\underset{\sim}{g}=0$ this yields $\underset{\sim}{k}$-conservation in optical transitions (vertical transitions). Since the core levels in the band-picture, however, are completely flat bands this selection rule is unimportant for the problems of this chapter.

The full program of evaluating eqs. (18) and (19) numerically for real metals is difficult to carry out and in those cases where bandstructures and wavefunctions have been obtained it is subject to considerable errors because of the necessary approximations. In a rough approximation the matrix element eq. (19) is set constant throughout the Brillouin zone. Then $\varepsilon_2(\omega)$ becomes an image of the density of states. Another approximation is to consider the local character of the matrix element eq. (19) as the important feature. Because $\psi_v(r)$ is different from zero only in the atomic core an atomic calculation of the matrix element appears to be a good starting point. This is the topic of the following section. A (local) density of states might come into play as a modulation of the atomic absorption cross section in the next higher approximation.

5.2. Atomic one-electron approximation

In atomic physics usually the atomic ionization cross section σ is calculated. This is related to the measured absorption coefficient by $\mu = N\sigma$. After COOPER [1962] and FANO and COOPER [1968] the ionization cross section for the n,l subshell is given by

$$\sigma_{nl}(\omega) = (4\pi\ \alpha\ a_o^3/3)\ h\omega\ (C_{l-1}\ R_{l-1}^2 + C_{l+1}\ R_{l+1}^2) \qquad (20)$$

here α is the fine structure constant, a_o the Bohr radius and the two terms in the last bracket describe two possible transitions to final states with angular quantum numbers l+1 and l-1.

$$R_{l\pm1} = \int_0^\infty P_{nl}(r)\ r\ P_{\varepsilon,l\pm1}(r)dr \qquad (21)$$

are radial matrix elements and the $C_{l\pm1}$ are statistical factors from averaging over initial states and summing over final states. It should be mentioned that the $R_{l\pm1}$ matrix elements are the dipole matrix elements in

the 'length' form while those in eq. (19) were given in the equivalent 'velocity' form. $P_{nl}(r)$ and $P_{\varepsilon,l\pm1}(r)$ in eq. (21) are the functions which really determine the behavior of the absorption coefficient. Let us consider how they are related to the initial and final state wave functions. The ground state wave function is $\psi_{nlms} = U_{nl}(r)\, Y_{lm}(\phi,\Theta)\chi_s$ where χ_s is a spin function, $Y_{lm}(\phi,\Theta)$ is a spherical harmonic and $U_{nl}(r) = P_{nl}(r)/r$ is a radial wave function. The wave function $P_{nl}(r)$ obeys a radial wave equation

$$d^2P_{nl}(r)/dr^2 + (2m/\hbar^2)\left(E_{nl}-V(r)-l(l+1)\hbar^2/2mr^2\right)P_{nl}(r) = 0. \qquad (22)$$

Continuum state radial wave functions $P_{\varepsilon l}(r)$ are obtained by solving eq. (22) with $P_{nl}(r)$ replaced by $P_{\varepsilon l}(r)$ and n replaced by ε. The Coulomb potential V(r) and the centrifugal 'potential' $l(l+1)\hbar^2/2mr^2$ in eq. (22) are combined to form an effective potential

$$V_{eff}(r) = V(r) + \frac{l(l+1)\hbar^2}{r^2\ 2m}\ . \qquad (23)$$

The evaluation of the matrix elements $R_{l\pm1}$ is straight-forward by making use of tabulated atomic one-electron wave functions for the bound states as e.g. those of HERMAN and SKILLMAN [1963] obtained from Hartree-Fock-Slater equations. The continuum-state functions are computed from eq. (22) after obtaining an appropriate potential again based on calculations like those of HERMAN and SKILLMAN [1963] .

A series of effective potentials (eq. (23)) for l =3 are shown in fig. 22 after MANSON and COOPER [1968] . It is realized that a potential barrier builds up which is responsible for the suppression of overlap between initial and final states at threshold. This is demonstrated for the 4f transitions of Bi in fig. 23 after COMBET FARNOUX [1969] . The wave function

marked ε=0 is the one at threshold and is zero in the region of overlap with the 4f shell. At ε=11.5 Ry (156 eV) the final state wave function has moved into the core region and an appreciable overlap with the 4f shell occurs. Figure 24 shows the calculated absorption coefficient with the onset of 4f electron transition at about 200 eV. A small edge appears due to the 4f→εd transitions but the major contribution to the oscillator strength is the 4f→εg contribution which comes into play only at higher energies. The experiments show the rise in the absorption above 200 eV in qualitative agreement. There is, however, no edge observed and the increase is less prominent than that in the calculations.

Calculations for several materials based on these theories have been performed by COOPER [1962] , MANSON and COOPER [1968] , COMBET FARNOUX and HENO [1967] , FANO and COOPER [1968] , JAEGLE et al. [1969] . McGUIRE [1968] has tabulated calculated cross sections for the elements Helium to Xenon using a different technique. The numerical potential from HERMAN and SKILLMAN [1963] is represented in successive radial intervals by hydrogenic potentials. Thereby the radial wave functions become piecewise analytic. This way of calculating the continuum wavefunctions is essentially equivalent to solving eq. (22).

5.3. Extended absorption fine structure (EXAFS)

The atomic approximation is essentially one where in eq. (19) the final state wave function $\psi_c(\underset{\sim}{k}_c, \underset{\sim}{r})$ is approximated by that of an isolated atom. The next step of approximation is to describe the final state as a superposition of an outgoing wave $\psi(r)$ with a sum over backscattered waves $\psi_{sc} = \sum_i \psi_i$ scattered from neighboring atoms located at positions i. In order

to calculate the matrix element it is only necessary to obtain the amplitude of ψ_{sc} at the position of the excited atom. Equation (19) becomes

$$\underset{\sim}{e}\cdot\underset{\sim}{M} \propto \int(\psi^{*}(\underset{\sim}{r}) + \psi^{*}_{sc}(\underset{\sim}{r}))\ \underset{\sim}{e}\cdot\underset{\sim}{\nabla}\ \psi_{v}(\underset{\sim}{r})d\underset{\sim}{r} \qquad (24)$$

We have omitted here the additional index k in the wave functions, which has no meaning in this model. If multiple scattering was included into ψ_{sc} this method when carried out correctly would build up the true one-electron wave-functions of the excited electrons.

Variations in the x-ray absorption spectrum as a function of the kinetic energy of the excited electron are now produced by the interference near the nucleus between the outgoing wave $\psi(\underset{\sim}{r})$ and the backscattered waves $\psi_{sc}(\underset{\sim}{r})$. When these waves add constructively there is an absorption maximum and when they add destructively there is a minimum.

The calculation is usually applied in an electron energy range where the scattering amplitude from a single atom is small. Therefore the multiple scattering contribution is neglected. Further it is assumed that the outgoing and the backscattered waves are rapidly damped through inelastic scattering. This is achieved by a damping factor $e^{-\gamma 2 r_i}$ where r_i is the distance to the scattering atom at position i. The assumption of rapid damping is well justified since $1/\gamma$ is in the order of 5-50 Å in the 100 eV - 1000 eV range (see e.g. LINDAU and SPICER [1974]). On the other hand, very strong electron-electron interactions cannot be described just by a simple damping.

Since the absorption cross section is proportional to $|\underset{\sim}{e}\cdot\underset{\sim}{M}|^2$ we obtain from eq. (24)

$$\sigma \propto \left| \int \psi_f^*(\underset{\sim}{r}) \underset{\sim}{e} \cdot \underset{\sim}{\nabla} \psi_v(\underset{\sim}{r}) d\underset{\sim}{r} + \int \psi_{sc}^*(\underset{\sim}{r}) \underset{\sim}{e} \cdot \underset{\sim}{\nabla} \psi_v(\underset{\sim}{r}) d\underset{\sim}{r} \right|^2 \qquad (25)$$

The first term squared gives the smoothly varying atomic absorption coefficient while the mixed term yields the oscillating part. This oscillating part of σ was first calculated by SHIRAIWA et al. [1958] and SHIRAIWA [1960] going back to an idea of KRONIG [1932] which he used to calculate the oscillations in the absorption cross section of molecular gases. (Earlier theories have been reviewed by AZAROFF [1963] .) The method was then improved by SAYERS et al. [1970] and was also inverted by this group in order to obtain radial distribution of nearest neighbor atoms in crystalline and amorphous materials from measured spectra (SAYERS et al. [1971] , STERN [1974]). Their expression for the oscillatory part of the cross section for K-shell excitations is

$$\sigma' = -k\, f(k) \sum_i \left(\exp(-\gamma 2r_i)/r_i^2\right) \exp(-\sigma_i^2 k^2/2) \sin\left(2kr_i + 2\eta(k)\right), \qquad (26)$$

where $\hbar k$ is the photoelectron momentum. $f(k)$ is the usual electron scattering factor, r_i is the distance from the absorbing atom to the i-th neighbouring atom. $\eta(k)$ is the phase shift caused by the potential in the absorbing atom. (This has to be counted twice since both the outgoing and the backscattered electron waves experience this shift), $\exp(-\sigma_i^2 k^2/2)$ is a Debye-Waller factor which through the mean square amplitude of the relative displacement of the atoms from their equilibrium positions includes both thermal and disorder effects.

Calculations based on this formalism are successful in explaining the oscillations in the absorption coefficient due to the excitation of K electrons to energies up to 1000 eV above threshold. The theory should fail quantitatively at very low energies where multiple scattering effects dominate, but

the qualitative feature of a moldulation of the absorption coefficient should occur also in the range of the first 100 eV above the edge. This will be the important point for the interpretation of structures in light metal absorption spectra of e.g. Al and Na as recently attempted by RITSKO et al. [1974] . ASHLEY and DONIACH [1974] have improved the calculations for low energies by including multiple scattering. The deficiencies of most of the present theories on EXAFS in the region near threshold become especially evident from the papers by FANO and LEE [1973] and FANO [1974]. They outline a considerably improved theoretical approach to this problem.

Another important point deserves mentioning. The phase shift $\eta(k)$ can be calculated only from a knowledge of the exact potential of the excited atom with a hole in the K-shell. Tabulations of atomic potentials like e.g. those of HERMAN and SKILLMAN [1963] do not list these potentials. Further the outer part of the potential will be modified compared to self consistent atomic Hartree-Fock potentials since metal electrons can shield the long tails. Therefore, in many calculations $\eta(k)$ is used only as a fitting parameter.

5.4. Multiplet splitting

Atomic calculations of the kind mentioned in section 5.2 are not limited to continuum transitions. Calculations of similar type serve as a first step for obtaining the discrete atomic excitations. Usually in going from atoms to solids, especially with solids in the metallic state, no correspondence between the rich line structure in atomic spectra and the few peaks, if any, at the onset of transitions in the solid can be established. A case of exception are the rare earth metals. These have partly filled f shells in configurations $4d^{10}4f^{N}$ which allow for excitations of the type $4d^{9}4f^{N+1}$.

We have intentionally omitted the metal electrons since it is known that rare earth metals consist of trivalent ionic cores embedded in and screened by the metal electrons. (BREWER [1971]).

Due to the compactness of the 4f wavefunctions these lie inside the $5s^2$ and $5p^6$ shells and are therefore screened from the environment of the solid. Calculations show that in excitations of the type $4d^{10}4f^N \rightarrow 4d^9 4f^{N+1}$ the additional f electron becomes bound inside the centrifugal barrier and overlaps the 4d wavefunction. Orbits with higher principal quantum numbers (5f,6f,...) remain outside the centrifugal barrier and have only weak overlap with the 4d wavefunction. Hence much of the oscillator strength of the 4d excitation will go into the transition to the $4d^9 4f^{N+1}$ configuration. From these considerations an atomic treatment of these excitations promises to be very successful also for the rare earth metals. The theory was published in a series of papers by DEHMER et al. [1971] , STARACE [1972] , SUGAR [1972] , DEHMER and STARACE [1972] .

The method used to obtain the splitting of the configuration $4d^9 4f^{N+1}$ into terms with different angular momentum and spin quantum numbers is a standard one of atomic physics (see e.g. CONDON and SHORTLEY [1970]). The starting point is a basis set obtained from an independent particle model such as Hartree-Fock-Slater or any of various central field models. Using this basis set linear combinations of Slater determinants are to be formed in some coupling scheme, which is usually taken to be L-S coupling. Let us denote these states by $|4d^9 4f^{N+1} \alpha\rangle$ where α incorporates all quantum numbers (angular momentum and spin) to uniquely identify the states of this configuration. All $|4d^9 4f^{N+1} \alpha\rangle$ states are eigenstates of the indenpendent particle model

Hamiltonian H_{mod} for the same energy eigenvalue E_{N+1}, which depends only on the configuration. The main task is now to diagonalize the matrix

$$\langle 4d^9 4f^{N+1} \alpha' | V_{res} | 4d^9 4f^{N+1} \alpha \rangle \qquad (27)$$

where V_{res} = H-Hmod and H is the complete Hamiltonian of the problem while H_{mod} is the model Hamiltonian used in calculating the states $|4d^9 4f^{N+1} \alpha\rangle$. V_{res} will contain electrostatic electron-electron interactions of the type $\sum_{i<j} 1/r_{ij}$ and the spin orbit interaction.

The result of the calculation are new eigenstates of the configuration say $|4d^9 4f^{N+1} \beta\rangle$ which are linear combinations of the $|4d^9 4f^{N+1} \alpha\rangle$'s and energies of these states $E_{N+1}+\varepsilon_\beta$ where the ε_β's are the diagonal elements of the matrix (27) after diagonalization. The new eigenstates allow for a calculation of the dipole matrix elements and thereby the oscillator strength of the individual lines.

Since a better approximation would have to allow for the admixing of other configurations than $4d^9 4f^{N+1}$ (configuration interaction) the energy values $E_{N+1}+\varepsilon_\beta$ are only a first order approximation. In the case of the rare earth metals a scaling by a factor of $\sim 2/3$ brings calculations and experiment into excellent agreement. This scaling as a substitute for taking configuration interaction into account is the weakest point of this calculation. As an example we give the result of the calculation by SUGAR [1972] for Ce^{3+} in table 3. The table also lists the experimental values by HAENSEL et al. [1970c]. Note that the ground state is a $^2F_{5/2}$ state. Since the optical selection rule $\Delta J = 0, \pm 1$ holds, only J = 3/2, 5/2 and 7/2 final states need be considered. Further the states are denoted in LS-coupling terminology. This does not

mean that LS coupling describes the $|4d^9,4f^2\beta\rangle$ states but it gives the character of these states. The main origin of the large splitting of the states of this configuration lies in the excellent overlap between the 4f and the 4d orbits. This results in a large value of the exchange integral which constitutes the most important parameter for the splitting of the terms. The most intense lines are pushed up into the continuum. They are broadened by interaction with the underlying continuum which needs special considerations as given in the next section.

Another group of metals where a similar theoretical approach could be relevant are the transition metals. In this case e.g. transitions of the type $3p^6 3d^N \rightarrow 3p^5 3d^{N+1}$ are considered. The 3d electrons are not as well shielded as the f electrons in rare earth metals but they are fairly localized at the transition metal atoms. Again the fact that the p and d electrons have the same principal quantum number will secure good overlap of the wavefunctions.

5.5. Configuration interaction and initial state correlations

If in a certain spectral region continuum excitations and discrete excitations overlap one would naively superimpose the intensities of these excitations in order to obtain the total absorption coefficient. In many cases, however, it is necessary to consider the interaction between the two excitations. FANO [1961] calculates separate probability amplitudes for the two transition processes and determines the absorption coefficient as the square of the sum of the separate probabilities. Interference destroys the simple Lorentzian line shapes and causes striking asymmetries. This gives also the means how to detect these interactions. Another result of the interaction is a broadening of the discrete excitation due to the decrease in lifetime because of autoionization.

The analytic equation for the cross section at energy E as given by FANO 1961 is

$$\sigma(\omega) = \sigma_c(\omega)\{\rho^2[(q+\varepsilon)^2/(1+\varepsilon^2)] + 1 - \rho^2\} \qquad (28)$$

here $\sigma_c(\omega)$ is the absorption cross section that would be observed in the absence of the discrete state at the photon energy $\hbar\omega$, ρ^2 is the fraction of $\sigma_c(\omega)$ which is capable of interference with the discrete state, q is a profile index determining the distortion of the line, Γ the width of the autoionization state is determined by the square of the overlap integral between discrete and continuum states and $\varepsilon=(\hbar\omega-E_r)/(\Gamma/2\Gamma)$ is a reduced energy variable, E_r being a nominal resonance energy. Figure 25 shows such line profiles as a function of q.

STARACE [1972] and DEHMER and STARACE [1972] have applied a similar approach to calculate the configuration interaction of those lines in the rare earth spectra (especially La) which are pushed into the continuum. In these cases a coupling and mixing of several continua is involved which results in broad intense peaks quite similar to those observed in the experiments (see e.g. fig. 4 in section 2).

The real break-through in obtaining a good quantitative description of these peaks (and peaks like the d-f maximum in the spectrum of Xe gas first measured by EDERER [1964]) came with the inclusion of initial state correlations into the calculations. These correlations involve an admixing of virtually excited states into the ground state wavefunction. These theories are reviewed in two recent papers by AMUSIA [1974] and WENDIN [1974] (see also references therein) We shall not attempt to deal with the details of these theories in the con-

text of this paper since they belong to atomic physics. Nevertheless, as will be seen in section 6.4, they are of considerable importance also for an understanding of the spectra of metals.

6. General absorption behavior

6.1. Simple metals: Li, Be, Na, Mg, Al

Figure 5 and fig. 26 display the absorption of the five lightest metals as measured by HAENSEL et al. [1970a]. The spectra of Na, Mg, and Al are shown in the region of the $L_{2,3}$ excitations while Li and Be are shown in the region of the K excitations. The positions of the structures are given in table 4. In all cases the transitions from the core level set in with a pronounced step-like increase in the absorption coefficient. The details of the edge shape and the peaks right at the edge will be discussed in section 7. Here we are concerned with the general shape of the spectra. We have to distinguish the region up to about 20 eV above threshold where narrow structures occur and the region up to more than 100 eV above threshold where large peaks are observed with a typical energy separation of 20 - 40 eV. Moreover in the Mg and Al spectra the weak L_1 edges can be identified. The narrow structures right above the edge are attributed to density of states structures (if possible) while the large wide peaks were the object of several theoretical attempts of interpretation. Here we only mention collective excitations and EXAFS (section 5.3).

6.1.1. K-edge (Li, Be)

The Li spectrum was obtained in addition to the absorption measurements shown in fig. 26 also with yield spectroscopy from solid and liquid samples by PETERSEN and KUNZ [1974] as shown in fig. 27. Absorption and yield of solid Li are in very good general agreement with each other. The shoulder B (fig. 26), however, could be shown to be very sensitive on sample cleanliness in the yield spectra and was absent in measurements performed on very clean samples. It is therefore ascribed to oxide. A shift of the edge

to higher energy compared to the absorption spectrum is partly due (+0.16 eV) to a calibrational error of the earlier result which is corrected in table 4. Also the temperature difference (77 K to 400 K) contributes to the shift of the edge (see fig. 57 in section 7.4.4).

The minimum at 57.7 eV about 2.3 eV above the edge is attributed to the onset of transitions to the second band in Li. MATHEWSON and MYERS [1972] find the optical threshold for transitions across the gap at 2.2 eV (at 298 K) and believe that the Fermi surface just touches the Brillouin zone boundary. The theoretical calculations of HAM [1962] imply an onset of transitions 2.87 eV above the edge. This correlates well with our result. In the spectrum of liquid Li this minimum is washed out, but a faint indication is still present. This might be due to the fact that the nearest neighbor distance remains quite well defined which could give rise to a decrease in the density of states in the liquid as well.

The results on Be shown in fig. 26 are in very good agreement with the transmission curves published by SAGAWA et al. [1966] and by SWANSON and CODLING [1968] . SAGAWA et al. [1966] have compared the absorption structures with an unpublished density of states calculation by LOUCKS [1964] which originates from the band structure calculation by LOUCKS and CUTLER [1964] . The minimum at the Fermi edge giving rise to the shoulder A is also present in the calculation by TERRELL [1966] . The Be spectrum establishes one of the rare cases of very good agreement of the structure in absorption spectra and a density of states calculation.

6.1.2. $L_{2,3}$ edges (Na, Mg, Al)

The earlier measurements on Na were performed by O'BRYAN [1940] . These disagree, however, with those of HAENSEL et al. [1970a]shown in fig. 5. For Mg there is good overall agreement with the results obtained by SKINNER and JOHNSON [1937] and for Al the results are in good general agreement with those of FOMICHEV [1967] obtained with classical sources and with the synchrotron radiation measurements by SAGAWA et al. [1966] , HAENSEL et al. [1969b], GÄHWILLER and BROWN [1970] , and EJIRI et al. [1970] . For both Mg and Al the earlier measurements do not show the details at the L_1 edge position and the details in the region 0 - 10 eV above the $L_{2,3}$ edges. Although in the measurements of HAENSEL et al. [1970a] an elimination of a contribution of surface oxide in the region right above the $L_{2,3}$ edges was achieved by dividing transmissivities offilms with different thicknesses,there is some doubt by now that these structures are intrinsic Al structures.

Recently BALZAROTTI et al. [1974] remeasured this region with a differential technique (see section 3.3). The samples, however, were evaporated under ordinary high vacuum conditions (10^{-6} torr) as those of HAENSEL et al. [1970a] and floated off in water before measuring. The results shown in fig. 28 (curve μ) are corrected for contributions from surface oxide which has prominent exciton structures in this region. Balzarotti et al. compared their results with a density of states calculation by CONNOLLY [1970] which is also displayed in fig. 28 (curve J_c). There is only partial coincidence between peaks in Connolly's density of states and peaks measured by Balzarotti et al..

GUDAT and KUNZ [1975] , GUDAT [1974] have remeasured this region with yield spectroscopy on samples evaporated in the 10^{-10} torr range with the same

accuracy as Balzarotti et al. namely ±0.2 %. The result is also displayed in fig. 28 (curve Y). No structures could be observed, the curves were completely flat in this region. (The change in slope at about 4.2 eV above threshold is explained as the threshold of electrons emitted directly into the vacuum from the L_3 level and thus would only be observed in yield spectroscopy.) Although yield spectra sample only a depth of ≈40 Å this appears to suffice for obtaining bulk properties. On the other hand HAGEMANN et al. [1974b] demonstrated a very strong influence of impurities on the absorption coefficient of Al before the onset of $L_{2,3}$ transitions when the samples were evaporated in a vacuum of about 10^{-6} torr. This would support a speculation that the samples of BALZAROTTI et al. [1974] contain trapped oxigen impurities which would not give rise to the typical Al_2O_3 spectrum but to additional structures.

The large peak in the spectra of Na, Mg and Al were subject to many speculations, because of the systematic variation of spacing between these peaks and their separations from the respective edges. The separations are smallest with Na and increase with the free electron density. Also Si appears to fit into this pattern (see BROWN [1974] , fig. 28 therein). All three metals have different crystal structures Na is bcc, Mg hcp and Al fcc. The peaks appear to be superimposed onto a smoothly varying background which closely follows the atomic calculation as demonstrated for Al with calculations by COOPER [1969] (fig. 26).

The first attempt to interpret these structures was based on the measurement of the Al spectrum by FOMICHEV [1967] . HEDIN and LUNDQVIST [1969] and HEDIN et al. [1971] have ascribed these structures to the excitation of plas-

marons. A plasmaron is a collective excitation of the free electron gas in which a plasma wave is coupled to a localized hole. By localizing the plasma wave the frequency is shifted from the free electron value at long wavelengths (15 eV in Al) to higher values through the mixing-in of short wavelength plasmons. Such short wavelength plasmons have higher frequencies by virtue of the dispersion relations (energy versus momentum relations). The magnitude of this effect could not be calculated, only the resonance energies were obtained. When applying the theory to Na and Mg it turns out that the peak positions do not scale properly with the particle density of free electrons.

Considerable progress was made when WOLFF et al. [1972] measured the spectrum of Na vapour which is displayed in fig. 29 with a photoelectric detector (in addition to photographic plates) thereby allowing for an extraction of the true shape of the continuum absorption. The spectrum demonstrates that the large maxima E, F, G in fig. 5 are absent in the Na vapour spectrum and are therefore a genuine solid state effect. The Na continuum follows nicely the atomic calculations by McGUIRE [1968 , 1970] .

In a recent experiment by PETERSEN and KUNZ [1975] (see also PETERSEN and KUNZ [1974] for a preliminary result) the yield spectrum of liquid Al was measured as shown in fig. 26. This result rules out completely any interpretations of the peaks F and G in the solid as a collective excitation since they are absent in the spectrum of the liquid. The spectrum closely resembles the atomic calculation.

A density of states calculation for Al by CONNOLLY [1970] shows a remarkable dip in the region between peaks F and G (fig. 26) but does not reproduce the other features of the spectrum. Connolly ascribes the dip to a shift of d-bands to lower energies. It is quite unexpected that such strong features appear in the density of states 30 eV above the Fermi level. The calculation ought to be repeated with a different method in order to see if it is relevant.

RITSKO et al. [1974a] after reproducing the Al spectrum with their electron energy loss spectrometer have calculated the Al and the Na spectra with a simple EXAFS calculation as explained in section 5.3. They are using a square well potential for the scattering atoms. Although the method used should be very insufficient near threshold the fact that they were able to reproduce the positions of maxima right down to the region of 10 eV above threshold (see fig. 30) makes it very probable that amplitude modulation of the final state wavefunction by scattering from the nearest neighbor atoms in the sense of section 5.3 is the cause of these structures. FANO [1974], however, has argued that a much more sophisticated theory for the region of low kinetic energy of the emitted electrons has to be developed. He points especially at the difference between the $L_{2,3}$ and the K spectrum, which is also shown in fig. 30. FANO [1974] proposes to match atomic with solid state wavefunctions at the edge of the atom along the lines of the paper by FANO and LEE [1973]. The matching condition will modulate the amplitude of the final state wavefunction at the position of the core level.

6.1.3. L_1 edge (Na, Mg, Al)

Weak structures at the expected positions of the L_1 edge are clearly identified in the Mg and the Al spectrum (fig. 26). These structures, however, do not have the shape of an edge. Depending on the background subtraction they can either be described as skewed or as broadened. Moreover, the fact that Mg shows three structures in this region is quite unexpected. The distortion of the edge is caused either by the edge anomalies discussed in section 7.2 or by a type of autoionization interaction as mentioned in section 5.5. This type of distortion is clearly to be seen in fig. 29 at the L_1 edge of Na vapour. There the 2s-transitions display profiles according to the Fano equation (28) (see fig. 25).

6.2. Alloys with Al

6.2.1. Wide range behavior

After first preliminary measurements by YAMAGUCHI et al. [1971], HAGEMANN et al. [1975] , HAGEMANN [1974] have performed a systematic investigation of several Al-transition metal alloys. Figure 31 shows the spectra of the ordered alloys VAl_3, FeAl, and $CuAl_2$. The partial absorption coefficient $\mu^*(\omega)$ is obtained by the differential technique described in section 3.3 and refers to the absorption of Al in V, Fe or Cu. It is obtained by putting a pure V, Fe or Cu film with equal amount of that metal per unit area as contained in the alloy film into the reference beam of the densitometer fig. 13. $\mu^*(\omega)$ is obtained from the transmissivity $T(\omega)$ of the alloy films relative to V, Fe, or Cu films by

$$\mu^*(\omega) = -\frac{1}{D_{Al}} \ln(T(\omega)) \qquad (29)$$

where D_{Al} is the thickness which would be obtained from the Al atoms in the alloy film if taken alone. Since the spectra of the other metals in the energy range above the onset of Al $L_{2,3}$ transitions are smooth and probably independent of the environment, we assume that spectra like those of fig. 31 measure the 'Al spectrum in the alloy environment'.

The striking change of these spectra compared to that of pure Al is the disappearance of the minimum at 105 eV. The EXAFS interpretation of the big maxima in the Al spectrum would predict rather a shift of these structures on alloying. A possible way of understanding the wash-out of structures would be to postulate a mean free path of the electrons shorter than twice the nearest neighbor distance. Then the factor $\exp(-2\gamma r_i)$ in eq. (26) causes a dramatic damping of the EXAFS oscillations. In this case, however, the theory in its present form will break down as was mentioned above.

Another feature of interest in the spectra of fig. 31 are the variations at the onset of the L_1 transition. In the spectrum of VAl_3 the onset looks very much like an edge. Quite obviously varying interactions between the L_1 edge and the $L_{2,3}$ continuum take place. A detailed interpretation, however, is not possible at the present state of knowledge on the electron states in these alloys.

6.2.2. Edge region

The vicinity of the $L_{2,3}$ edges is displayed in fig. 32 after HAGEMANN et al. [1974a]. In addition fig. 32 shows the $AuAl_2$ spectrum after GUDAT et al. [1973], HAGEMANN [1974] and GUDAT [1974]. The onset of L_3 transitions shifts with different alloys between -1.2 eV and +0.3 eV with respect to pure Al. In

table 5 (HAGEMANN et al. [1975]) these shifts are compared with the shifts observed in fluorescence emission. There is a very good correspondence between the two types of measurement. An interpretation in terms of charge transfer between the alloy components, however, is difficult as discussed by WATSON et al. [1973] for $AuAl_2$ on the basis of XPS measurements. All the spectra displayed in fig. 32 but that of $CuAl_2$ show a second rise in the absorption coefficient after the Al $L_{2,3}$ edge culminating in a peak. The ordered alloys show sharper structures than the disordered alloys as would be expected. Especially the slopes in the rise towards the peaks with the ordered alloys $AuAl_2$ and NiAl are edge-like. The structure in the spectrum of $AuAl_2$ shows clearly the spin orbit splitting of the $L_{2,3}$ level and also with the NiAl there is an indication of this feature. No other examples of so sharp structures in the spectra of metals at higher energies than the edge are known. The samples were therefore carefully checked against mixed phases and the spectrum of $AuAl_2$ was reproduced at several stages of improved sample preparation and measuring techniques. Among these improvements was also the measurement of bulk samples with yield spectroscopy (GUDAT and KUNZ [1975] , GUDAT [1974]).

Both spectra ($AuAl_2$ and NiAl) could be compared with density of states calculations. The comparison of the $AuAl_2$ spectrum (GUDAT et al. [1973]) with the density of states calculated by SWITENDICK [1971] from a band structure calculation by SWITENDICK and NARATH [1969] showed a faint indication of the peak at 74.7 eV. Much better agreement between theory (CONNOLLY and JOHNSON [1971]) and experiment (HAGEMANN [1974a]) is found with the NiAl spectrum as was shown in fig. 6 (section 2.5). Here the rise in the absorption coefficient conincides quantitatively with a very pro-

nounced steep rise in the density of states. A corresponding structure occurs at the Ni edge which is also displayed in fig. 6. This appears to show quite clearly that prominent density of states structures must be present in the absorption spectra. It would be interesting to see also calculations of this type for some of the other ordered alloys on which data are now available (fig. 32). The local character of the density of states extracted this way manifests itself in the absence of any indication of the unfilled transition metal d-states. These are not seen since the d wavefunctions probably have small amplitudes at the Al sites.

6.3. Noble and heavy metals

In this section we want to bring further examples of the suppression of oscillator strength near threshold and the shift of oscillator strength to higher energies which is typical for noble and several other heavy metals. Many of the edges in transition metals and rare earth metals behave the same way and only a few transitions in these latter two classes of metals show the large structures at threshold introduced in section 2.3 and explained in section 5.4 and 5.5.

Figure 33 gives a comparison of the absorption behavior of all three noble metals in the energy range 10 - 200 eV after HAGEMANN et al. [1974b]. First, it is interesting to note the slow decay of the absorption coefficient of Cu to higher energies compared to a fairly abrupt decrease for Ag. The minimum at 125 eV can be ascribed to a so called 'Cooper minimum' for the 4d transitions in Ag. Such a minimum was first explained by COOPER [1962] and occurs when the initial state wavefunction has one or more nodes. Figure 34 shows a scetch of the wavefunctions in order to explain how the matrix element

R_{l+1} (eq. (21)) changes its sign when the final state moves into the core. The change of sign implies a zero crossing of R_{l+1} at an energy ε intermediate between ε_1 and ε_2 for which wavefunctions are scetched in fig. 34. The result of actual calculations of R_{l+1} and σ for the Ag^+ and Cu^+ d→f transitions as carried out by COOPER [1962] is shown in fig. 35 . The calculations are in good overall agreement with the measured absorption of Ag and Cu in fig. 33.

Although we do not want to give an extensive discussion of the excitations of loosely bound d bands in this context we want to point at the prominent structures in the region below 40 eV in the spectra of all three noble metals. These peaks are due to d electron excitations. The question arises whether these structures can be explained in terms of an EXAFS type theory or have to be attributed to the density of states or other phenomena.

Recently OLSON et al. [1974] using synchrotron radiation have performed a very interesting thermomodulation measurement in reflection on Au in the region from 6 to 35 eV which shows structure of unexpected sharpness. The authors ascribe these structures to transitions into empty f states.

Figure 36 shows the spectrum of Bi which was composed by HAGEMANN et al. [1974b] from a recent remeasurement and previous results by HAENSEL et al. [1968] , ZACHARIAS [1973], SASAKI and EJIRI [1966] and JAEGLE et al. [1967].
The Bi spectrum is dominated by the d excitations which set in near 25 eV with the spin orbit split edges. The edges are due to d→p transitions while the d→f transitions are delayed and give rise to the broad peak at about 40 eV above threshold. This delay is very typical for d electron transitions and is found in a similar way in the spectra of Sn, In and other metals.

Further JAEGLE et al. [1969] have measured Au, Bi, Pt, Ta between 80 eV and 500 eV and compared these data with atomic calculations (see also fig. 24). The agreement for Ta and Pt is not very striking. There exists a large number of reflectivity measurements on metals in the region below 40 eV which we do not want to review in this context. Electron energy loss data are available on Pd, Pt, Cu, Ag, and Au in the region up to 70 eV as reviewed by DANIELS et al. [1970] and up to 150 eV on Cu, Al, Au, Ir, U, Bi, Pb, and transition metals Ti to Ni by WEHENKEL and GAUTHE [1974a,b,c]. Further CUKIER et al. [1974] give results on U and Ir up to 500 eV comparing them with atomic theory. Again the agreement is not very good. These calculations give the absorption coefficients only to zeroth order for heavy atoms. Configuration interaction as mentioned in section 5.5 probably has a strong influence on parts of these spectra.

6.4. Rare earth metals, La, Ba

6.4.1. Rare earth metals

The first results on the 4d absorption of the rare earth metal series were obtained using a classical x-ray tube as the source and were published in two successive papers by ZIMKINA et al. [1967] and by FOMICHEV et al. [1967]. These spectra together with those of the preceeding elements in the periodic table Sn, Te, Xe and La are shown in fig. 37. They display very nicely the systematics of the absorption behavior due to the lowering in energy of the empty f states and finally the filling of f states. The large peak due to transitions into the empty part of the 4f states migrates towards the ionization limit while the binding energy of the 4d level increases at the same time giving rise to a shift of the whole feature to higher photon energies. Finally in Lu the 4f states are filled with 14 electrons and the peak has disappeared. Several of these huge resonances show a skewed line shape which is obviously due to an interaction with the underlying continuum

according to eq. (28). This is especially obvious in the spectra of Dy, Ho, Er, Tu and Yb.

Figure 38 shows the fine structure regions omitted from fig. 37. The fine structures are simple in La then attain considerable complexity while the number of filled f states increases. Finally in Yb^{3+} with only one empty f state the structures are very simple again. The two peaks in Yb are separated by 8.3 eV which ought to be the spin orbit splitting of the final state configuration $4d^9 4f^{14}$ into the states $D_{5/2}$ and $D_{3/2}$. This is supported by an XPS measurement on Yb vapor by FADLEY and SHIRLEY [1970] in which case the atoms have a ground state configuration $4d^{10} 4f^{14}$ (WYBOURNE [1965]). The ejected 4d electrons show the spin orbit splitting of the $4d^9 4f^{14}$ configuration left behind of 8.43 eV in good agreement with the value given above.

The spectra of the rare earths between Ce and Lu are very complicated. It was shown, however, already in fig. 4 to which extent the theoretical calculations by SUGAR [1972] were able to account for these structures in terms of a splitting of the configuration $4d^9 4f^{N+1}$ by the exchange interaction. HAENSEL et al. [1970] and RABE [1970] have remeasured several of these spectra. In addition they could demonstrate that oxidation of the rare earth metals changes mainly the line strength but not so much the energy positions of the lines. Table 3 in section 5.4 compares theory and experiments on La and Ce showing excellent agreement.

An example of the atomic character of these transitions is the spectrum of $PrAl_2$ (fig. 39) as obtained by HAGEMANN et al. [1975], HAGEMANN [1974]. In this spectrum the sharp lines up to 120 eV and also the broader maxima of the Pr spectra at 123.9 eV and 131.4 eV are not changed in any obvious way. This is demonstrated especially well when looking at μ^* (according to eq. (29))

in the lower part of fig. 39. In the μ^* spectrum the structures of the pure Pr metal and those of $PrAl_2$ have cancelled because they are identical.

6.4.2. La

The La spectrum is of interest in several respects. It is much simpler than the rare earth spectra proper, nevertheless it furnishes the simplest case of the d-f electron coupling. While La in its ground state has an empty 4f shell the 4f states are almost bound and the extra charge in the excited $4d^9$ state due to the hole lowers the potential well even further so that it is capable of binding the excited 4f electron. According to SUGAR [1972] the configuration $4d^9 4f^1$ splits into three relevant levels (see table 3) $^3P_1$, $^3D_1$, $^1P_1$ with relative oscillator strengths 1:11.1:1993. The strongest line $^1P_1$ is pushed up into the continuum and is broadened as can be seen in fig. 37. DEHMER and STARACE [1972] have calculated the configuration interaction of this line with the underlying $4d^9 \varepsilon f$ continuum, and WENDIN [1974] has performed a calculation taking ground state correlations into account (section 5.5) within the random-phase-approximation including exchange. Both calculations give a broadening of approximately the right magnitude but the peak positions do not agree very well with the experiment and among the two different theories.

There is a superficial peak C at 103.7 eV in the La spectrum of fig. 38 which does not fit into the scheme of table 3. RABE [1974] did not find this extra peak in a careful reinvestigation of this spectrum. Thus all features in the La spectrum are quite well understood.

6.4.3. Ba

Figure 40 shows the spectra of Ba metal and Ba vapour as given by RABE et al.

[1974] . The authors have performed a Hartree-Fock calculation taking into account multiplet splitting and spin-orbit interaction. There is excellent agreement with the line positions. It is interesting to note that although Ba has one atomic number less than La the spectrum is very similar to that of La. The reason is, in a simple picture, the charge of the 4d hole which pulls the 4f wavefunction into the inner well. Again WENDIN [1973] has performed a calculation of the large $^1P_1$ reasonance within the random-phase-approximation and finds the broad feature about 2/3 in width of the observed structure.

Although all the features discussed in this section are predominantly determined by the atoms and only slightly influenced by the metallic state it is important to understand these spectra. Only since a fairly detailed atomic understanding of what is going on in these spectra is reached it is possible now to see the limitations of learning something from these spectra about the solid especially the metallic state. In addition these very interesting phenomena deserve attention in their own right.

6.5. Transition metals

6.5.1. Ti-Ni

The transitions $3p^6 3d^N - 3p^5 3d^{N+1}$ in the metals Sc to Ni bear a very close similarity to the transitions $4d^{10} 4f^N - 4d^9 4f^{N+1}$ of the rare earth metals which were treated in the previous section. The major difference, however, is the spatial extension of the 3d wavefunctions which are less compact than the f wavefunctions and the lack of closed shells outside the 3d shell. In solid state physics the d-states are frequently described in terms of Bloch functions. Band structures of transition metals are calculated producing a

considerable width of the d-bands in the order of 5 eV. The d-bands have great importance in explaining many solid state properties of transition metals, on the other hand in many cases an atomic treatment of d states furnishes an excellent first order description of these solids.

The first relevant measurement on the $3p^6 3d^N - 3p^5 3d^{N+1}$ transitions was performed using synchrotron radiation by SONNTAG et al. [1969] . Figure 41 shows these spectra from Ti to Ni including Cu. The huge peak near the expected onset of $M_{2,3}$ transitions is decreasing in strength when going from Ti to Ni and collapses almost completely in the spectrum of Cu. At the same time the background onto which it is superimposed increases in strength. This is quite reasonable, since the number of d electrons, which are responsible for the background absorption, increases. The $3p^5 3d^{N+1}$ peak, however, cannot be taken as an image of the empty part of the d band in which case it should display a narrow peak about 5 eV wide for Ti and then decrease continuously to a very small width in Ni. A replica of this peak should follow at a distance of about 2 eV because of the spin-orbit splitting of the 3p level. Instead, the peaks are up to 25 eV wide (FWHM for Cr) and the initial slope is not edge-like but has a minimum width of $\sim$2 eV.

For some time it was anticipated that probably configuration splitting in a way quite similar to the rare earths (sections 5.4, 6.4) would explain the shapes of these peaks (DEHMER et al. 1971). Only recently COMBET FARNOUX [1974] and COMBET FARNOUX and LAMOUREUX [1974] have performed an atomic calculation on Ti, V and Co yielding a multiplet splitting of the $3p^5 3d^{N+1}$ configuration having the right order of magnitude to explain the spread of oscillator strength. In these spectra the background absorption is much stronger than in the rare earths and interaction with the continuum needs

to be calculated in the next step before a direct comparison with the spectra is possible.

KOTANI and TOYOZAWA [1973a,b] have pointed out the importance of considering the s-d mixing interaction and the interaction of the hole with the conduction electrons. They have treated these interactions in a model calculation. The interaction with the conduction electrons is considered along the lines of the many-body spike theory which will be treated in section 7. Since (as will be shown in section 7) this theory has unresolved difficulties in explaining the behavior even of simple metals it is difficult to evaluate the relevance of this theory for the much more complicated transition metals. Multiplet splitting is completely disregarded in the model of Kotani and Toyozawa.

It is interesting to note that transition metal compounds show sharp structures near the onset. NAKAI et al. [1974] have measured several halides of Cr, Mn, Fe, Co, and Ni all of them displaying fine-structure at the onset. Figure 42 shows spectra of Mn halides with rich line structure quite analogous to that in the rare earth metal spectra. Probably s-d mixing (as suggested by KOTANI and TOYOZAWA [1973a,b]) is responsible for the blurring of these structures in the metallic state.

A special problem arises in the interpretation of the Ni spectrum. In this case a situation very similar to that of Yb (see fig. 37) should occur. The transition $3p^6 3d^9 \rightarrow 3p^5 3d^{10}$ leaves the final state with a filled d band. No multiplet splitting in addition to the spin orbit splitting will occur. We therefore expect to observe two narrow bands $\sim$.3 eV wide (see the band structure calculation by ZORNBERG [1970]) with a separation of about 2 eV. Instead

an edge-like structure is measured (fig. 41). DIETZ et al. [1974a,b] who have reproduced this structure with electron energy loss measurements fit their results with a Fano profile with $E_r = 66.1 \pm 0.2$ eV, $\Gamma = 2 \pm 0.2$ eV and $q = 0.9 \pm 0.1$ according to eq. (28). A theoretical estimate is in quite good agreement with these values. Even the superposition of two such lines with the spin orbit separation is consistent with the data according to Dietz et al.. (BROWN et al. [1971] and GUDAT and KUNZ [1972a] have actually observed an indication of the spin orbit splitting in the Ni spectra.) Such a strong interaction with the background continuum is also prompted by the skewed shapes of structures in several other spectra namely the Mn, Fe and Co structures in fig. 41. Speculations on these line shapes were already expressed in the papers by SONNTAG et al. [1961] , FANO and COOPER [1969] , and GERLACH [1971] .

6.5.2. Ta - Pt

Figure 43 shows the spectra of the third series of transition metals Ta to Pt as measured by HAENSEL et al. [1969c] augmented by results of LEYSER [1970] on Os and Ir. Results on Ir are published also by CUKIER et al. [1974] in fair agreement with Leyser's results and with the energy loss measurements by WEHENKEL and GAUTHE [1974a] showing, however, much less details. The interesting feature in these spectra is again the strong $5p^6 5d^N \rightarrow 5p^5 5d^{N+1}$ transition. Since the spin orbit splitting is large in these metals it manifests itself in a splitting of the broad features into two peaks. (The edge positions as marked have to be considered with caution.)

The second interesting feature is the onset of the 4f ($N_{6,7}$) electron transitions. These transitions overtake the 5p peaks when going from Ta to Au. There appears to be a configuration interaction between the 4f and 5d levels which is changing phase when the transitions come to lie on the higher energy side of the 5p peaks. In the Ta, W and Re spectra the 4f structures can barely be identified. However, in the spectra of Os, Ir and Pt they become more and more prominent. In the Pt spectrum there appears to be a dip before the onset of the $N_{6,7}$ transitions. This would correspond to positive values of q in eq. (28) (see fig. 25). The 4f structures in Au are weak again, they were not resolved in the older measurements shown here (but see fig. 3 or 33). Because of the filling of the 5d band in Au 4f→5d transitions are no longer possible. Note also that in the $4f^{14}5d^{N}\rightarrow 4f^{13}5d^{N+1}$ transitions the main quantum numbers of the f and d shells differ. This corresponds to a low overlap of initial and final state wavefunctions and explains the relative weakness of these transitions at threshold.

No measurements on the systematics of the $4p^{6}4d^{N}\rightarrow 4p^{5}4d^{N+1}$ transitions in the series Zr to Pd are available in the literature to our knowledge. A very similar behavior as with the other transition metals in approximately the same spectral range is expected to occur.

6.6. Alloys with transition metals

Two different groups of alloys with transition metals have been investigated. These are alloys among transition metals of the series Ti to Ni (and Cu-Ni alloys) and alloys of these transition metals with Al. The transition metal alloys have a long history which is especially connected with that of the rigid band model (see e.g. MOTT [1964]). According to the rigid band model

the Ni d states in an alloy of Cu-Ni (1:1) should be just filled. This would imply a disappearance of the Ni 3p structure in the absorption spectrum.

The result of the absorption measurement of GUDAT and KUNZ [1972a] on CuNi is shown in fig. 44. The transmittance of Cu and Ni films is shown together with the transmittance of a Cu+Ni sandwich film and a Cu-Ni (1:1) alloy film. The sandwich and the alloy films show almost identical spectra the difference can be accounted for by inaccuracies in composition or film thicknesses. The same result, namely a superposition of the spectra of the individual components in the alloy spectrum, was also observed with other ratios of Cu and Ni and with alloys of the Fe-Mn and Cr-Mn systems. This result is in obvious contradiction with the rigid band model.

A theoretical approach completely different from the rigid band model is due to SOVEN [1967] , LANG et al. [1968] and KIRKPATRIK et al. [1970] , the coherent potential approximation (CPA). The CPA is a self-consistent scattering approach with which actual calculations on the filled Cu-Ni valence states were carried out by STOCKS et al. [1971] . These calculations are in excellent agreement with XPS measurements by HÜFNER et al. [1972] . The result is roughly characterized by stating that each Ni atom carries approximately one unfilled d-hole with it irrespective of the Cu environment. This characterizes also very well the results by GUDAT and KUNZ [1972a].

Figure 45 shows the spectra of alloys of Al with Fe and Ni after HAGEMANN et al. [1975] , HAGEMANN [1974]. The FeAl spectrum differs only slightly from the spectrum of pure Fe at the onset of the Fe 3p transitions while the Ni spectrum undergoes a considerable shift by about 2.5 eV in $NiAl_3$.

Moreover, the absolute change in the absorption coefficient in NiAl is only 1/5 of what would be expected from a simple superposition. The shift and the decrease in edge height can be ascribed to a filling of the Ni d states in these alloys. In this case the rigid-band model provides a first order understanding of the result. The high density of states in Fe allows only for small shifts of the Fermi level. On the other hand the Ni d-hole will be filled already at low concentrations of Al since additional electrons are supplied from Al. At higher concentrations the Fermi level undergoes large shifts assuming a low density of states in the region above the Ni d band.

7. Edge shape in simple metals

7.1. History

The soft x-ray measurements of edge-shapes in simple metals began with the emission measurements of O'BRYAN and SKINNER [1931]. Figure 46 displays these historical results (LANDOLT BÖRNSTEIN [1955]) which have not changed in essence in the meantime in spite of much improved measuring techniques. Such spectra gave the first direct image of the filled part of the conduction band in free-electron metals. They are in very good general agreement with the expected behavior and, most important, they show relatively sharp edges. The main interest turned to those minor features which did not agree with the simple picture. The blurring at the low energy end was attributed to Auger transitions. The little peak in the Na L_3 spectrum right at the edge (and similar peaks for Mg and Al) and the broad decrease of intensity at the Li K edge beginning at a peak well below the edge were not explained satisfactorily. ALLOTEY [1967] explained the Li peak as a electron-hole p-scatering resonance but the explanation was not generally accepted because of the difficulties in obtaining a realistic self consistent electron-hole potential in a metal. The situation of the theoretical understanding of these features before the advent of the Mahan, Nozieres-DeDominicis (MND) many-body theory is best described in the proceedings of the Strathclyde conference (1967) on the 'Soft X-Ray Band Spectra' edited by FABIAN [1968].

It was in 1967 that MAHAN [1967] published the paper which initiated the many-body interpretation of edges. He treated the excited electron in the incompletely shielded potential of the hole from an excitonic point of view and predicted a power law divergence at threshold. NOZIERES and DeDOMINICIS [1969] were able to give a more rigorous foundation of this theory in terms

of the phase shifts of the electron hole scattering. The theory gave an explanation of both the edge peak at the Na $L_{2,3}$ edge as well as the peculiar shape of the Li K edge. Moreover, the theory is applicable both to the edge shapes in emission and absorption spectra. From the theoretical point of view the two cases are complementary.

At about this time the edge shapes of the absorption spectra of Li and Na were obtained for the first time in good quality by HAENSEL et al. [1969a] and KUNZ et al. [1971] (figs. 5 and 47). These spectra showed beyond doubt a very prominent peak at the $L_{2,3}$ absorption edge of Na (fig. 5) and a broadening of the Li K edge giving the direct complement to the emission behavior. Moreover, absorption data in principle are more reliable since they are not subject to self-absorption and efficiency corrections of the monochromator-detector combination which have to-be applied to emission results. MAHAN [1974 a] has reviewed the status of the subject at this stage.

In 1973 DOW [1973] and DOW and SONNTAG [1973] undertook again a careful analysis of the absorption spectra near K and L edges of Li, Na, Al and Mg and found inconsistencies with a qualitative application of the MND theory. In the meantime Dow and collaborators have pointed at further inconsistencies in the spectra when interpreted with the MND theory and have proposed alternative explanations of the width of the Li K edge. The controversy about this subject is documented in the proceedings of the IV. conference on VUV Radiation Physics, Hamburg (1974) in two invited papers by MAHAN [1974b] and DOW [1974a].

Most recently RITSKO et al. [1974b] have failed to observe a change of the Li K edge shape with increasing momentum transfer in an electron energy loss scattering experiment. This change of the edge shape was predicted as a consequence of the MND theory by DONIACH et al. [1972]. In another recent experiment KUNZ et al. [1974] have observed a strong temperature dependent increase in the edge width of Li above lq. N_2 temperature. The data suggest that most of the Li K edge width is due to a phonon induced broadening. No better theory, however, than the MND theory has been brought forth up to now to explain the shape at the L edge. At the present moment it is difficult to predict in which direction the theory of the edge shape will move.

7.2. Many-body theory of edge anomalies

7.2.1. Edge shapes

According to the theory of MAHAN [1967] and NOZIERES and DeDOMINICIS [1969] called the 'MND' theory, the 'metal-exciton' theory or the 'spike' theory, the imaginary of ε is given in the vicinity of the K, L, M and higher edges by a universal threshold law

$$\varepsilon_2(\omega) \propto \sum_{\ell=0}^{\infty} B_\ell \left(\frac{\hbar\omega - E_T}{\xi}\right)^{-\alpha_\ell} \Theta(\hbar\omega - E_T) \qquad (30)$$

with

$$\alpha_\ell = 2\delta_\ell(k_F)/\pi - \sum_{j=0}^{\infty} 2(2j+1)\left(\delta_j(k_F)/\pi\right)^2 \qquad (31)$$

Here B_ℓ is essentially the square of a dipole matrix element for a transition between the one-electron core level and a state with angular momentum quantum number ℓ in the conduction band; ξ is an energy in the order of magnitude of the Fermi energy (the correct value of ξ is controversial among theorists); E_T is the threshold energy; Θ is the unit step function which

guarantees observance of the Pauli principle; $\delta(k_F)$ is the phase shift of a Fermi energy electron in the screened potential of the hole and k_F is the Fermi wave vector. The phase shifts δ_j are restricted by Friedel's sum rule.

$$1 = \sum_{j=0}^{\infty} 2(2j+1) \frac{\delta_j}{\pi} . \qquad (32)$$

Under the assumption that the screened hole potential is well localized in a small volume, δ_o will be the dominant phase shift, thus from (32) $\delta_o \approx \frac{\pi}{2}$, $\delta_\ell \approx 0$ for $\ell \geq 1$. It follows $\alpha_o = 0.5$ and $\alpha_\ell = -0.5$ for $\ell \geq 1$. This by far oversimplifies the situation but it illustrates best which line shapes should occur. For a transition from an s level (e.g. Li) all B_ℓ's are zero except B_1. Since α_1 is negative the edge is expected to be rounded from eq. (30). On the other hand if the core level has p symmetry as in the Na $L_{2,3}$ transitions then B_o and B_2 are non-zero. In this case the B_o term in eq. (30) with a positive α_o dominates $\varepsilon_2(\omega)$ and gives rise to an integrable singularity at threshold.

7.2.2. Simplified interpretation

It is always difficult to figure out a non-mathematical physical explanation for the result of a many-body calculation. Nevertheless, let us try to give a simple picture which could perhaps convey a first order understanding of the mechanism involved.

As we have mentioned in section 2.4 the core level excitation gives rise to the sudden creation of a hole potential. As a reaction the conduction electrons rush in, in order to shield this potential since we deal with a metal. The scattering is characterized by phase shifts δ_ℓ in a partial wave analysis.

An infinite number of electrons near the Fermi energy will become excited. This follows from a theorem by ANDERSON [1967] which states that the many-body ground state in the presence of a localized potential well is orthogonal to the many-body state in the absence of the potential since an infinite number of electrons undergo an infinitesimal change of their states in order to adjust to the local potential. This theorem was one of the starting points of the edge theory. The situation is illustrated in fig. 48. The change of the free electron states can be visualized in the energy plot as an infinite number of transitions near the Fermi surface excited by the sudden creation of the core hole potential. The excitation spectrum f(E) of these transitions across the Fermi level is such that the transitions with the lowest excitation energy E are the most probable ones. It is described by

$$f(E) \propto \frac{1}{E^A}\,\Theta(E) \tag{33}$$

with an exponent $A < 1$ (HOPFIELD [1969]). This excitation spectrum is drawn schematically in fig. 49.

HOPFIELD [1969] has pointed at the analogy between impurity excitations coupled to a phonon spectrum and our present problem. (Using such an approach SCHOTTE and SCHOTTE [1969] could give a different derivation of the Nozieres-DeDominicis result.) The equivalent to the phonon spectrum is the spectrum of one electron excitations across the Fermi level f(E). Take the simple case that we have an x-ray transition between two bound levels of an atom in a metal which would show up as a δ-function line in the spectrum of the isolated atom. Since this atom, however, is immersed in the Fermi sea, excitations of the Fermi sea will be coupled to this transition. The coupling is achieved through the sudden change of the potential when the hole goes from the lower state to the excited state. Then the

δ-function line will obtain a side band as shown in fig. 49a. Moreover, because of ANDERSON's [1967] 'orthogonality catastrophe' the 'zero phonon' line, the δ-function, will disappear. Such distortions of line shapes in x-ray fluorescence emission and in photoelectron spectroscopy were calculated by DONIACH and SUNJIC [1969] . Recently HÜFNER et al. [1974] and SHEVCHIK [1974] have shown experimental evidence of this feature.

In the next step of our explanation we have now to compose the classical absorption spectrum from a continuous distribution of δ-function excitations as shown in fig. 49b. This distribution sets in with a step at E_T and is given by $\Theta(E'-E_T)$ (curve β). Through the coupling with the Fermi sea each of these δ-lines atan energy E' will develop a sideband distribution $f(E'-\hbar\omega)$ and the δ-lines disappear. In order to obtain the edge shape of $\varepsilon_2(\omega)$ we have to integrate over all these distributions and obtain (curve η)

$$\varepsilon_2(\omega) \propto (\hbar\omega-E_T)^{1-A}\ \Theta(\hbar\omega-E_T) \qquad (34)$$

The Fermi sea excitation spectrum must have an integrable singularity , $A<1$ and therefore $1-A>0$. Thus $1-A$ corresponds to the term $\sum_{j=0}^{\infty} 2(2j+1)\left(\delta_j(k_F)/\pi\right)^2$ in eq. (31).

The previous argument made the rounding of edges plausible. The explanation of the edge singularity in simple terms is more difficult. Here a picture due to FRIEDEL [1969] helps for an understanding. We did not yet consider the fact that the electron which was taken from the deep hole state will not go into a free electron state but will also end up in one of the scattering states due to the hole potential. If it ends up in a state near the Fermi energy it will go into a region of the energy distribution of electrons where

an infinite number of rearrangements have been taking place. This gives rise to a severe influence on the dynamics of the excited electron which eventually is the reason for the spike at the edge as sketched in fig. 49 (curve γ).

According to Friedel we can imagine three types of transitions which contribute to the absorption spectrum which are sketched in fig. 50. Figure 50a shows a direct transition which as we know is suppressed. Figure 50b shows the transitions coupled to the Fermi sea excitations which are responsible for the rounding of the edge. Figure 50c, finally, shows a replacement transition where the core electron goes into one of the hole states created by the Fermi sea excitations. Friedel has performed a simplified model calculation in which the terms due to the processes fig. 50a to c could be identified. The replacement transitions are those which give rise to the singularity at threshold (curve γ in fig. 49). Intuitively this is to be expected since the possible number of such transitions leading to net excitations close to the edge is divergent. Thus, in this picture the edge singularity is caused by a statistical factor counting the number of possible replacement transitions.

7.3. Auger and phonon broadening

Apart from possible density of states anomalies near the edges Auger and phonon processes will contribute to the edge shape. These processes will always give rise to a broadening of edges. Therefore these processes are in competition with the edge rounding of the MND many-body theory. Because of imperfect experimental resolution and the necessity to subtract a background etc., it will usually be difficult to make a decision on the different

processes involved on the basis of the line shapes alone (MND: according to eq. (30), Auger: Lorentzian, phonons: Gaussian).

Auger widths of edges are fairly difficult to calculate. For example in the Li atom no Auger decay of the 1s level is possible from energy considerations. In the metallic state the Auger width will depend crucially on the values of the conduction electron wavefunctions at the position of the 1s orbit. A recent attempt to calculate the Auger lifetime ($\tau = h/\Gamma$ for Li by FRANCESCHETTI and DOW [1974] and FRANCESHETTI [1974] has demonstrated these difficulties. Depending on the wavefunctions values of the width ranging from 2.5 meV to 130 meV were obtained. The authors believe that 130 meV is a lower limit to the actual Auger width.

Phonon broadening could come into play in several different ways.

1. Fermi edge broadening is proportional to $k_B T$ (k_B = Boltzman constant), at room temperature about 60 meV.

2. A calculation of the MND theory at finite temperature by FERRELL [1969] gave a temperature width of the spectrum at small energies which is proportional to $k_B T$ times the square of the phase shift. This makes it a small effect in the same order of magnitude as the Fermi edge broadening.

3. The coupling of phonons to the hole state was first estimated by McALLISTER [1969] following a suggestion by Overhauser. The model is based on calculating the dynamic change in potential energy of a charge sitting at the position of the core hole due to the deformation potential and the fluctuating dilations and compressions of the lattice brought about by the phonons. His values at 300° K for the inner level half widths (FWHM) are for Li: 370 meV, and for Na: 250 meV. An improved model of this inter-

action by BERGERSEN et al. [1971] yielded considerably smaller values in the order of 50-100 meV for Li and Na depending on the potentials chosen to evaluate the model.

4. DOW et al. [1973] have argued that an indirect coupling of the core state to the lattice mediated through a fluctuation of the conduction electron density inside the 1s orbit could result in additional broadening with FWHM of 460 meV for Li. The model calculation, however, was crude and better calculations have not been published. The paper was criticized by BERGERSEN et al. [1974] .

7.4. Experimental results and discussion

7.4.1. Li, Be, Na, Mg, Al

Figure 47 and the inset in fig. 5 show the spectra of the five lightest metals in the vicinity of the K resp. $L_{2,3}$ edges as obtained by HAENSEL et al. [1969a] and KUNZ et al. [1971] . The Li edge, however, was shifted by +.16 eV because of a recent recalibration. All spectra were measured with the sample at 77° K. As discussed in section 6.1.1. the feature A in the spectrum of Be is considered to be a band structure feature. The spectra of Na, Mg and Al show the spin orbit splitting of the L_2 and L_3 levels. The edge shape analysis using the lifetime broadened theoretical shape eq. (30) as described in DOW and SONNTAG [1973] and DOW et al. [1974] gave excellent fits in all three cases with the theoretical ratio $L_3:L_2=2:1$ (SONNTAG 1974). The spin orbit energies as determined by DOW et al. [1974] are 0.16 eV for Na, 0.27 eV for Mg, and 0.43 eV for Al.

It would be very helpful if one could relate the exact edge positions in emission and in absorption spectra with respect to each other. Unfortunately the two types of experiments are usually performed with different samples, different instruments and at different locations. The absolute calibration of a Rowland monochromator is a difficult task and therefore usually uncertainties of a few tenth of an eV are involved. One exception is the Al L_3 edge which was measured by CODLING and MADDEN [1968] in absorption at 72, 73 ± 0.02 eV and by SKINNER [1940] in emission at 72, 70 ± 0.02 eV. The edges coincide within 0.03 eV which is well within the common error bars. This result is important since it shows that no relaxation occurs between the absorption and the emission processes. This differs considerably from the luminescence behavior in the visible and near VUV.

KOSUCH et al. [1974] using synchrotron radiation have performed a measurement of the emission and absorption spectrum of Li with the same sample and the same monochromator. Their result shows an overlap of the two edges at about their 40 % points. The result appears to contradict the many body theory since this theory demands that the two edges meet at their onsets. Only broadening mechanisms of the type described in section 7.3 can account for an overlap of the edges.

The Li absorption spectrum is compared in fig. 47 with the respective emission spectrum by AITA and SAGAWA [1969] . This spectrum was inverted and shifted in order to match the two spectra at the edges. The shape of the Li K edge is in excellent agreement in emission and absorption. The edge peak at the Na L_3 edge, however, is by an order of magnitude weaker in emission than in absorption as is recognized when comparing figs. 5 and 46. This is surprising since the MND theory was claimed to be symmetric in emission and absorption.

DOW and SONNTAG [1973] and DOW et al. [1974] have fitted the $L_{2,3}$ spectra figs. 5 and 47 in the vicinity of the edge with a Gaussian broadened curve of the type eq. (30) with $B_\ell=0$ for $\ell\geq 1$. Note that the authors assume that the p→d transitions can be neglected: $B_2 \approx 0$. The result of the analysis are the values of α_o plotted in fig. 51. The value of α_o for Li was obtained from a value of $\alpha_1 = -0.3$ as obtained from a fit by YUE and DONIACH [1973] . Under the assumption $\alpha_\ell = 0$ for $\ell\geq 2$ it is easy to derive a functional connection between α_o and α_1 from eqs. (31) and (32), the so called compatibility relation (DOW [1973])

$$\alpha_o = \alpha_1 - \frac{1}{3} + \frac{2}{3}\,(1-6\alpha_1)^{1/2}. \qquad (35)$$

The straight line connecting the α_o values of Al, Mg, and Na in fig. 51 is the empirical law $\alpha_o = 0.068 r_s$, with $r_s = (3/(4\pi n a_o))^{1/3}$, a_o being the Bohr radius and n being the electron gas density. The dashed line is a theoretical curve in which the MND exponent α_o was calculated from a self consistent screening field. The Al, Mg and Na data points are in disagreement with the theoretical curve. No obvious solution was proposed up to now for this inconsistency. Nevertheless, the fact that α_o is linearily proportional to r_s is an important empirical result.

A further method of testing the MND theory is to extract α_o from the $L_{2,3}$ edge and α_1 from the K edge of one and the same metal. This was carried out by DOW 1974a on the basis of the results by NEDDERMEYER [1973a,b] and he found inconsistencies with the compatibility relation (35) as shown in fig. 52. NEDDERMEYER [1974] has reanalyzed his data correcting them for self-absorption and the resolution of his spectrometer showing them to be consistent with the compatibility curve (fig. 52). Since most of the width of the K edges in his analysis is ascribed to the resolution of the spectrometer the α_1's are approximately 0 and the many-body effect would be irrelevant for these K edges (see DOW et al. [1974]).

SLOWIK and BROWN [1972] and SLOWIK [1973] have measured the Mg $L_{2,3}$ edge in alloys of the type Mg_xSb_{1-x}. Depending on the composition the electrical resistivity of the amorphous alloy films varies from 10^{-6} Ω cm to 10^6 Ω cm. The high conductivity occurs near x=0.6. Positive values of α_o varying between 0.2 and 1.0 have been extracted from the shape of the Mg $L_{2,3}$ edges. The α_o values increase monotonically with restivity, however, the connection with r_s is not known. Also, the question arises whether or not these

amorphous alloys can be considered to be subject to a theory set-up for metals and, moreover, the fact that α_o approaches 1 violates the compatibility relation (35) see also DOW et al. [1974] .

7.4.2. Li-Cu alloys

DOW and SMITH [1973] have proposed that the inversion symmetry around a Li atom is destroyed by introducing a Cu atom into an adjacent lattice site. This should make $B_o \neq 0$ and thereby admix a contribution with a spike into $\varepsilon(\omega)$ in eq. (30). The shape of the Li K edge for different ratios of B_o/B_1 is shown in fig. 53. The calculations were carried out with $\alpha_o = .46$ and $\alpha_1 = -0.30$.

SONNTAG [1973] measured the K edge in Li_{1-x} Cu_x alloys up to concentrations $x = 0.35$ as shown in fig. 54. No change of the edge shape is observed . The prediction of DOW and SMITH [1973] on the basis of the MND theory failed.

7.4.3. Influence of momentum transfer on the Li edge shape

DONIACH et al. [1971] have calculated the effect of the break-down of the dipole selection rule on the B_ℓ's in eq. (30) when the excitation of the core hole is accompanied by a momentum transfer $\hbar q$. The Li spectrum should show a spike at large values of q.

Such a momentum transfer can be provided in x-ray Raman scattering experiments and in electron energy loss experiments (see section 3.5). RITSKO et al. [1974] have obtained the result shown in fig. 55 using the energy loss technique. No change in the shape is detectable which is larger than the error bars when q is increased. The change in the edge as expected from the MND theory when going from q=0 to q=1.2 Å^{-1} is shown in fig. 56. The theory was evaluated using

B_o/B_1 = 0.43 (for q = 1.2 $Å^{-1}$) as suggested by DONIACH et al. [1971], the phase shifts as calculated by AUSMAN and GLICK [1969], and ξ = 4.9 eV, the Li Fermi energy. The theoretical curves from eq. (30) were convoluted with a Gaussian function of FWHM = .38 eV asuming an unspecified additional broadening not originating from the MND mechanism. This gave agreement with the q=0 data (dots) in the region of the edge. If the effect was there it should clearly have been detected.

There are several alternative ways to set limits from this result to the MND parameters of eq. (30) and (31):

(1) The result fig. 55 sets a limit to B_o/B_1 of a maximum value of 2 %.

(2) Another way to interpret the result is to extract an upper limit to ξ of 0.01 eV. However, LONGE [1973] has calculated ξ and found that it is always greater than the Fermi energy (4.9 eV).

(3) Still another interpretation sets a limit to δ_o namely $0.22<\delta_o<0.5$. This would yield positive α_o and α_1 and limit $|\alpha_o - \alpha_1| \leq 0.17$ using the compatibility relation. Such restrictions would result in very unusual edge shape parameters.

7.4.4. Temperature dependence of Li edge shape

CRISP [1972] has measured the Li emission spectrum at 77 K and 4 K and has found no change in the edge shape. When taking self absorption corrections into account there was no change which could be attributed to the temperature change between these spectra and those taken previously by CRISP and WILLIAMS [1960] at room temperature. This result is especially surprising since Li undergoes two phase transitions between room temperature and 4 K.

HAENSEL et al. [1970b] have measured the absorption spectrum of Li at 77 K and 4 K and did not find any change. They also made a crude measurement at room temperature which did not show any appreciable difference to the other spectra, it was, however, affected by oxide contributions. This led KUNZ [1970] to the statement that there is "no change of the shape of the absorption edge between room temperature and liquid helium temperature".

Recently, KUNZ et al. [1974] have measured the temperature changes at the Li edge using yield spectroscopy (section 3.4) between room temperature and above the melting point (443 K) of Li. The result is shown in fig. 57 together with the older low temperature absorption spectra. There is an appreciable shift and a broadening of the edge by almost a factor of 2. The width of the edge is plotted against the rms lattice displacement δR as taken from the neutron scattering data by SMITH et al. [1968] in fig. 58. A linear dependence of the width on δR with a slope of 1.3 eV/Å gives a good fit to the data points. Only the two low temperature points are a little higher. This result shows quite convincingly that most of the width of the Li K edge is a phonon induced effect. Which o of the mechanism proposed in section 7.3 is causing this broadening cannot be decided. Our result is in good agreement with the theoretical estimates of McALLISTER [1969] and of DOW et al. [1973] . At 4 K the main part of the edge width will be caused by zero-point phonons. The small additional width could in principle be the many-body effect or an Auger width. The many-body effect therefore does not appear to be the dominant factor shaping the Li K edge.

Acknowledgement

The author is grateful to all of his colleagues at DESY for many enlightening discussions on the subjects of this article. In particular he is indebted to B. Sonntag for a critical reading of the manuscript and helpful comments and suggestions. Special thanks go to E. Thumann for the typing of this manuscript and to V. Fischer, W. Knaut, K. Köhler and D. Stanusch for preparing the figures and to W. Eberhardt, E.E. Koch, H. Petersen, P. Rabe, and H.W. Wolff for pointing out errors in the manuscript and for making useful suggestions.

References

ABELÈS, F., ed., 1966, Proceedings of the conference on Optical Properties and Electronic Structure of Metals and Alloys (North-Holland, Amsterdam)

ABELÈS, F. and M.L. THÈYE, 1966, Surface Sci. 5, 325

AGARWAL, B.K. and M.P. GIVENS, 1957, Phys.Rev. 107, 62

AITA, O. and T. SAGAWA, 1969, J.Phys.Soc. Japan 27, 164

ALLOTEY, F.K., 1967, Phys.Rev. 157, 467

ALTARELLI, M., D.L. DEXTER and H.M. NUSSENZVEIG, 1972, Phys.Rev. B6, 4502

AMUSIA, M.Ya., 1974, in: Koch, E.E., R. Haensel, C. Kunz eds., Proceedings of the IV. Int. Conf. on Vacuum Ultraviolet Radiation Physics, Hamburg, July 1974 (Pergamon/Vieweg, Braunschweig) p. 205

ANDERSON, P.W., 1967, Phys.Rev.Lett. 18, 1049

ASHLEY, C.A. and S. DONIACH, 1974, submitted to Phys.Rev. B

AUSMAN, G.A. and A.J. GLICK, 1969, Phys.Rev. 183, 687

AXELROD, N.N. and M.P. GIVENS, 1960, Phys.Rev. 120, 1205

AZAROFF, L.V., 1963, Rev.Mod.Phys. 35, 1012

BALZAROTTI, A., A. BIANCONI and E. BURATTINI, 1974, Phys.Rev. B9, 5003

BEARDEN, A.J. and A.F. BURR, 1967, Rev.Mod.Phys. 39, 78

BERGERSEN, B., P. JENA and T. McMULLEN, 1974, preprint

BERGERSEN, B., T. McMULLEN and J.P. CARBOTTE, 1971, Can.J.Phys. 49, 3155

BORN, M. and E. WOLF, 1959, Principles of Optics (Pergamon, London) p. 36

BREWER, L., 1971, J.Opt.Soc.Am. 61, 1101

BROWN, F.C., 1974, Ultraviolet Spectroscopy of Solids with the Use of Synchrotron Radiation. In: Ehrenreich, H., F. Seitz and D. Turnbull eds. Vol. 29, Solid State Physics (Academic Press, New York, London) p. 1

BROWN, F.C., C. GÄHWILLER and A.B. KUNZ, 1971, Solid State Commun. 7, 597

CANFIELD, L.R. and G. HASS, 1965, J.Opt.Soc.Am. 55, 61

CODLING, K., 1973, Applications of Synchrotron Radiation, Rep.Progr.Phys. 36, 54

CODLING, K. and R.P. MADDEN, 1968, Phys.Rev. 167, 587

COMBET FARNOUX, F., 1969, J. Physique 30, 521

COMBET FARNOUX, F., 1974, in Åberg, T., E. Källne, and R. Manne eds., Proceedings of the Int. Conf. on X-Ray Processes in Matter, Otaniemi, Finland (Physica Fennica, Vol. 9, Suppl. S1) p. 80

COMBET FARNOUX, F. and Y. HÉNO, 1967, Compt.Rend. 264B, 138

COMBET FARNOUX, F. and M. LAMOUREUX, 1974, in Koch, E.E., R. Haensel, C. Kunz eds., Proceedings of the IV. Int. Conf. on Vacuum Ultraviolet Radiation Physics, Hamburg, July 1974 (Pergamon/Vieweg, Braunschweig) p. 89

CONDON, E.U. and G.H. SHORTLEY, 1970, The Theory of Atomic Spectra (Cambridge University Press, Cambridge)

CONNOLLY, J.W.D., 1970, Int.J. Quantum Chem. S 3, 807

CONNOLLY, J.W.D. and K.H. JOHNSON, 1971, in: Bennett, L.H. ed., Electronic Density of States (NBS Spec.Publ. 323, Washington) p. 19

COOPER, J.W., 1962, Phys.Rev. 128, 681

COOPER, J.W., 1969, private communication

CRISP, R.S., 1972, Phil. Mag. 25, 167

CRISP, R.S. and S.E. WILLIAMS, 1960, Phil. Mag. 5, 525

CUKIER, M., P. DHEZ, F. WUILLEUMIER, P. JAEGLÈ, M. LAMOUREUX and F. COMBET FARNOUX, 1974, in Koch, E.E., R. Haensel, C. Kunz eds., Proceedings of the IV. Int. Conf. on Vacuum Ultraviolet Radiation Physics, Hamburg, July 1974 (Pergamon/Vieweg, Braunschweig) p. 102

DAMANY, H., G. MEHLMAN and J. ROMAND, 1974, in Koch, E.E., R. Haensel, C. Kunz eds., Proceedings of the IV. Int. Conf. on Vacuum Ultraviolet Radiation Physics, Hamburg, July 1974 (Pergamon/Vieweg, Braunschweig) p. 720

DANIELS, J., C. v.FESTENBERG, H. RAETHER, and K. ZEPPENFELD, 1970, in: Höhler, G. ed., Springer Tracts in Modern Physics, Vol. 54 (Springer, Berlin, New York, Heidelberg) p. 77

DEHMER, J.L. and A.F. STARACE, 1972, Phys.Rev. B5, 1792

DEHMER, J.L., A.F. STARACE, U. FANO, J. SUGAR and J.W. COOPER, 1971, Phys.Rev.Letters 26, 1521

DIETRICH, H. and C. KUNZ, 1972, Rev.Sci.Instrum. 43, 434

DIETZ, R.E., E.G. McRAE, Y. YAFET and C.W. CALDWELL, 1974a, in Koch, E.E., R. Haensel, C. Kunz eds., Proceedings of the IV. Int. Conf. on Vacuum Ultraviolet Radiation Physics, Hamburg, July 1974 (Pergamon/Vieweg, Braunschweig), p. 472

DIETZ, R.E., E.G. McRAE, Y. YAFET and C.W. CALDWELL, 1974b, Phys.Rev.Lett. 33, 1372

DONIACH, S. and M. SUNJIC, 1970, J.Phys. C: Proc. Phys. Soc., London 3, 285

DONIACH, S., P.M. PLATZMAN and J.T. YUE, 1971, Phys.Rev. B4, 3345

DOW, J.D., 1973, Phys.Rev.Letters 31, 1132

DOW, J.D., 1974a, in Koch, E.E., R. Haensel, C. Kunz eds., Proceedings of the IV. Int. Conf. on Vacuum Ultraviolet Radiation Physics, Hamburg, July 1974 (Pergamon/Vieweg, Braunschweig) p. 649

DOW, J.D., 1974b, to be published

DOW, J.D. and D.L. SMITH, 1973, J.Phys. F: Metal Phys. 3, L001

DOW, J.D. and B.F. SONNTAG, 1973, Phys.Rev. Letters 31, 1461

DOW, J.D., J.E. ROBINSON and T.R. CARVER, 1973, Phys.Rev.Letters 31, 759

DOW, J.D., J.E. ROBINSON, J.H. SLOWIK and B.F. SONNTAG, 1974a, Phys.Rev. B10, 432

DOW, J.D., D.L. SMITH and B.F. SONNTAG, 1974b, Phys.Rev. B10, 3092

EDERER, D.L., 1964, Phys.Rev.Letters 13, 760

EHRENREICH, H. and H.R. PHILIPP, 1962, Phys.Rev. 128, 1622

EJIRI, A., S. YAMAGUCHI, M. SARUWATARI, M. YOKOTA, K. INAYOSHI and G. MATSUOKA, 1970, Opt. Commun. 1, 349

FABIAN, D.J. ed, 1968, Soft X-Ray Band Spectra and the Electronic Structure of Metals and Materials, (Academic Press, London and New York)

FADLEY, C.S. and D.A. SHIRLEY, 1970, Phys.Rev. A2, 1109

FANO, U., 1961, Phys.Rev. 124, 1866

FANO, U., 1974, in Koch, E.E., R. Haensel, C. Kunz eds., Proceedings of the IV. Int. Conf. on Vacuum Ultraviolet Radiation Physics, Hamburg, July 1974 (Pergamon/Vieweg, Braunschweig) p. 84

FANO, U. and J.W. COOPER, 1968, Rev.Mod.Phys. 40, 441

FANO, U. and J.W. COOPER, 1969, Rev.Mod.Phys. 41, 724

FANO, U. and C.M. LEE, 1973, Phys.Rev.Letters 31, 1573

FERRELL, R.A., 1969, Phys.Rev. 186, 399

FOMICHEV, V.A., 1967, Sov.Phys.-Solid State 8, 2312

FOMICHEV, V.A., T.M. ZIMKINA, S.A. GRIBOVSKII and I.I. ZHUKOVA, 1967, Fiz.Tverd. Tela 9, 1490 (Sov.Phys.-Sol.State 9, 1163).

FRANCESCHETTI, D.R., 1974, in Koch, E.E., R. Haensel, C. Kunz eds., Proceedings of the IV. Int. Conf. on Vacuum Ultraviolet Radiation Physics, Hamburg, July 1974 (Pergamon/Vieweg, Braunschweig) p. 663

FRANCESCHETTI, D.R. and J.D. DOW, 1974, J.Phys. F4, L 151

FRIEDEL, J., 1969, Comments Solid State Phys. 2, 21

GÄHWILLER, C. and F.C. BROWN, 1970, Phys.Rev. B2, 1918

GERLACH, R.L., 1971, J.Vac.Sci.Tech., 8, 599

GIRAULT, P., S. SEIGNAC, M. PRIOL and S. ROBIN, 1968, Comt.Rend. B266, 688

GOWDIN, R.P. 1969, Synchrotron Radiation as a Light Source, in Höhler, G. ed., Springer Tracts in Modern Physics, Vol. 51 (Springer, Berlin, New York, Heidelberg) p. 1

GREENAWAY, D.L. and G. HARBEKE, 1968, Optical Properties and Band Structure of Semiconductors (Pergamon, London) p. 9

GUDAT, W., 1974, Thesis University Hamburg

GUDAT, W. and C. KUNZ, 1972a, phys.stat.sol. (b) 52, 433

GUDAT, W. and C. Kunz, 1972b, Phys.Rev. Letters 29, 169

GUDAT, W. and C. KUNZ, 1973, in: Faessler, A. and G. Wiech, eds. Proceedings of the International Symposium, X-Ray Spectra and Electronic Structure of Matter, München, September 1972, Vol. I (München) p. 131

GUDAT, W. and C. Kunz, 1975, to be published

GUDAT, W., J. KARLAU and C. KUNZ, 1973, in Faessler, A. and G. Wiech, eds., Proceedings of the International Symposium, X-Ray Spectra and Electronic Structure of Matter, München, September 1972, Vol. I (München) p. 205

GUDAT, W., C. KUNZ and J. KARLAU, 1974, Appl. Optics 13, 1412

HAENSEL, R. and C. Kunz, 1967, Z. Angew. Physik 23, 276

HAENSEL, R., C. KUNZ, T. SASAKI and B. SONNTAG, 1968, Appl.Opt. 7, 301

HAENSEL, R., G. KEITEL, P. SCHREIBER, B. SONNTAG and C. KUNZ, 1969a, Phys.Rev. Letters 23, 528

HAENSEL, R., C. KUNZ, T. SASAKI and B. SONNTAG, 1969b, J.Appl.Phys. 40, 3046

HAENSEL, R., K. RADLER, B. SONNTAG and C. KUNZ, 1969c, Sol.State Comm. 7, 1495

HAENSEL, R., G. KEITEL, B. SONNTAG, C. KUNZ and P. SCHREIBER, 1970a, phys.stat.sol. (a) 2, 85

HAENSEL, R., C. KUNZ, U. NIELSEN and B. SONNTAG, 1970b, unpublished

HAENSEL, R., P. RABE and B. SONNTAG, 1970c, Sol.State Comm. 8, 1845

HAGEMANN, H.-J., 1974, Internal Report DESY F41-74/4

HAGEMANN, H.-J., R. KLUCKER and U. NIELSEN, 1973, Internal Report DESY F41-73/10 (DESY, Hamburg)

HAGEMANN, H.-J., W. GUDAT and C. KUNZ, 1974a, Sol. State Comm. 15, 655

HAGEMANN, H.-J., W. GUDAT and C. KUNZ, 1974b, Report DESY SR-74/7 (DESY, Hamburg)

HAGEMANN, H.-J., W. GUDAT and C. KUNZ, 1975, to be published

HAM, F.S., 1962, Phys.Rev. 128, 2524

HEAVENS, O.S., 1964, in: Hass, G. and R.E. Thun, eds., Physics of Thin Films, Vol. 2 (Academic Press, New York) p. 193

HEDIN, L. and S. LUNDQVIST, 1969, Solid State Physics 23, 135

HEDIN, L., B.I. LUNDQVIST and S. LUNDQVIST, 1971, in: Bennett, L.H. ed., Electronic Density of States (NBS Spec.Publ. 323, Washington) p. 233

HERMAN, F. and S. SKILLMAN, 1963, Atomic Structure Calculations (Prentice Hall, Inc., Englewood Cliffs, N.J.)

HODGSON, J.N., 1954, Proc. Phys. Soc. (London) B67, 269

HODGSON, J.N.,1970, Optical Absorption and Dispersion in Solids (Chapmann and Hall, Ltd., London)

HOPFIELD, J.J., 1969, Comments Solid State Phys. 2, 40

HUBBELL, J.H., 1971, Atomic Data 3, 241-297

HÜFNER, S., G.K. WERTHEIM, R.L. COHEN and J.H. WERNICK, 1972, Phys.Rev.Lett. 28, 488

HÜFNER, S., G.K. WERTHEIM, D.N.E. BUCHMANN and K.W. WEST, 1974, Phys.Lett. 46A, 420

IRANI, G.B., T. HUEN and T. WOOTEN, 1971, J.Opt.Soc.Am. 61, 128

JAEGLÉ, P. and G. MISSONI, 1966, Compt.Rend. 262, 71

JAEGLÉ, P., G. MISSONI and P. DHEZ, 1967, Phys.Rev.Lett. 18, 887

JAEGLÉ, P., F. COMBET FARNOUX, P. DHEZ, M. CREMONESE and G. ONORI, 1969, Phys.Rev. 188, 30

JOHNSON, P.B. and R.W. CHRISTY, 1972, Phys.Rev. B6, 4370

KAPOOR, Q.S., L.M. WATSON, D. HART and D.J. FABIAN, 1972, Sol. State Comm. 11, 503

KIRKPATRICK, S., B. VELICKÝ and H. EHRENREICH, 1970, Phys.Rev. B1, 3250

KLUCKER, R. and U. NIELSEN, 1973, Computer Phys. Comm. 6, 187

KOCH, E.E., R. HAENSEL and C. KUNZ, eds., 1974, Proceedings of the IV. Int. Conf. on Vacuum Ultraviolet Radiation Physics, Hamburg, July 1974 (Pergamon/ Vieweg, Braunschweig)

KOSUCH, N., G. WIECH and A. FAESSLER, 1974, in Koch, E.E., R. Haensel, C. Kunz, eds., Proceedings of the IV. Int. Conf. on Vacuum Ultraviolet Radiation Physics, Hamburg, July 1974 (Pergamon/Vieweg, Braunschweig) p. 398

KOTANI, A. and Y. TOYOZAWA, 1973a, J.Phys.Soc. Japan 35, 1073

KOTANI, A. and Y. TOYOZAWA, 1973b, J.Phys.Soc. Japan 35, 1082

KRONIG, R. de L., 1932, Z. Physik 75, 468

KUNZ, C., 1971, J. de Physique 32-C4, 180

KUNZ, C., 1973a, in: Marr, G.V. and I.M. Munro eds., International Symposium for Synchrotron Radiation Users, Daresbury, DNPL Report R26

KUNZ, C., 1973b, Comm. on Solid State Phys. 5, 31

KUNZ, C., 1974, in Koch, E.E., R. Haensel, C. Kunz eds., Proceedings of the IV. Int. Conf. on Vacuum Ultraviolet Radiation Physics, Hamburg, July 1974 (Pergamon/Vieweg, Braunschweig) p. 753

KUNZ, C., R. HAENSEL, G. KEITEL, P. SCHREIBER and B. SONNTAG, 1971, in: Bennett, L.H. ed (NBS Spec. Publ. ed. (NBS Spec. Publ. 323 Washington) p. 275

KUNZ, C., H. PETERSEN and D.W. LYNCH, 1974, Phys.Rev. Letters 33, 1556

LANDOLT BÖRNSTEIN, 1955, Vol. I/4, Atom- und Molekularphysik, ed. Hellwege, K.H. (Springer, Berlin, Göttingen, Heidelberg) p. 772

LANG, N.D. and H. EHRENREICH, 1968, Phys. Rev. 168, 605

LEYSER, E., 1972, Diplomarbeit University Hamburg

LINDAU, I. and W.E. SPICER, 1974, J. Electr. Spectr. 3, 409

LONGE, P., 1973, Phys.Rev. B8, 2572

LOUCKS, T.L., 1964, unpublished

LOUCKS, T.L. and P.H. CUTLER, 1964, Phys.Rev. 133, A819

LUKIRSKII, A.P., O.A. ERSHOV, T.M. ZIMKINA and E.P. SAVINOV, 1966, Sov.Phys.-Solid State 8, 1422

MADDEN, R.P., 1974, in: Azaroff, L.V. ed., X-Ray Spectroscopy, International Series in Pure and Applied Physics (McGraw-Hill, New York) p. 338

MADDEN, R.P. and K. CODLING, 1967, Instrumental Aspects of Synchrotron XUV Spectroscopy, Applied Opt. 6, 31

MAHAN, G.D., 1967, Phys.Rev. 163, 612

MAHAN, G.D., 1974a, Many-Body Effects on X-Ray Spectra of Metals, in: Ehrenreich, H., F. Seitz, and D. Turnbull, eds., Solid State Physics, Vol. 29 (Academic Press, New York and London) p. 75

MAHAN, G.D., 1974b, in Koch, E.E., R. Haensel, C. Kunz eds., Proceedings of the IV. Int. Conf. on Vacuum Ultraviolet Radiation Physics, Hamburg, July 1974 (Pergamon/Vieweg, Braunschweig) p. 635

MANSON, S.T. and J.W. COOPER, 1968, Phys.Rev. 165, 126

MARR, G.V. and I.H. MUNRO eds. 1973, International Symposium for Synchrotron Radiation Users, Daresbury, DNPL Report R26

MARR, G.V., J.H. MUNRO and J.C.C. SHARP, 1972, Synchrotron Radiation a Bibliography, Report DNPL/R24 (Daresbury Nuclear Physics Laboratory)

MARR, G.V., I.H. MUNRO and J.C.C. SHARP, 1974, Synchrotron Radiation a Bibliography, Supplement August 72 to Febr. 74, Report DL/TM 127 (Daresbury Nuclear Physics Laboratory)

MATHEWSON, A.G. and H.P. MYERS, 1972, Phil.Mag. 25, 853

McALLISTER, A.J., 1969, Phys.Rev. 186, 595

McGUIRE, E.J., 1968, Phys.Rev. 175, 20

McGUIRE, E.J., 1970, Sandia Laboratories Research Report No. SC-RR-721

MOTT, N.F., 1964, Adv.Phys. 13, 325

MYERS, H.P., L. WALLDÉN and Å. KARLSSON, 1968, Phil.Mag. 18, 725

NAKAI, S., M. NAKAMORI, H. TOMITA, K. TSUTSUMI, M. NAKAMURA and C. SUIGIURA, 1974, Phys.Rev. B9, 1870

NEDDERMEYER, H., 1973a, in D.J. Fabian and L.M. Watson eds., Band Structure Spectroscopy of Metals and Alloys (Academic Press, London) p. 62

NEDDERMEYER, H., 1973b, Phys.Lett. 44A, 181

NEDDERMEYER, H., 1974, in Koch, E.E., R. Haensel, C. Kunz eds., Proceedings of the IV. Int. Conf. on Vacuum Ultraviolet Radiation Physics, Hamburg, July 1974 (Pergamon/Vieweg, Braunschweig) p. 665

NIELSEN, U., 1973, Int. Report, DESY F41-73/4 (DESY, Hamburg)

NILSSON, P.-O., 1968, Appl.Opt. 7, 435

NOZIERES, P. and C.T. De DOMINICIS, 1969, Phys.Rev. 178, 1097

O'BRYAN, H.M., 1940, Phys.Rev. 57, 995

O'BRYAN, H.M. and H.W.B. SKINNER, 1931, Phys.Rev. 38, 1797

OLSON, C.G., M. PIACENTINI and D.W. LYNCH, 1974, to be published

PARRATT, L.G., 1959, Rev.Mod.Phys. 31, 616

PETERSEN, H. and C. KUNZ, 1974, in Koch, E.E., R. Haensel, C. Kunz eds., Proceedings of the IV. Int. Conf. on Vacuum Ultraviolet Radiation Physics, Hamburg, July 1974 (Pergamon/Vieweg, Braunschweig) p. 587

PETERSEN, H. and C. Kunz, 1975, to be published

PHILIPP, H.R. and H. EHRENREICH, 1964, J.Appl.Phys. 35, 1416

PINES, D., 1963, Elementary excitations in solids (Benjamin, New York, Amsterdam) p. 200

RABE, P., 1970, Internal Report DESY, F41-70/3 (DESY, Hamburg)

RABE, P., 1974, Internal Report DESY, F41-74/2 (DESY, Hamburg)

RABE, P., K. RADLER and H.-WOLFF, 1974, in Koch, E.E., R. Haensel, C. Kunz eds., Proceedings of the IV. Int. Conf. on Vacuum Ultraviolet Radiation Physics, Hamburg, July 1974 (Pergamon/Vieweg, Braunschweig) p. 247

RITSKO, J.J., S.E. SCHNATTERLY and P.C. GIBBONS, 1974a, Phys.Rev.Letters 32, 671

RITSKO, J.J., S.E. SCHNATTERLY and P.C. GIBBONS, 1974b, Phys.Rev. B to be published

SAGAWA, T., Y. IGUCHI, M. SASANUMA, A. EJIRI, S. FUJIWARA, M. YOKOTA, S. YAMAGUCHI, M. NAKAMURA, T. SASAKI and T. OSHIO, 1966, J.Phys.Soc. Japan 21, 2602

SAMSON, J.A.R., 1967, Techniques of Vacuum Ultraviolet Spectroscopy (John Wiley, New York, London, Sidney)

SASAKI, T. and A. EJIRI, 1966, in Abelés, F. ed., Proceedings of the Conference on Optical Properties and Electronic Structure of Metals and Alloys (North Holland, Amsterdam) p. 417

SAYERS, D.E., F.W. LYTLE and E.A. STERN, 1970, in: Henke, B.L., J.B. Newkirk and G.R. Mallett, eds., Advances in X-Ray Analysis, Vol. 13 (Plenum Press, New York) p. 248

SAYERS, D.E., E.A. STERN and F.W. LYTLE, 1971, Phys.Rev.Lett. 27, 1204

SCHOTTE, K.D. and U. SCHOTTE, 1969, Phys.Rev. 182, 479

SENEMAUD, C. and M.T. LIMA, 1973, in: Faessler, A. and G. Wiech, eds., Proceedings of the International Symposium, X-Ray Spectra and Electronic Structure of Matter, München, September 1972, Vol. I (München) p. 216

SHEVCHIK, N.J., 1974, Phys.Rev.Lett. 33, 1336

SHIRAIWA, T., 1960, J.Phys.Soc. Japan 15, 240

SHIRAIWA, T., T. ISHIMURA and M. SAWADA, 1958, J.Phys.Soc. Japan 13, 847

SIEGBAHN, K., C. NORDLING, A. FAHLMAN, R. NORDBERG, K. HAMRIN, J. HEDMAN, G. JOHANSSON, T. BERGMARK, S.E. KARLSSON, I. LINDGREN, B. LINDBERG, 1967, Atomic, Molecular and Solid State Structure Studied by Means of Electron Spectroscopy (Almqvist and Wiksells, Uppsala)

SKINNER, H.W.B., 1940, Phil.Trans.Roy.Soc. London A239, 95

SKINNER, H.W.B. and J.E. JOHNSTON, 1937, Proc.Roy.Soc. A161, 420

SLOWIK, J.H., 1974, Phys.Rev. B10, 416

SLOWIK, J.H. and F.C. BROWN, 1972, Phys.Rev.Lett. 29, 934

SMITH, H.G., G. DOLLING, R.M. NICKLOW, P.R. VIJAYARAGHAVAN and M.K. WILKINSON, 1968, Proc. 4B IAEA Symposium on Neutron Inelastic Scattering, Copenhagen (International Atomic Energy Agency, Vienna) p. 149

SOKOLOV A.A. and J.M. TERNOV, 1968, Synchrotron Radiation (Pergamon Press, Oxford) 207 p. (translated from the Russian)

SONNTAG, B., 1969, Internal Report DESY-F41/1 (DESY, Hamburg)

SONNTAG, B.F., 1973, J.Phys. F: Metal Phys. 3, L255

SONNTAG, B., 1974, private communication

SONNTAG, B., R. HAENSEL and C. KUNZ, 1969, Sol. State Comm. 7, 597

SOVEN, P., 1967, Phys.Rev. 156, 809

STARACE, A.F., 1972, Phys.Rev. B5, 1773

STERN, E.A., 1974, Phys.Rev. B10, 3027

STOCKS, G.M., R.W. WILLIAMS and J.S. FAULKNER, 1971, Phys.Rev. Letters 26, 253

SUGAR, J., 1972, Phys.Rev. B5, 1785

SWANSON, N. and K. CODLING, 1968, J.Opt.Soc.Amer. 58, 1192

SWITENDICK, A.C., 1971, in: Bennett, L.H., ed., Electronic Density of States (NBS Spec. Publ. 323, Washington) p. 297

SWITENDICK, A.C. and A. NARATH, 1969, Phys.Rev.Letters 22, 1423

TERRELL, J.H., 1966, Phys.Rev. 149, 526

TOLL, J.S., 1956, Phys.Rev. 104, 1760

TOMBOULIAN, D.H., 1957, in: Flügge, S., ed., Handbuch der Physik, Vol. 30 (Springer, Berlin, Göttingen, Heidelberg), p. 246

TOMBOULIAN, D.H., D.E. BEDO and W.M. NEUPERT, 1957, J.Phys.Chem. Solids, 3, 282

WATSON, L.M., Q.S. KAPOOR and D. HART, 1973, in Faessler, A. and G. Wiech, eds., Proceedings of the International Symposium, X-Ray Spectra and Electronic Structure of Matter, München, September 1972, Vol. I (München) p. 135

WATSON, R.E. and M.L. PERLMAN eds., 1972, Study Symposium on Research Applications of Synchrotron Radiation, Brookhaven National Lab. 25-28 Sept. 1972, BNL Report 50 381

WEHENKEL, C. and B. GAUTHÉ, 1974a, in: Koch, E.E., R. Haensel, C. Kunz, eds., Proceedings of the IV. Int. Conf. on Vacuum Ultraviolet Radiation Physics, Hamburg, July 1974 (Pergamon/Vieweg, Braunschweig) p. 455

WEHENKEL, C. and B. GAUTHÉ, 1974b, phys.stat.sol. (b) 64, 515

WEHENKEL, C. and B. GAUTHÉ, 1974c, Sol.State Comm. 15, 555

WENDIN, G., 1973, Phys.Lett. 46A, 119

WENDIN, G., 1974, in Koch, E.E., R. Haensel, C. Kunz, eds., Proceedings of the IV. Int. Conf. on Vacuum Ultraviolet Radiation Physics, Hamburg, July 1974 (Pergamon/Vieweg, Braunschweig) p. 225

WOLFF, H.-W. K. RADLER, B. SONNTAG and R. HAENSEL, 1972, Z. Physik 257, 353

WYBOURNE, B.G., 1965, Spectroscopic Properties of Rare Earths, (Interscience Publishers - John Wiley, New York, London, Sydney) p. 3

YAMAGUCHI, S., S. SATO, E. ISHIGURO, O. AITA, T. HANYU and H. KOIKE, 1971, Nakai, Y. ed. Proc. III Int. Conf. on VUV Rad.Phys. (Tokyo) Contribution 2a C2-4

YUE, J.T. and S. DONIACH, 1973, Phys.Rev. B8, 4578

ZACHARIAS, P., 1973, Opt.Comm. 8, 142

ZIMKINA, T.M., V.A. FOMICHEV, S.A. GRIBOVSKII, and I.I. ZHUKOVA, 1967, Fiz.Tverd. Tela 9, 1447 (Sov. Phys.-Sol. State 9, 1128)

ZORNBERG, E.I., 1970, Phys.Rev. B1, 244

TABLE 1.

Synchrotrons (SY) or storage rings (ST) used (or considered) as light sources
E = particle energy, R = magnet radius, I = max. current (during acceleration for SY), ε_c = critical photon energy

Name	Location	Type	E(GeV)	R(m)	I(mA)	ε_c(eV)	Remarks
	USA						
SURF I	NBS Washington	SY	.17	.83	1	13	closed down
SURF II	NBS Washington	ST	.24	.83	50	37	dedicated, teste
TANTALUS I	PLS Stoughton/Wisc.	ST	.24	.64	20	48	dedicated
TANTALUS II	PLS Stoughton/Wisc.	ST	1.76	4.5	100	2690	proposed, dedica
SPEAR (II)	SLAC Stanford/Calif.	ST	4.0	12.7	60	11200	
CEA	Cambridge/Mass.	SY/ST	6.0	26.0	30	18400	closed down
CORNELL III	Ithaca/N.Y.	SY	12	∿120	2	32000	
PEP	SLAC Stanford/Calif.	ST	15	170	100	44000	proposed
	GERMANY						
BONN I	Univ. Bonn	SY	.5	1.7	30	163	
BONN II	Univ. Bonn	SY	2.5	7.65	30	4530	
DESY	DESY Hamburg	SY	7.5	31.7	30	29500	
DORIS	DESY Hamburg	ST	3.5	12.12	900	7850	
PETRA	DESY Hamburg	ST	19	200	90	75500	proposed
	GREAT BRITAIN						
NINA I	DNPL Daresbury	SY	5.0	20.8	50	13300	
NINA II	DNPL Daresbury	ST	2.0	5.55	1000	3200	proposed, dedica
EPIC	Rutherford Lab.	ST	14	171.89	22	35000	proposed
	FRANCE						
ACO	Orsay	ST	.55	1.11	35	333	
DCI	Orsay	ST	1.8	3.82	400	3390	under constructi
	JAPAN						
INS-SOR I	INS-Tokyo	SY	1.3	4.0	60	1220	
INS-SOR II	INS-Tokyo	ST	.3	1.1	100	54	dedicated, teste
PHOT-FACT		ST	2.5	∿8		∿4300	proposed
	SOVIET UNION						
C-60	Lebedev Moscow	SY	.68	2	10	349	
PACHRA	Krasnaja Pachra near Moscow	SY/ST	1.3	4	10/300	1220	under constructi
ARUS	Erewan	SY	6.0	24.65	22	19500	
VEPP-3	Novosibirsk	ST	2.5	6.15	∿100	5600	
	ITALY						
FRASCATI	Frascati	SY	1.1	3.6	14	821	
ADONE	Frascati	ST	1.5	5.0	60	1500	no radiation lal

TABLE 2.

Summary of numerical evaluation of sum rules. n_o = number of conduction electrons, $\Delta n_{cond} = B \int_0^{\omega_{core}} \omega\, \varepsilon_2(\omega) d\omega$, ω_{core} being the frequency of first onset of core transitions, $n_K = c\, B \int_{\omega_k}^{\infty} \mu(\omega) d\omega$, ω_k being the onset of K-transitions, Z = total number of electrons, $n_{eff}(\varepsilon_2)$, $n_{eff}(\mu)$, $n_{eff}(\mathrm{Im}\varepsilon^{-1})$ are the limiting values ($\omega_o \to \infty$) of eqs. 13,14,15 respectively. The absolute values and the deviations from Z in percent are given. (After HAGEMANN et al. [1974b]).

	n_o	Δn_{cond}	Δn_k	Z	$n_{eff}(\varepsilon_2)$	$n_{eff}(\mu)$	$n_{eff}(\mathrm{Im}\hat{\varepsilon}^{-1})$
Mg	2	2.2	1.3	12	12.2 +1.7 %	12.6 +5 %	12.6 + 5 %
Al	3	2.8	1.5	13	13.4 +3 %	13.6 + 4.5%	13.6 +4.5 %
Cu	1	0.6	1.2	29	27.6 -5 %	27.6 -5 %	27.6 -5 %
Ag	1	0.9	1.3	47	47.5 +1 %	47.7 +1.5 %	47.6 +1.3 %
Au	1	0.9	1.3	79	78.9 -0.1 %	79.0 ±0 %	79.0 ±0 %
Bi			1.25	83	82.3 -1 %	82.3 -1 %	82.3 -1 %

TABLE 3

Calculated absorption maxima and relative theoretical oscillator strength gf for La^{3+} and Ce^{3+} near the 4d edges. Positions of peaks (in eV) are given whose gf values are $\geq$ 5 % of maximum peak in regions of low and high absorption respectively, the regions are separated by a dotted line. Measured peak positions (HAENSEL et al. [1970c]) appear in last column. (From SUGAR 1972).

Transition		E_{calc}	gf Rel.	E_{obs}
La^{3+} $4d^{10}$	$^1S_0$-			
$4d^9 4f$	$^3P_1$	97.2	1.0	96.9
	$^3D_1$	101.3	11.1	101.6
		...		(103.7)
	$^1P_1$	117.0	1993	117
Ce^{3+} $4d^{10}4f$	$^2F_{5/2}$-			
$4d^9 4f^2$	$(^3H)^4F_{3/2}$	101.8	0.2	101.25
	$(^1I)^2G_{7/2}$	103.5	0.9	103.48
	$(^3H)^4G_{5/2}$	103.7	0.5	
	$(^3H)^4G_{5/2}$	104.4	0.8	104.56
	$(^3H)^4G_{7/2}$	104.6	1.2	
	$(^1D)^2D_{5/2}$	105.4	1.4	
	$(^3F)^4G_{7/2}$	105.7	6.8	105.77
	$(^3F)^4G_{5/2}$	106.0	2.0	106.06
	$(^3F)^4F_{3/2}$	106.2	1.1	
	$(^3H)^4H_{7/2}$	106.6	0.5	
	$(^3F)^4H_{7/2}$	106.8	3.4	106.58
	$(^1G)^2D_{5/2}$	108.0	0.7	
	$(^3P)^4D_{3/2}$	108.2	2.2	108.06
	$(^3F)^4D_{7/2}$	108.3	0.8	
	$(^3F)\ D_{5/2}$	108.5	0.7	
	$(^3F)^4D_{7/2}$	108.8	1.3	108.93
	$(^3P)^4P_{3/2}$	109.5	1.6	109.70
	$(^3P)^4F_{7/2}$	109.8	2.0	
	$(^1D)^2P_{3/2}$	110.0	0.6	
	$(^3F)^4H_{7/2}$	110.1	10.4	110.36
	$(^1D)^2G_{7/2}$	111.7	4.6	111.52
		...		
	$(^3H)^2G_{7/2}$	120.4	1088	
	$(^3F)^2D_{3/2}$	124.4	781	
	$(^3F)^2D_{5/2}$	124.8	40	124.3
	$(^3H)^2F_{5/2}$	125.3	1215	
	$(^3H)^2F_{7/2}$	125.4	85	

TABLE 4

Position of edges and absorption maxima in the absorption spectra of Li, Be, Na, Mg, and Al. The fourth column gives the temperatures at which the tabulated energy positions were measured. (RT romm temperature, LNT liquid nitrogen temperature). (After HAENSEL et al. [1970a], however, Li K-edge and A corrected see text).

Metal	Maximum	Energy (eV)	Temperature
Li	K-edge	54.86 ± 0.15	LNT
	A	55.4 ± 0.2	LNT
	B	58 ± 0.5	LNT
	C	64 ± 0.5	LNT
Be	K-edge	112.1 ± 0.2	RT
	A	112.3 ± 0.2	RT
	B	113.65 ± 0.4	RT
	C	119 ± 0.5	RT
	D	122 ± 0.5	RT
	E	126 ± 0.5	RT
Na	L_3	30.68 ± 0.1	LNT
	A	30.74 ± 0.1	LNT
	L_2	30.84 ± 0.1	LNT
	B	30.88 ± 0.1	LNT
	C	32.5 ± 0.4	LNT
	D	35 ± 1	LNT
	E	48.5 ± 1	LNT
	F	65.5 ± 1	LNT
Mg	L_3	49.60 ± 0.1	LNT
	A	49.66 ± 0.1	LNT
	L_2	49.87 ± 0.1	LNT
	B	49.9 ± 0.1	LNT
	C	51.7 ± 0.2	RT
	D	52.9 ± 0.3	RT
	E	55.5 ± 0.3	RT
	F	58 ± 0.5	RT
	G	72 ± 0.5	RT
	H	82 ± 0.5	RT
	I	85 ± 0.5	RT
	J	89.5 ± 1	RT
Al	L_3	72.72	Calibration point
	A	72.8 ± 0.1	LNT
	L_2	73.15 ± 0.1	LNT
	B	73.25 ± 0.1	LNT
	C	74.9 ± 0.2	RT
	D	77.3 ± 0.2	RT
	E	84.3 ± 0.3	RT
	F	97 ± 1	RT
	G	113.5 ± 1	RT
	H	118 ± 0.5	RT
	I	124 ± 1	RT

TABLES 5.

Shift of the onset of Al $L_{2,3}$ absorption (after HAGEMANN et al. [1975] , HAGEMANN [1974]) and the onset of Al $L_{2,3}$ emission (after WATSON et al. [1973] , $AuAl_2$ after KAPOOR et al. [1972]).

material	shift of the onset (eV) absorption (±0.1 eV)	emission (±0.05 eV)
Al (onset)	72.6	72.76
V-Al 16 %	- 1.1	-1.25 (10 %)
V-Al 28 %	- 1.1	-1.10 (24 %)
V-Al 41 %	- 0.7	-0.95 (40 %)
VAl_3	- 0.4	-0.65
Fe-Al 11 %	- 1.0	--
FeAl	- 0.7	- 0.75
NiAl	- 0.3	- 0.55
$NiAl_3$	- 0.3	--
$CuAl_2$	+ 0.4	--
$PrAl_2$	- 0.6	--
$AuAl_2$	+ 0.3	+ 0.3

Figure Captions

Fig. 1 Absorption and emission spectroscopy in the density of states approximation. (From KUNZ [1973b].)

Fig. 2 Variation of binding energy for different atomic shells as a function of atomic number. The photon wavelengths at the excitation threshold are given.

Fig. 3 Absorption coefficient of Au as composed from different experiments (JAEGLE and MISSONI [1966], HAENSEL et al. [1968], GUDAT et al. [1973]) and one-electron atomic calculation (COMBET FARNOUX and HENO [1967], MANSON and COOPER [1968]. (From KUNZ [1973b].)

Fig. 4 Absorption from Pr 4d-4f transitions after HAENSEL et al. [1970] and calculation of multiplet lines after SUGAR [1972], the length of the lines is a measure of the theoretical intensity.

Fig. 5 Absorption coefficient from Na $L_{2,3}$ transitions showing the edge singularity after HAENSEL et al. [1969a, 1970a]. (From KUNZ [1973b].)

Fig. 6 Absorption coefficient at the Al-2p and the Ni-3p edges of NiAl by HAGEMANN et al. [1974] in comparison with a density of states calculation (dashed line) by CONNOLLY and JOHNSON [1971]. (From HAGEMANN et al. [1974a].)

Fig. 7 Geometry of synchrotron radiation emission. (From KUNZ [1974].)

Fig. 8 Angular distribution of intensity components with electrical vector parallel ($I_{\parallel}$) and normal ($I_{\perp}$) to the plane of the synchrotron, linear polarization, and circular polarization (from decomposition into left (I_L) and right (I_R) hand circularly polarized components: ψ according to fig. 7.

Fig. 9 Spectral distribution of intensity into a 2 cm x 2 cm wide aperture at the laboratory distance of 40 m from the source for the accelerator DESY and the storage rings DORIS (see table 1).

Fig. 10 Absorption coefficient of Cr in the region of 3p-3d transitions. The synchrotron radiation results of DESY (SONNTAG [1969] , SONNTAG et al. [1969]) are compared with results obtained with classical sources which have been scaled (TOMBOULIAN et al. [1957], AGARWAL and GIVENS [1957], AXELROD and GIVENS [1960], GIRAULT et al. [1968]). (From SONNTAG [1969] .)

Fig. 11 Arrangement of a Rowland monochromator at the DESY synchrotron. EO = electron orbit, V = vacuum valve, BS = beam shutter, VT = vacuum pipe, SH = sample holder, M = focusing mirror, ES = entrance slit, G = grating B = exit slit and detector, RA = rotating arm, Sh = shielding. (From HAENSEL et al. [1968] .)

Fig. 12 Fixed exit slit monochromator at the DESY laboratory, I monochromator with DM = drive mechanism, D = aperture diaphragm, M = plane mirror, G = grating, F = focusing mirror, GP and TVP vacuum pumps; II differential pumping stage; III UHV sample chamber with ES = exit slit. (After GUDAT [1974] .)

Fig. 13 Two-beam densitometer with rotating beam splitter; M_1, M_2 = plane mirrors, D_1, D_2 = detectors, S_1, S_2 = thin film samples. (After GUDAT et al. [1974].)

Fig. 14 Comparison of yield and absorption spectrum of Al. The yield is given as measured against an uncalibrated reference detector (see fig. 15). (After GUDAT [1974], GUDAT and KUNZ [1975].)

Fig. 15 Arrangement for yield-spectroscopy. The reference detector uses photoemission from the non-reflected part of the light. The electron detector is located behind the plane of this figure. (From GUDAT and KUNZ [1973].)

Fig. 16 Kramers-Kronig consistent reflectivity R and absorption coefficient μ (solid curves). Other results are shown a: EHRENREICH and PHILIPP [1962], b: CANFIELD and HASS [1965], c: HAENSEL et al. [1968]. (From HAGEMANN et al. [1974b].)

Fig. 17 Kramers-Kronig consistent real (ε_1) and imaginary (ε_2) part of the dielectric constant. Other result a: by MYERS et al. [1968]. (From HAGEMANN et al. [1974b]).

Fig. 18 Kramers-Kronig consistent real (n) and imaginary (k) part of the optical constant. Other result a: by JOHNSON and CHRISTY [1972]. (From HAGEMANN et al. [1974b].)

Fig. 19 Kramers-Kronig consistent energy loss function Im$-1/\varepsilon$. Experimental result a: DANIELS et al. [1970]. (From HAGEMANN et al. [1974b].)

Fig. 20 Check of sum rules yielding $n_{eff}(\omega)$, see text. (From HAGEMANN et al. [1974b].)

Fig. 21 Check on sum rules on $\mu(n-1)$ and on $(n-1)$. (From HAGEMANN et al. [1974b].)

Fig. 22 Effective potential V_{eff} according to eq. (23) for $\ell=3$ electrons in several atoms. (From MANSON and COOPER [1968].)

Fig. 23 Bi, core function $P_{4f}(r)$ (dashed), and continuum functions $\varepsilon=0$ (at threshold), $\varepsilon=11.5$ rydberg. The radial distance r is given in units of the Bohr radius. (From COMBET FARNOUX [1969].)

Fig. 24 Absorption cross section of Bi. Solid line: theory and dashed line: experiment by JAEGLE et al. [1969], dash-dotted: line experiment by HAENSEL et al. [1968]. (From JAEGLE et al. [1969].)

Fig. 25 Autoionization profiles according to eq. (28). (From FANO [1961].)

Fig. 26 Absorption spectra of light metals in the region of 1s transitions (Li, Be) and 2p transitions (Mg and Al). The Be spectrum is compared with a density of states calculation by LOUCKS [1974], the Al spectrum with an atomic calculation by COOPER [1969]. The yield spectrum of liquid Al after PETERSEN and KUNZ [1975] is also shown. Energy positions of peaks are listed in table 4. (After HAENSEL et al. [1970a].)

Fig. 27 Yield spectrum of solid and liquid Li. (After PETERSEN and KUNZ [1974].)

Fig. 28 Region above $L_{2,3}$ edges of Al (blow-up). μ = absorption spectrum after BALZAROTTI et al. [1974], Y = yield spectrum after GUDAT [1974], J_F = free electron density of states, J_C = density of states as calculated by CONNOLLY [1970].)

Fig. 29 Absorption cross section of atomic Na (solid line) after WOLFF et al. [1972] in comparison with metallic Na (dashed line, arbitrary units, after HAENSEL et al. [1970a]), and an atomic calculation by McGUIRE [1970]. (From WOLFF et al. [1972].)

Fig. 30 Comparison of an EXAFS calculation by RITSKO et al. [1974], with the absorption spectra in the region of $L_{2,3}$ transitions (HAENSEL et al. [1970]) and in the region of K transition (SENEMAUD and LIMA [1973].)

Fig. 31 Partial absorption coefficient μ^* according to eq. (29) of the Al $L_{2,3}$ transitions in several ordered phase alloys. (After HAGEMANN [1974].)

Fig. 32 Partial absorption coefficient μ^* (eq. (29)) of several alloys at the Al $L_{2,3}$ edge. The onset of the 2p transitions of pure Al is marked. (After HAGEMANN et al. [1974a].)

Fig. 33 Absorption coefficient of the noble metals Cu, Ag and Au showing the behavior of d-valence electron transitions. (After HAGEMANN et al. [1974b].)

Fig. 34 Overlap of continuum wavefunctions $P_\varepsilon(r)$ for two energies $\varepsilon_1 < \varepsilon_2$ with the core 4d function $P_i(r)$ to demonstrate change of sign of the matrix element R_{l+1} (schematic).

Fig. 35 Matrix element for d-f transitions R_{l+1} and total absorption cross section σ as a function of electron kinetic energy for Ag^+ and Cu^+. (From COOPER [1962].)

Fig. 36 Absorption coefficient of Bi in the region of 5d transitions. The sum orbit split edges and the delayed peak around 60 eV are clearly identified. (After HAGEMANN et al. [1974b].)

Fig. 37 Evolution and disappearance of the 4d-4f 'resonance' transitions from Sn^{50} to Lu^{71}. The region of fine structure below the onset of the large maxima is interpolated in this figure but is shown in fig. 38 in an expanded scale. (From ZIMKINA et al. [1967].)

Fig. 38 Fine-structures for 4d-4f transitions into bound states for the rare earths series. (After FOMICHEV et al. [1967].)

Fig. 39 Absorption coefficient for Pr and $PrAl_2$ (upper part). The lower part shows the partial absorption coefficient μ^* for Al in $PrAl_2$ after eq. (29). (From HAGEMANN [1974a].)

Fig. 40 Absorption behavior of Ba in the region of 4d-4f transitions for vapor and solid. The lines show the result of a Hartree-Fock calculation. The broad peak (theory) results from a many-body calculation by WENDIN [1973]. (After RABE et al. [1974].)

Fig. 41 Absorption spectra of 3p-3d transitions in the transition metal series Ti to Ni and Cu. The expected edge positions are marked after BEARDEN and BURR [1967]. (After SONNTAG et al. [1969].)

Fig. 42 Absorption coefficient at the 3p-3d threshold for several Mn-halides. (From NAKAI et al. [1974].)

Fig. 43 Absorption spectra of 5p-5d and 4f-5d transitions for the transition metal series Ta to Pt and Au. The expected edge positions are marked after SIEGBAHN et al. [1967]. (After HAENSEL et al. [1969c] and LEYSER [1970].)

Fig. 44 Transmittance of a Cu-Ni (1:1) alloy film (∿300 Å thick) and a Cu+Ni sandwich film separated by a carbon layer to prevent diffusion in the region of Ni 3p-3d transitions. In addition the transmittances of pure (∿150 Å thick) Cu and Ni films are shown. (From GUDAT and KUNZ [1972].)

Fig. 45 Absorption coefficient at the Fe and Ni 3p edges for several Al transition metal alloys in comparison with the pure transition metal spectra. (After HAGEMANN [1974].)

Fig. 46 Emission spectra of light metals after SKINNER [1940]. (From LANDOLT BÖRNSTEIN [1955].)

Fig. 47 Shape of the absorption edges of light metals after KUNZ et al. [1971]. The resolution is marked. The mirror-image of the Li emission spectrum as measured by AITA and SAGAWA [1969] was shifted for comparing with the absorption spectrum.

Fig. 48 Shielding of a suddenly created hole in space a) and in an energy picture b) (schematic).

Fig. 49 a) Side band of electron transitions near the Fermi level (fig. 48b)), to a discrete line spectrum in contact with an electron gas. b) Smearing of a one-electron absorption spectrum β because of the effect shown in part a) resulting in a spectrum η. γ shows the edge-singularity effect (schematic).

Fig. 50 The three processes contributing to the core-hole excitation spectrum of a metal. (After FRIEDEL [1969].)

Fig. 51 Edge exponents α_o for different metals plotted against r_s. The solid line is an interpolation, the dashed line is the result of a calculation using a self-consistent screening field. (From DOW et al. [1974].)

Fig. 52 Compatibility relationship (eq. (35)) for the exponents α_o and α_1. The circles give an evaluation of the data of NEDDERMEYER [1973a,b] by DOW [1974b], the points with error bars give a recent re-evaluation by NEDDERMEYER [1974]. (From NEDDERMEYER [1974].)

Fig. 53 Theoretical Li K absorption shape from eq. (30) assuming various values for B_o/B_1 assuming $\xi = 5$ eV, $\alpha_o = 0.46$, $\alpha_1 = -0.30$. (From SONNTAG [1963].)

Fig. 54 Li K absorption edge in Li_{1-x} Cu alloys. (From SONNTAG [1973].)

Fig. 55 Dependence of Li K edge as obtained from energy loss measurements on momentum transfer q. (From RITSKO et al. [1974b].)

Fig. 56 Predictions of theory eq. (30), the theoretical curve was convoluted with a broadening function in order to give a good fit at q=0. (From RITSKO et al. [1974b].)

Fig. 57 Li K edge at different temperatures. The curve at 4 K was obtained from absorption measurements by HAENSEL et al. [1970b], the other curves by yield spectroscopy. All the yield curves coincide with the dashed curve below 54.5 eV. (From KUNZ et al. [1974].)

Fig. 58 Li K edge width ΔW vs. rms lattice displacement δR as obtained from neutron scattering measurements by SMITH et al. [1968]. The dashed line is an interpolation. (From KUNZ et al. [1974].)

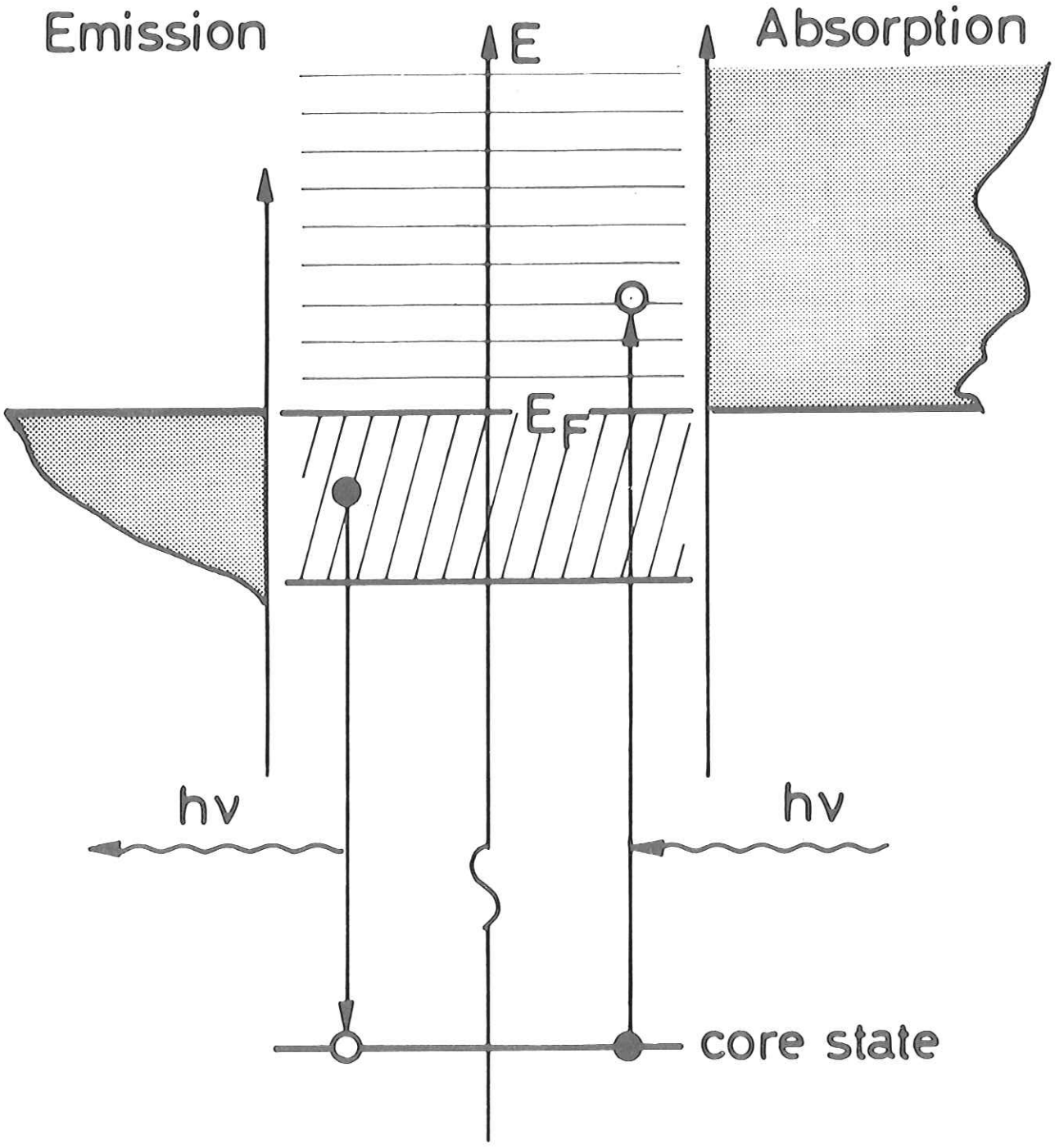

Fig. 1

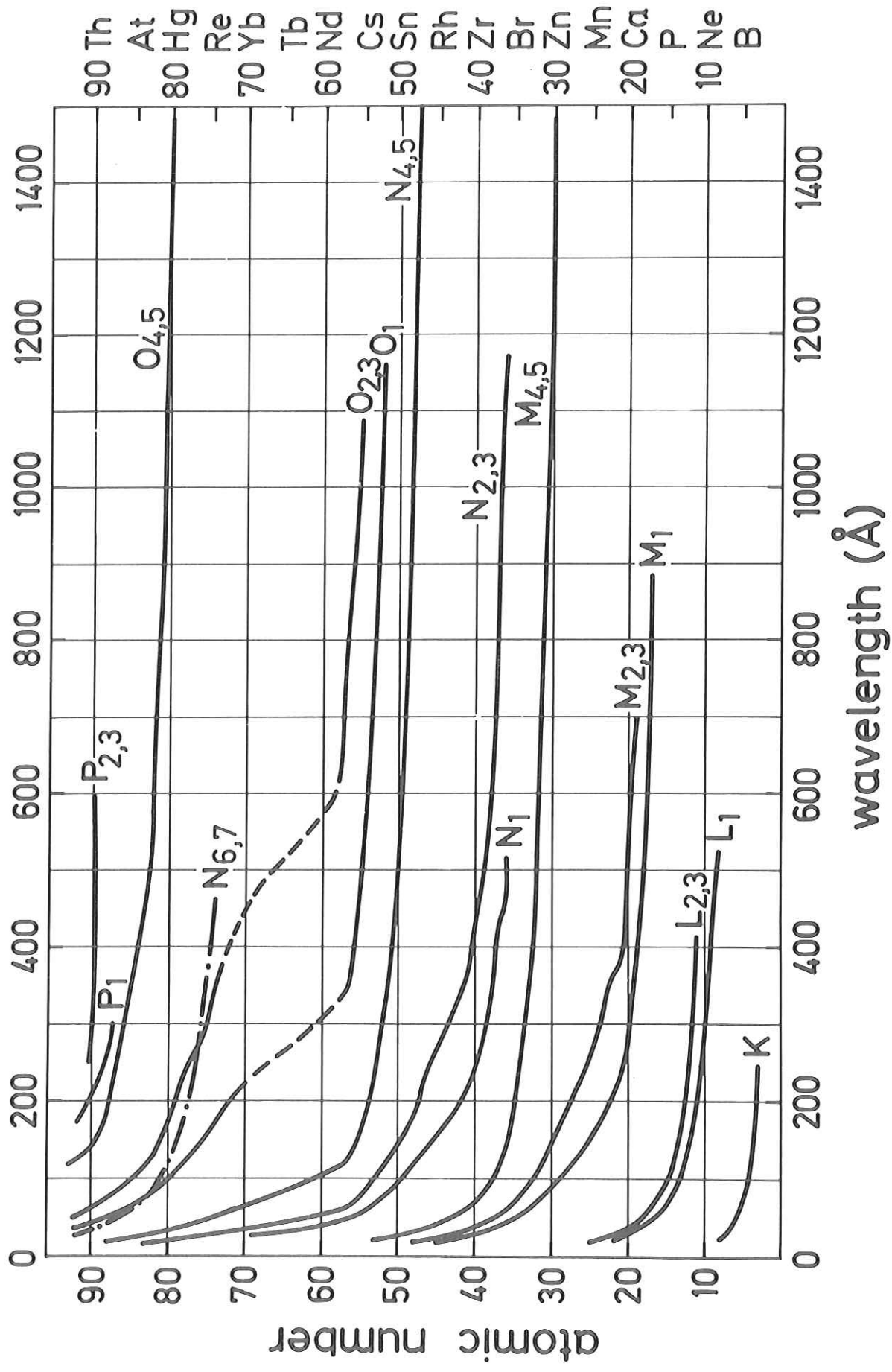
atomic number
wavelength (Å)
90 Th
At
80 Hg
Re
70 Yb
Tb
60 Nd
Cs
50 Sn
Rh
40 Zr
Br
30 Zn
Mn
20 Ca
P
10 Ne
B
0
200
400
600
800
1000
1200
1400
P2,3
P1
O4,5
N6,7
O2,3
O1
N4,5
N2,3
M4,5
N1
M2,3
M1
L2,3
L1
K

Fig. 2

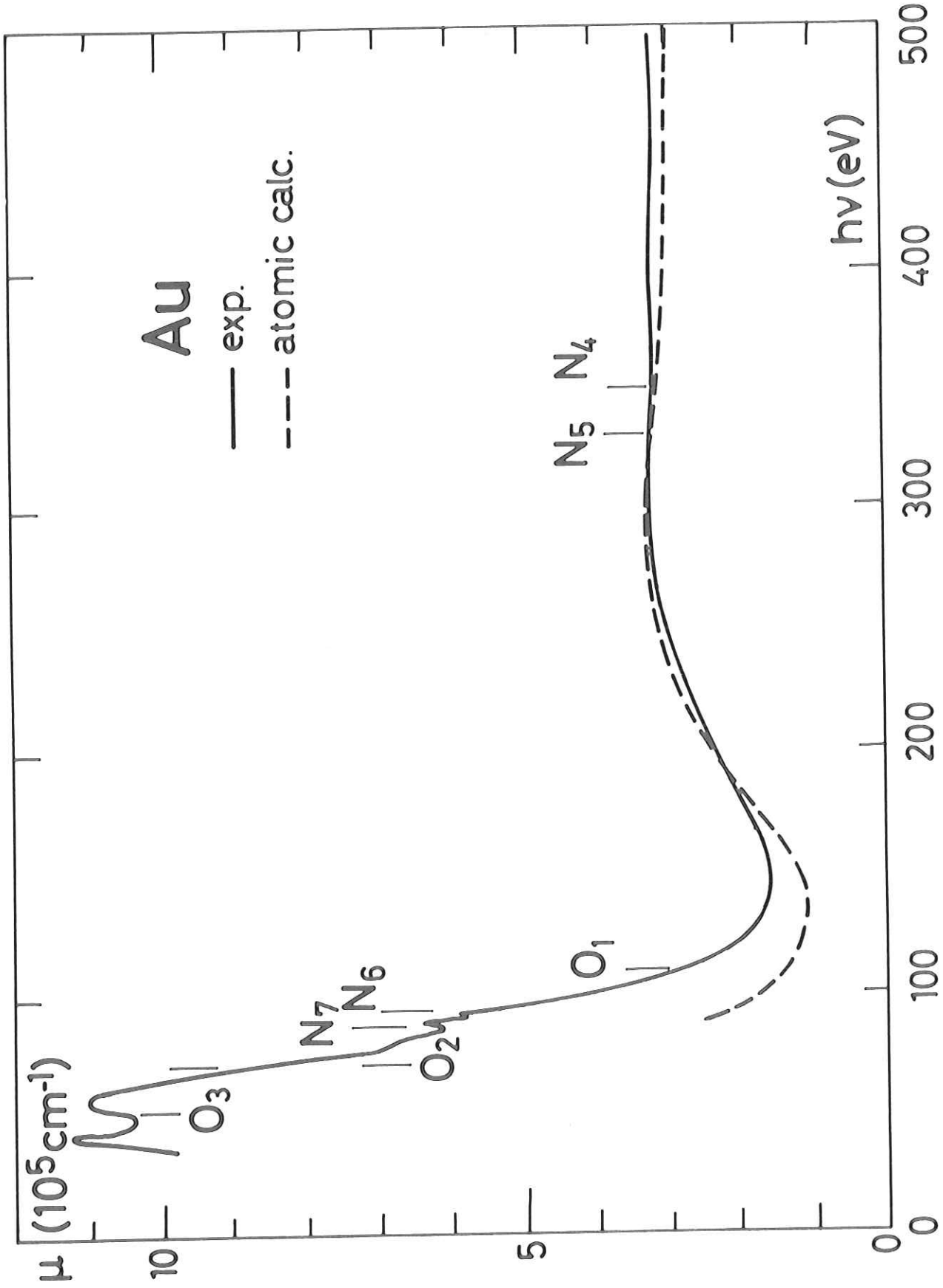
Au
exp.
atomic calc.
μ (10⁵cm⁻¹)
hν(eV)
O3
N7
N6
O2
O1
N5
N4
0
5
10
100
200
300
400
500

Fig. 3

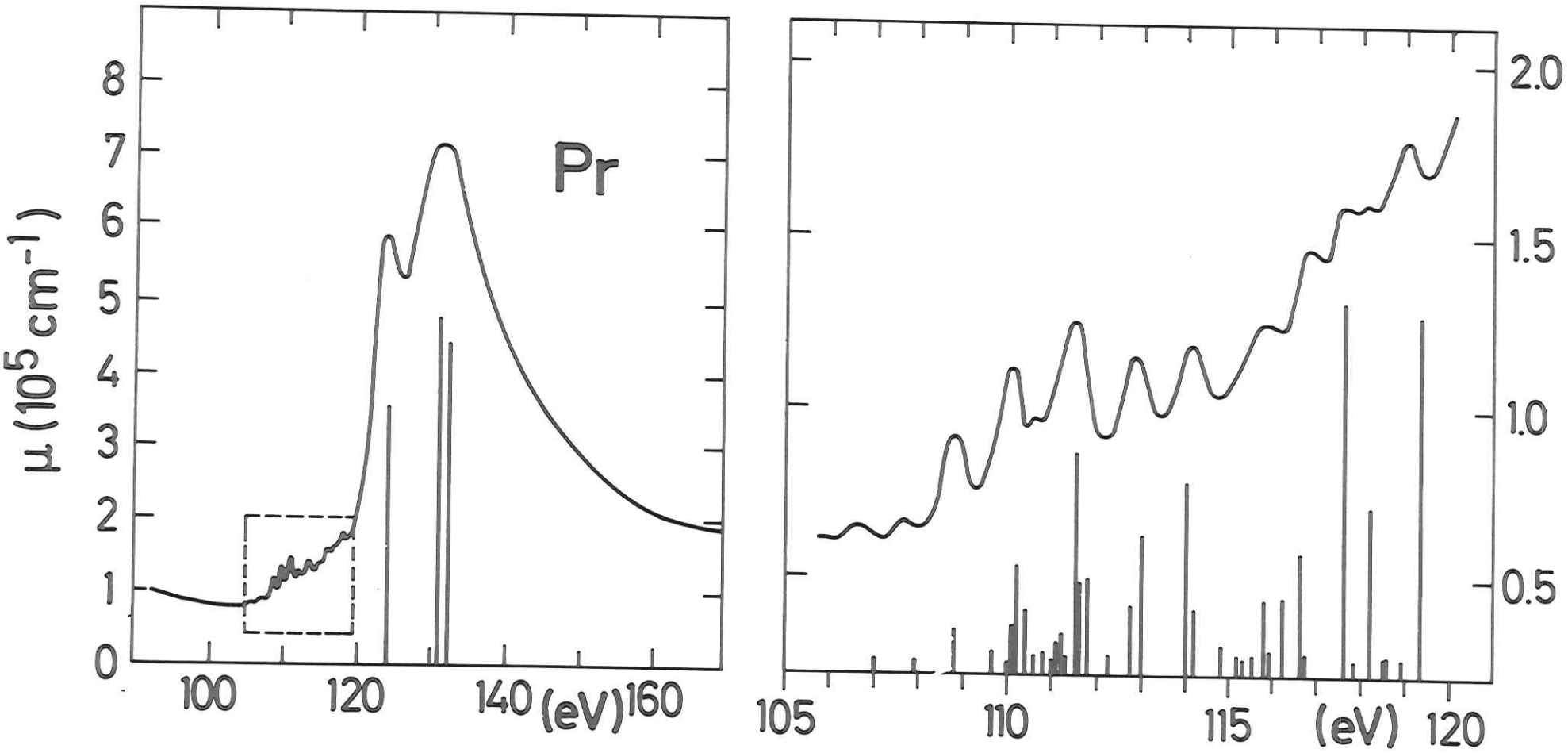
Pr
μ (10^5 cm^-1)
0
1
2
3
4
5
6
7
8
100
120
140
(eV)
160
105
110
115
(eV)
120
0.5
1.0
1.5
2.0

Fig. 4

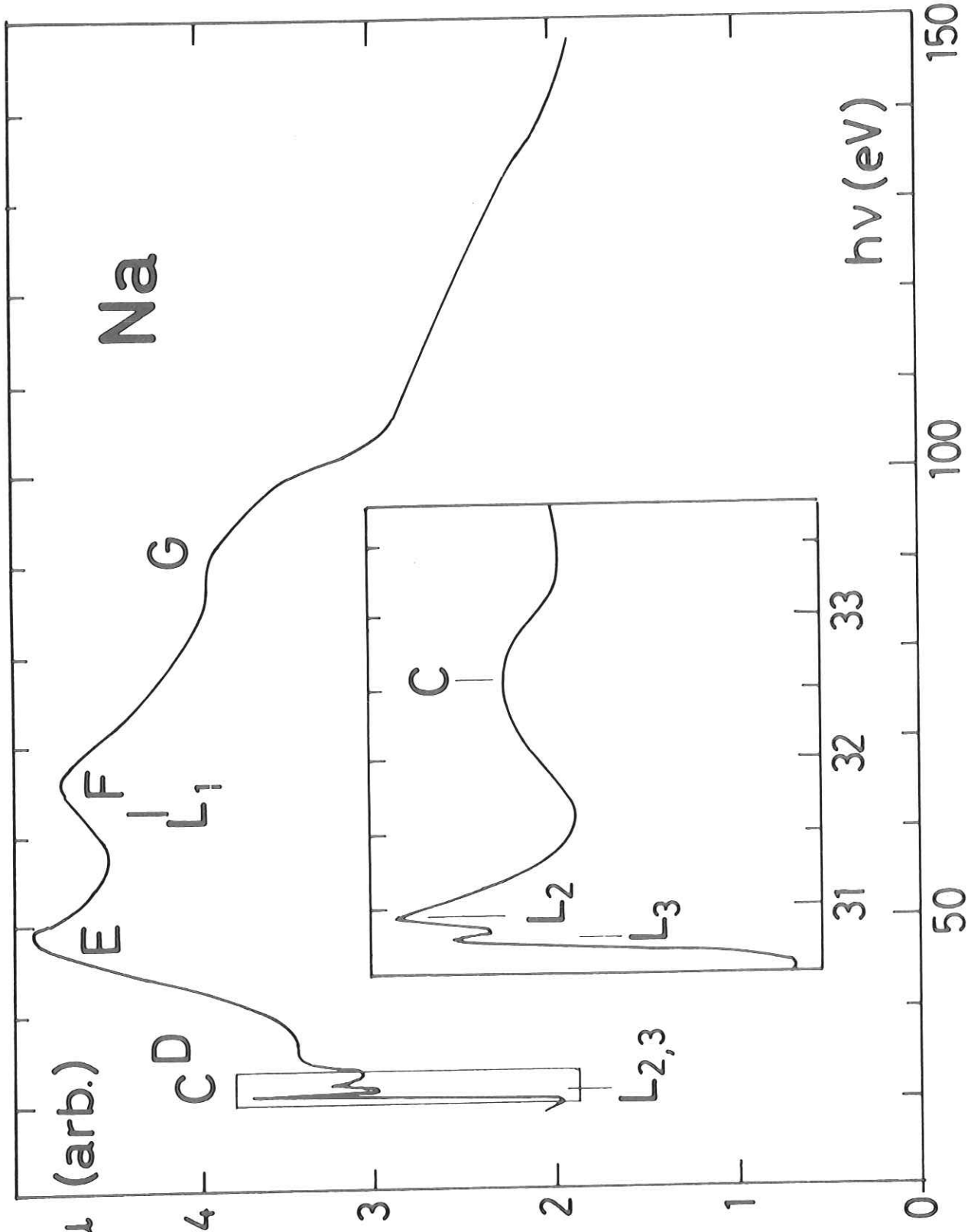

Fig. 5

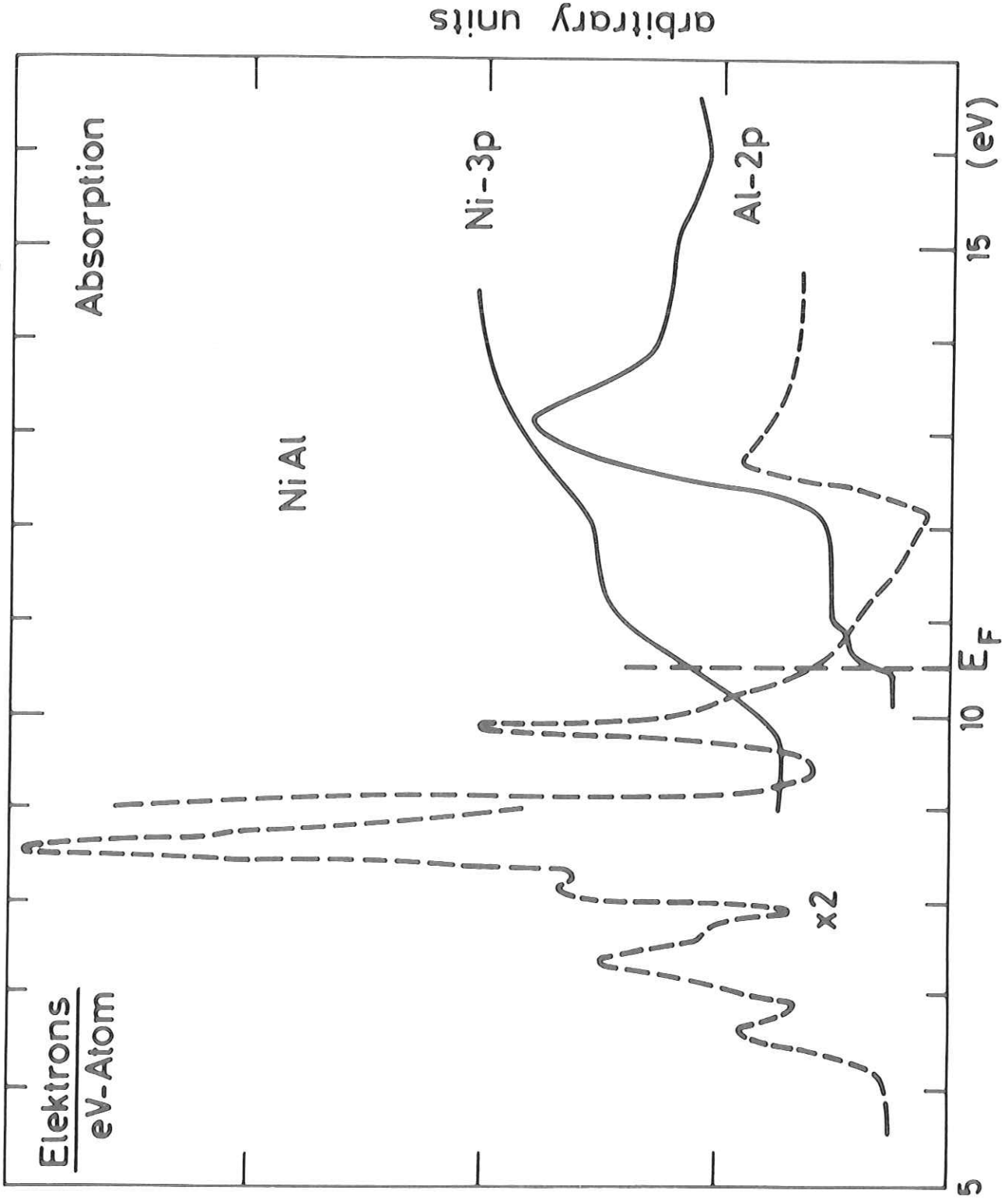
arbitrary units
Absorption
NiAl
Ni-3p
Al-2p
Elektrons
eV-Atom
x2
5
10
15
(eV)
E_F

Fig. 6

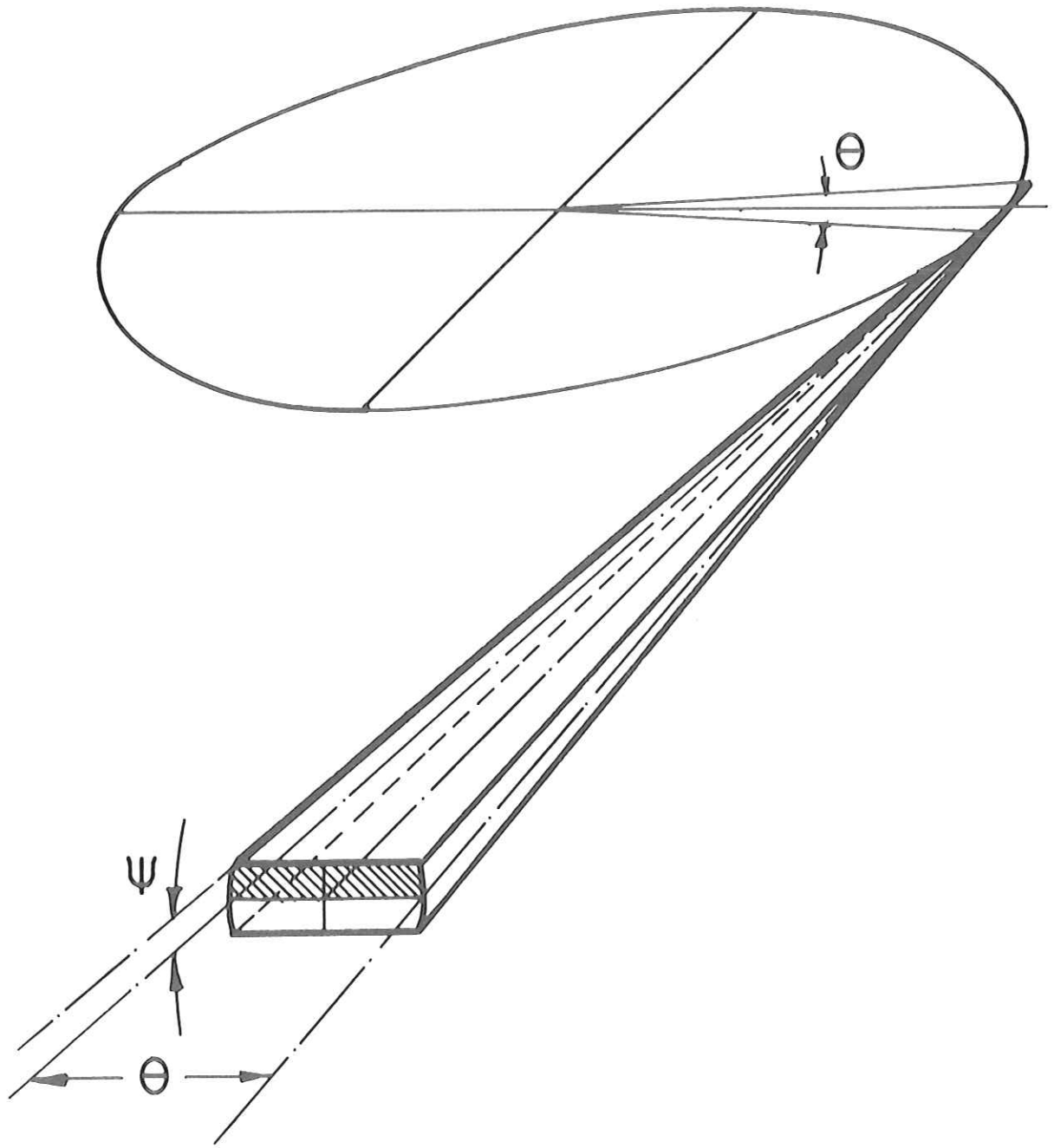

Fig. 7

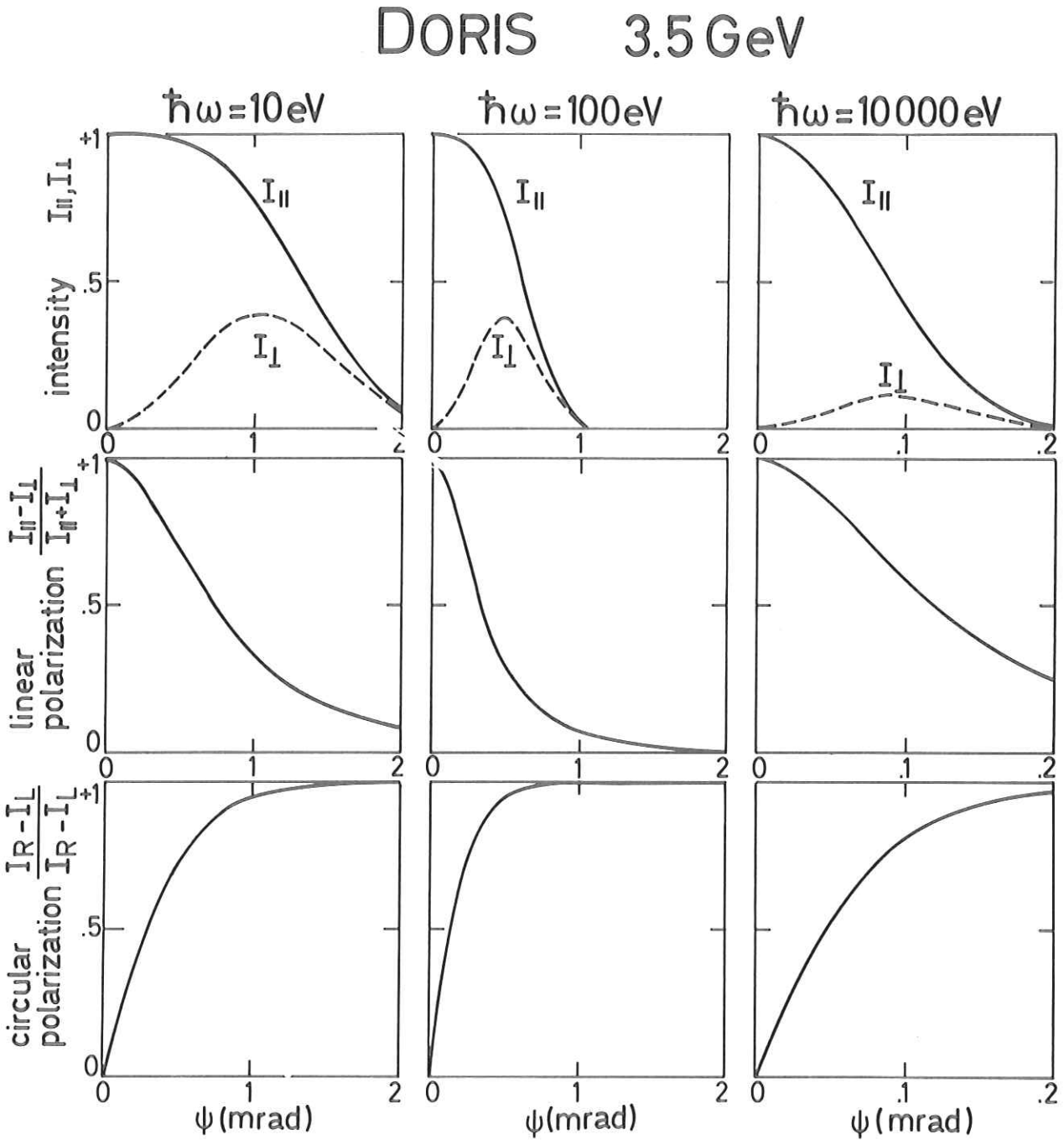
DORIS 3.5 GeV
ħω = 10 eV
ħω = 100 eV
ħω = 10000 eV
intensity $I_{\parallel}, I_{\perp}$
$I_{\parallel}$
$I_{\perp}$
linear polarization $\frac{I_{\parallel}-I_{\perp}}{I_{\parallel}+I_{\perp}}$
circular polarization $\frac{I_R-I_L}{I_R-I_L}$
+1
.5
0
1
2
.1
.2
ψ (mrad)

Fig. 8

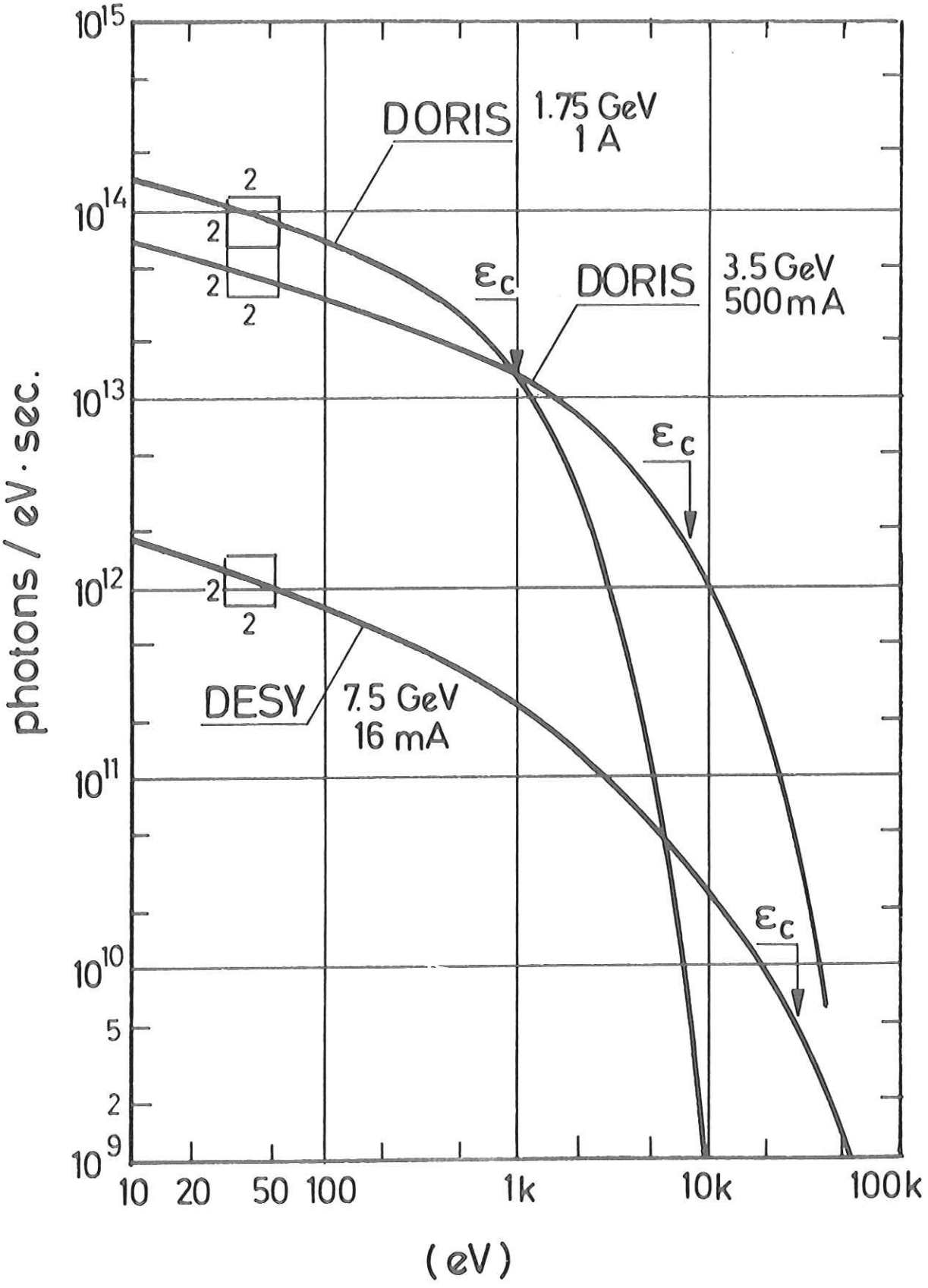
DORIS
1.75 GeV
1 A
DORIS
3.5 GeV
500 mA
DESY
7.5 GeV
16 mA
ε_c
ε_c
ε_c
2
2
2
2
2
2
photons / eV · sec.
10^{15}
10^{14}
10^{13}
10^{12}
10^{11}
10^{10}
5
2
10^{9}
10 20 50 100 1k 10k 100k
(eV)

Fig. 9

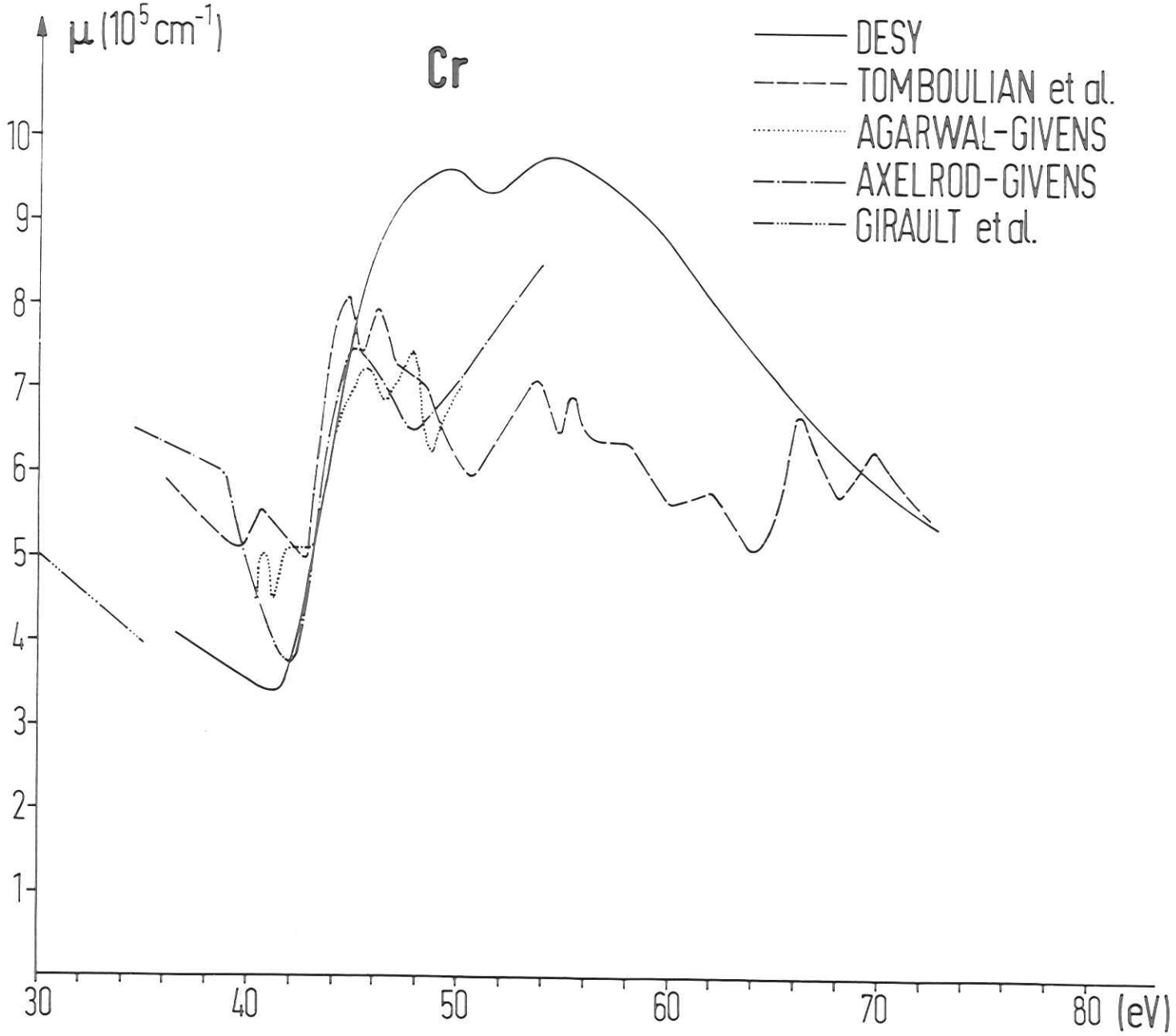
μ (10⁵ cm⁻¹)
Cr
DESY
TOMBOULIAN et al.
AGARWAL-GIVENS
AXELROD-GIVENS
GIRAULT et al.
10
9
8
7
6
5
4
3
2
1
30
40
50
60
70
80 (eV)

Fig. 10

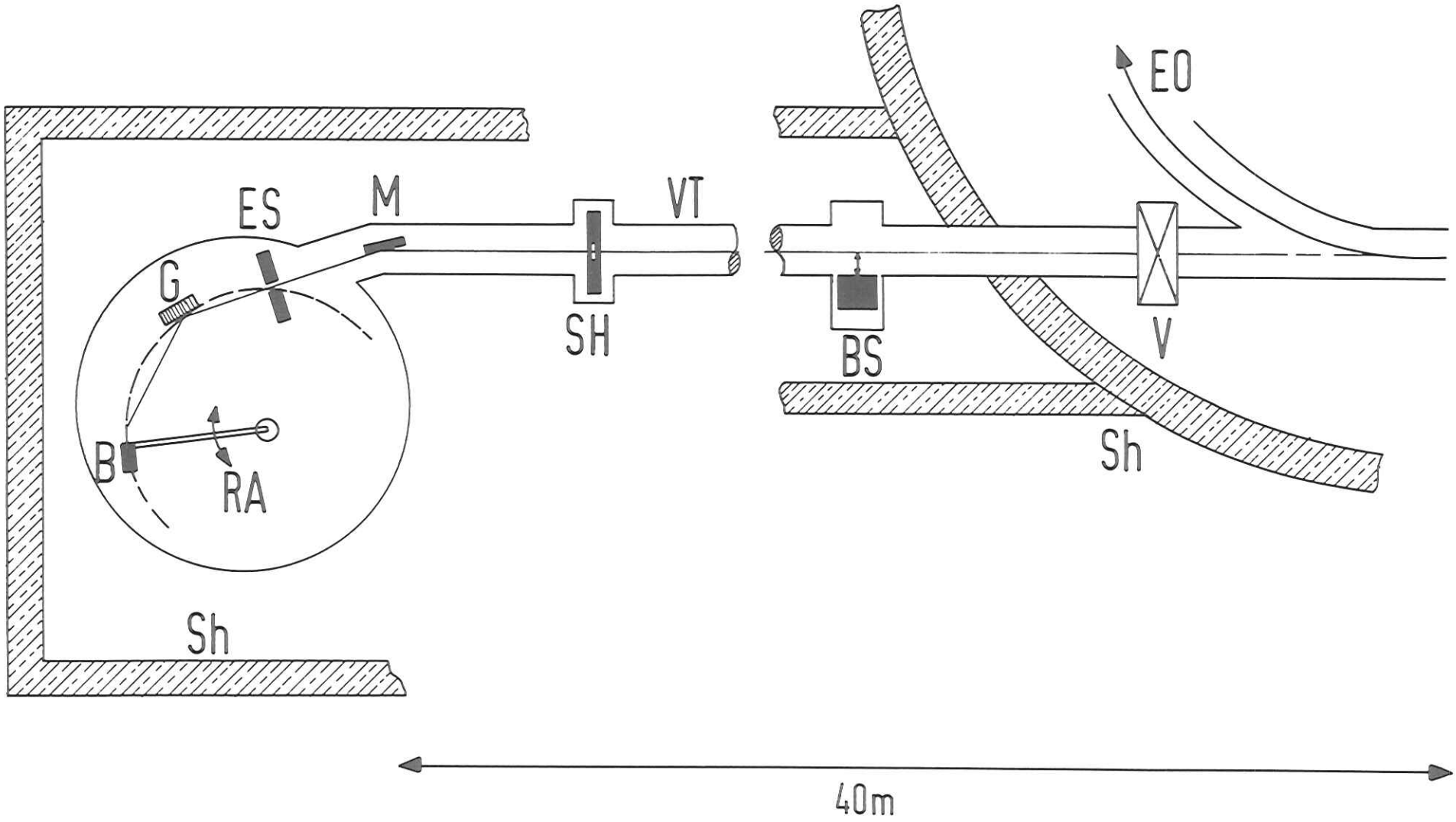

Fig. 11

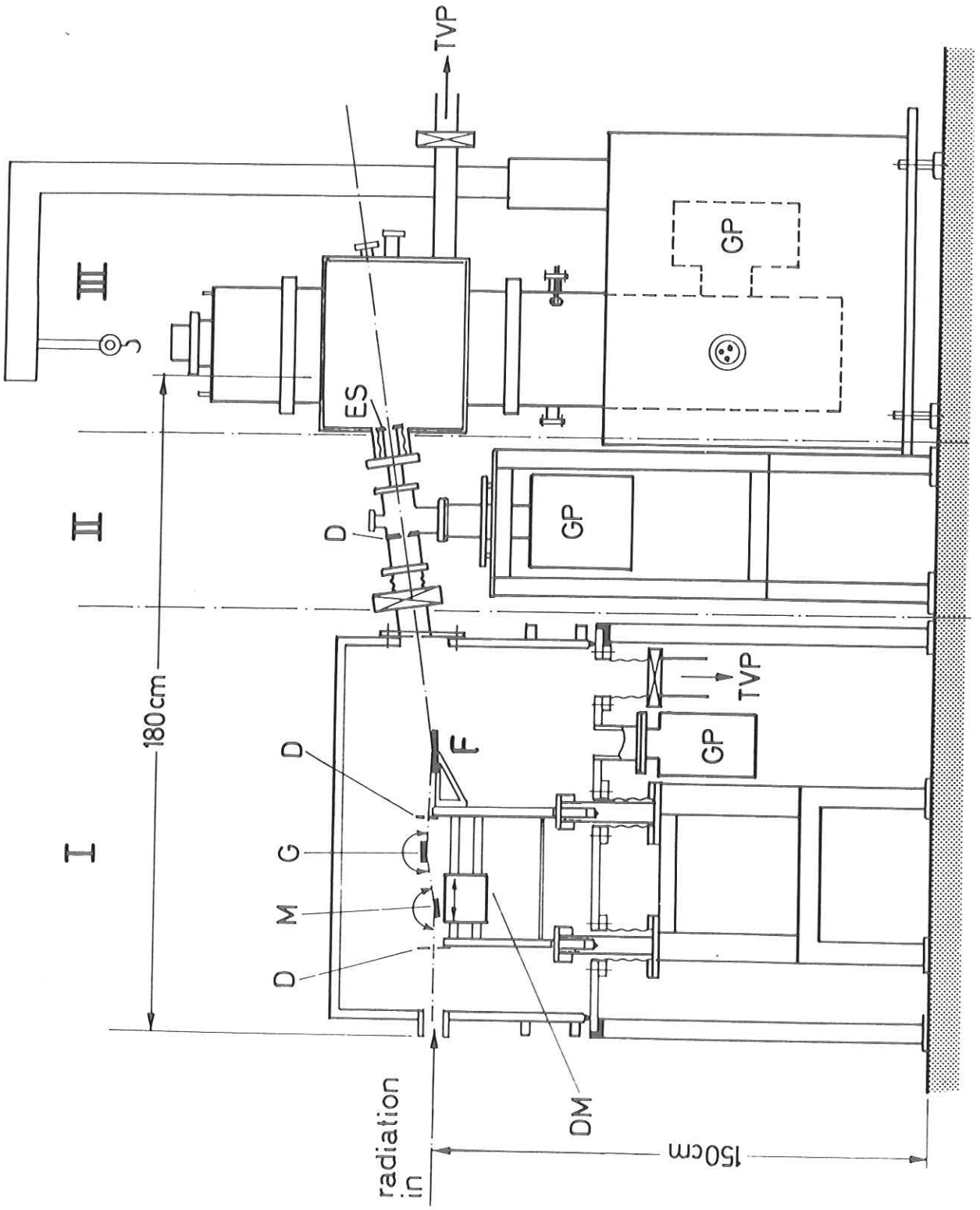

Fig. 12

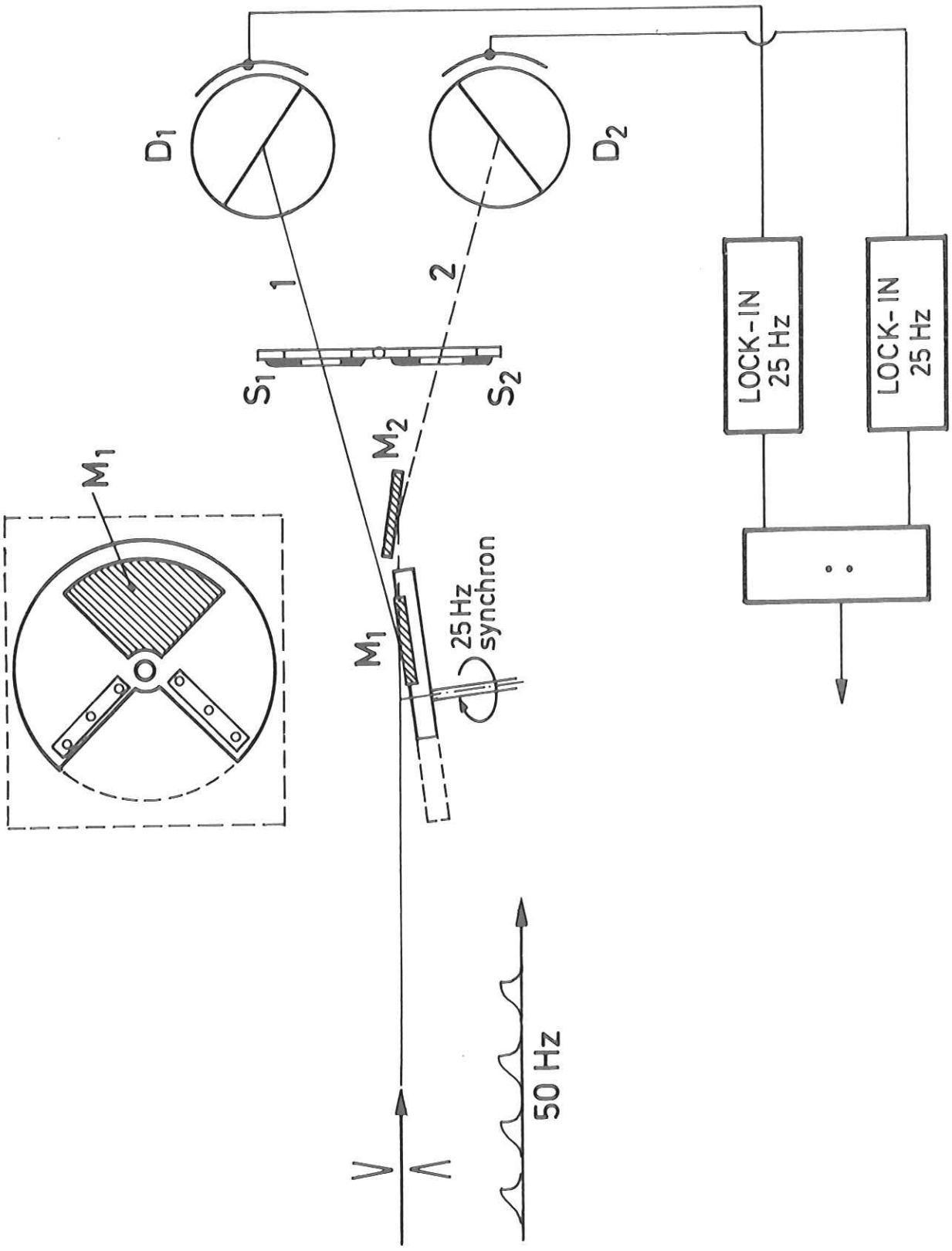
D1
D2
1
2
S1
S2
M2
M1
M1
25 Hz
synchron
LOCK-IN
25 Hz
LOCK-IN
25 Hz
50 Hz

Fig. 13

photoelectric yield (arb. units)
absorption coefficient (10^5 cm^{-1})
Al
yield
absorption
(eV)
0
2
4
6
8
10
20
60
100
140
1
3
5

Fig. 14

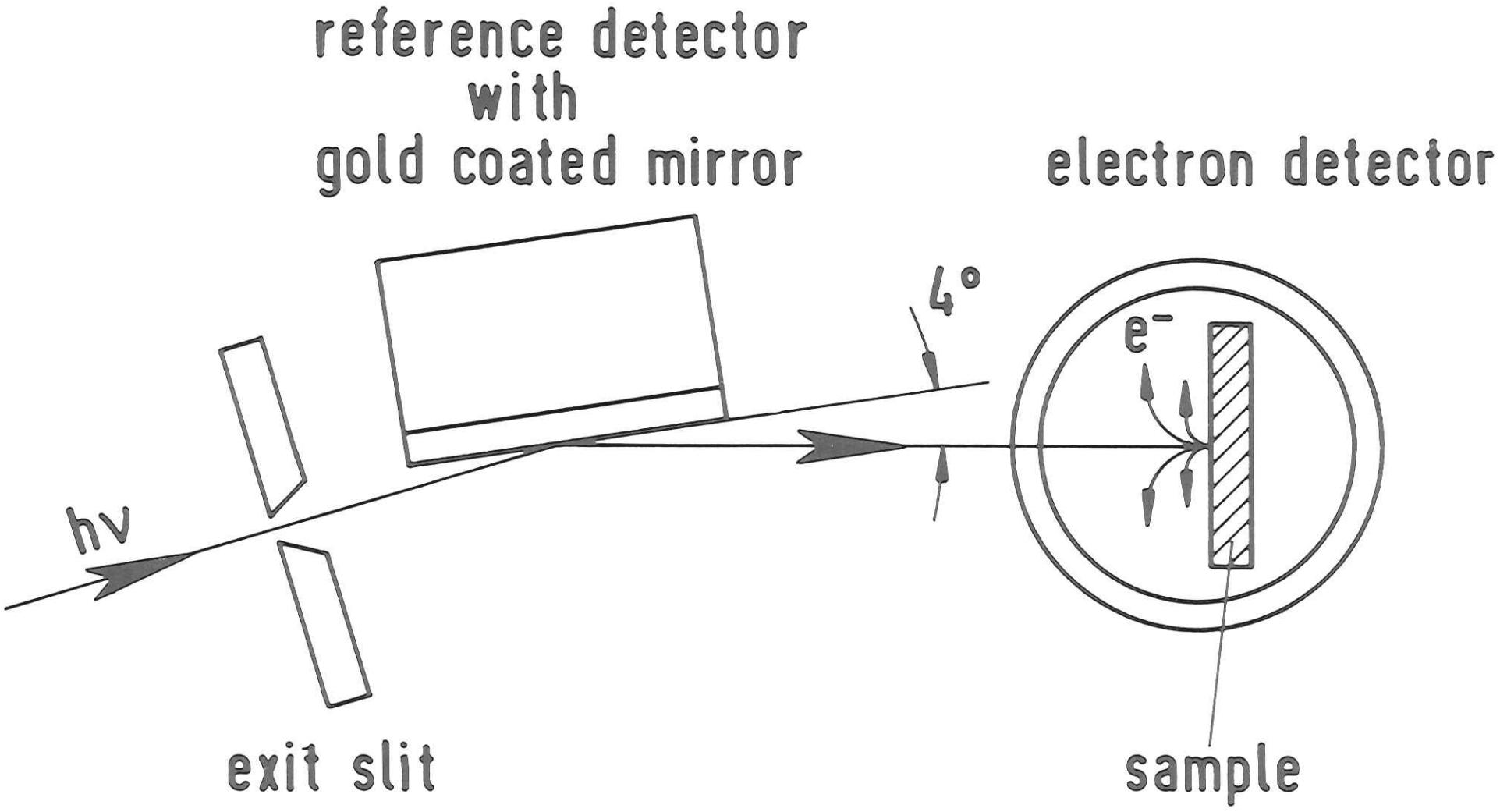
reference detector
with
gold coated mirror
electron detector
4°
e⁻
hν
exit slit
sample

Fig. 15

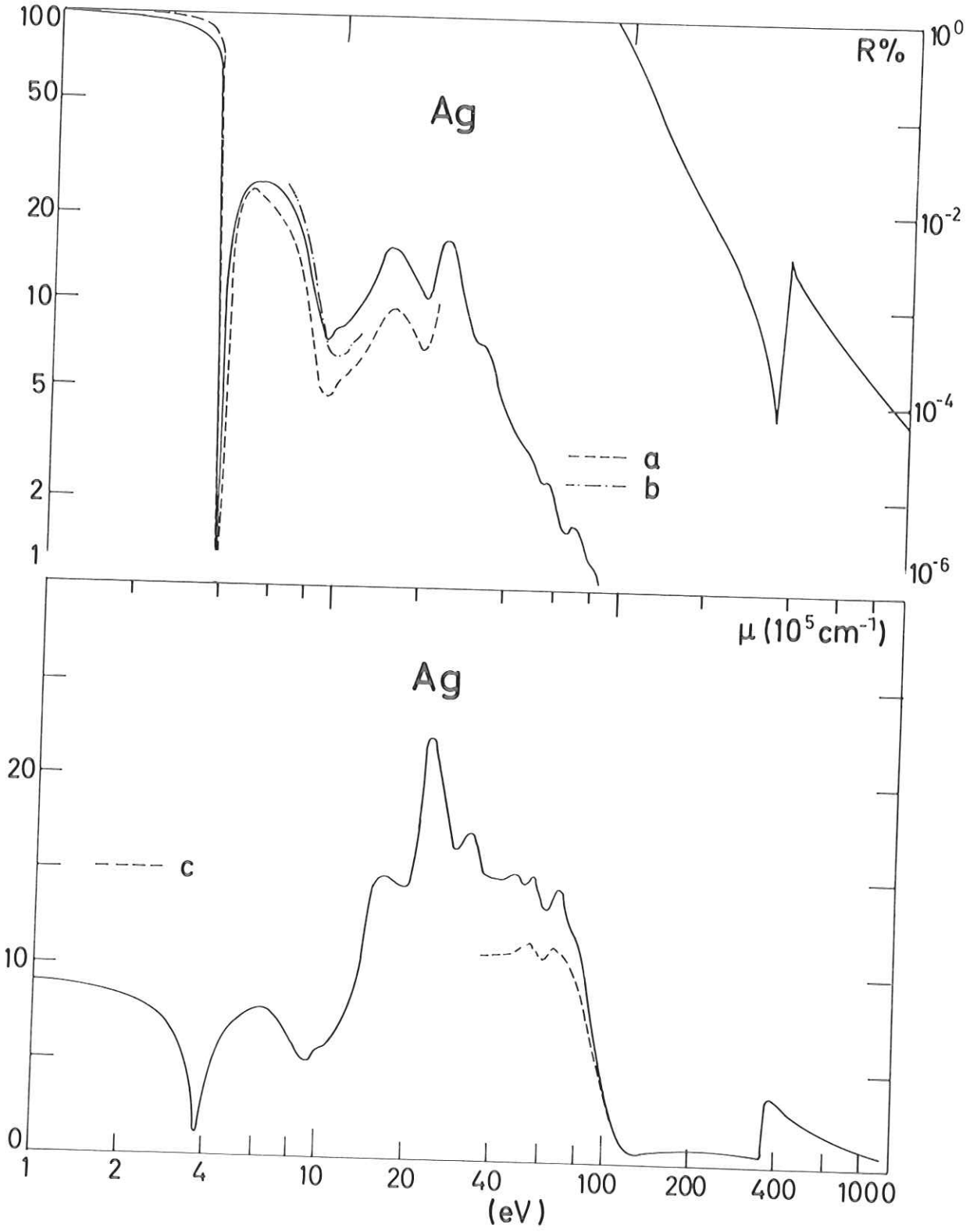

Fig. 16

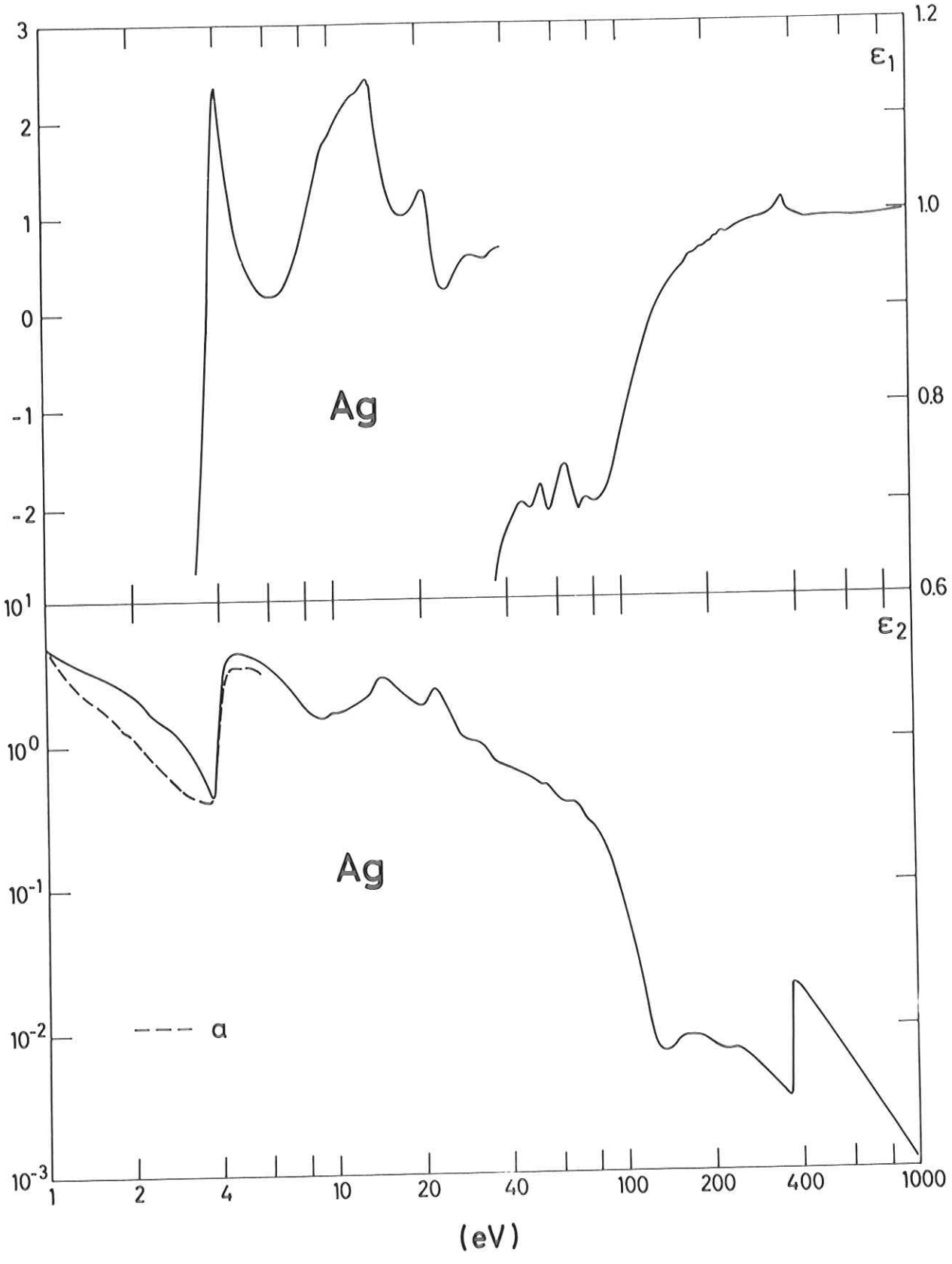
3
2
1
0
-1
-2
10^1
10^0
10^{-1}
10^{-2}
10^{-3}
1.2
1.0
0.8
0.6
ε_1
ε_2
Ag
Ag
a
1
2
4
10
20
40
100
200
400
1000
(eV)

Fig. 17

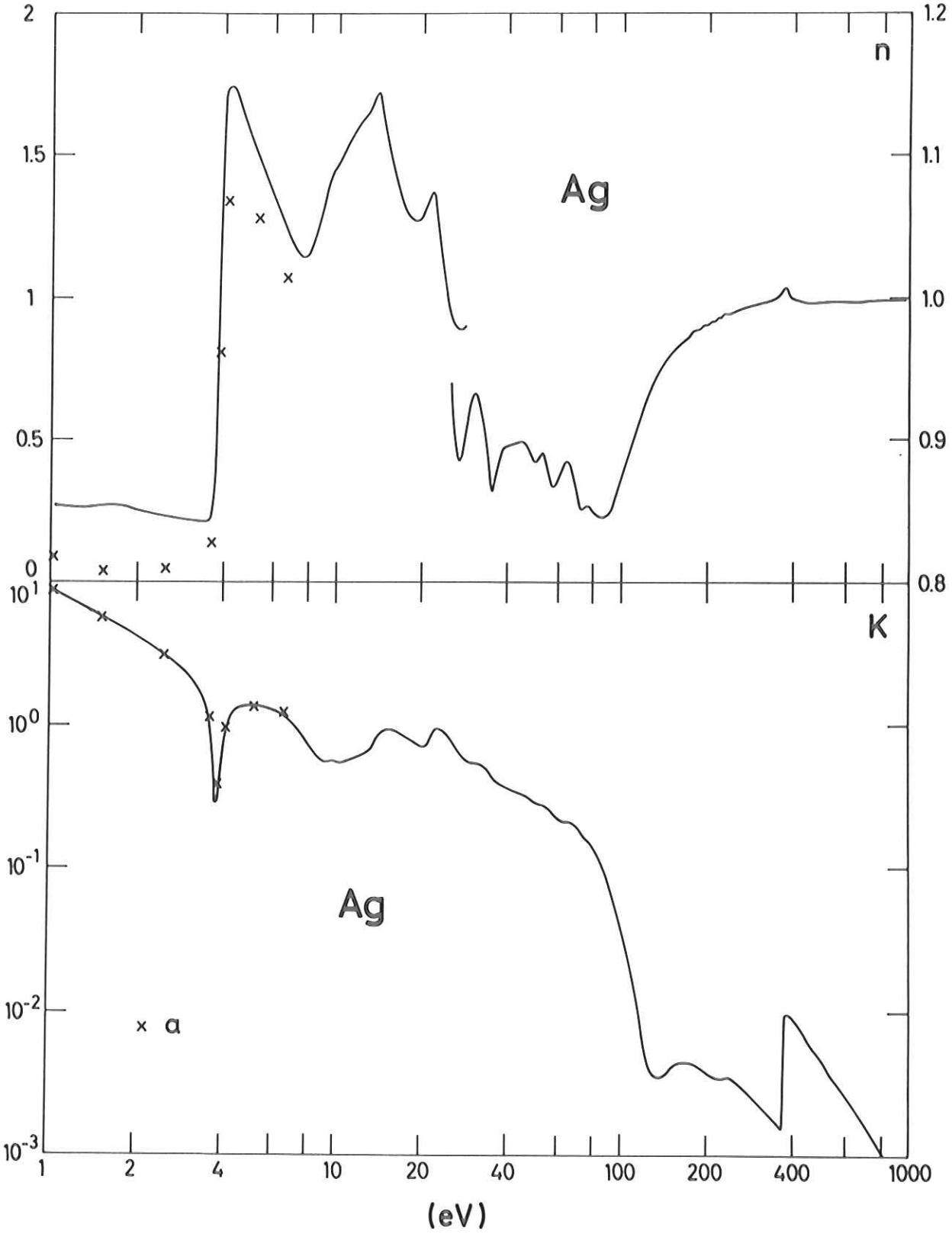

Fig. 18

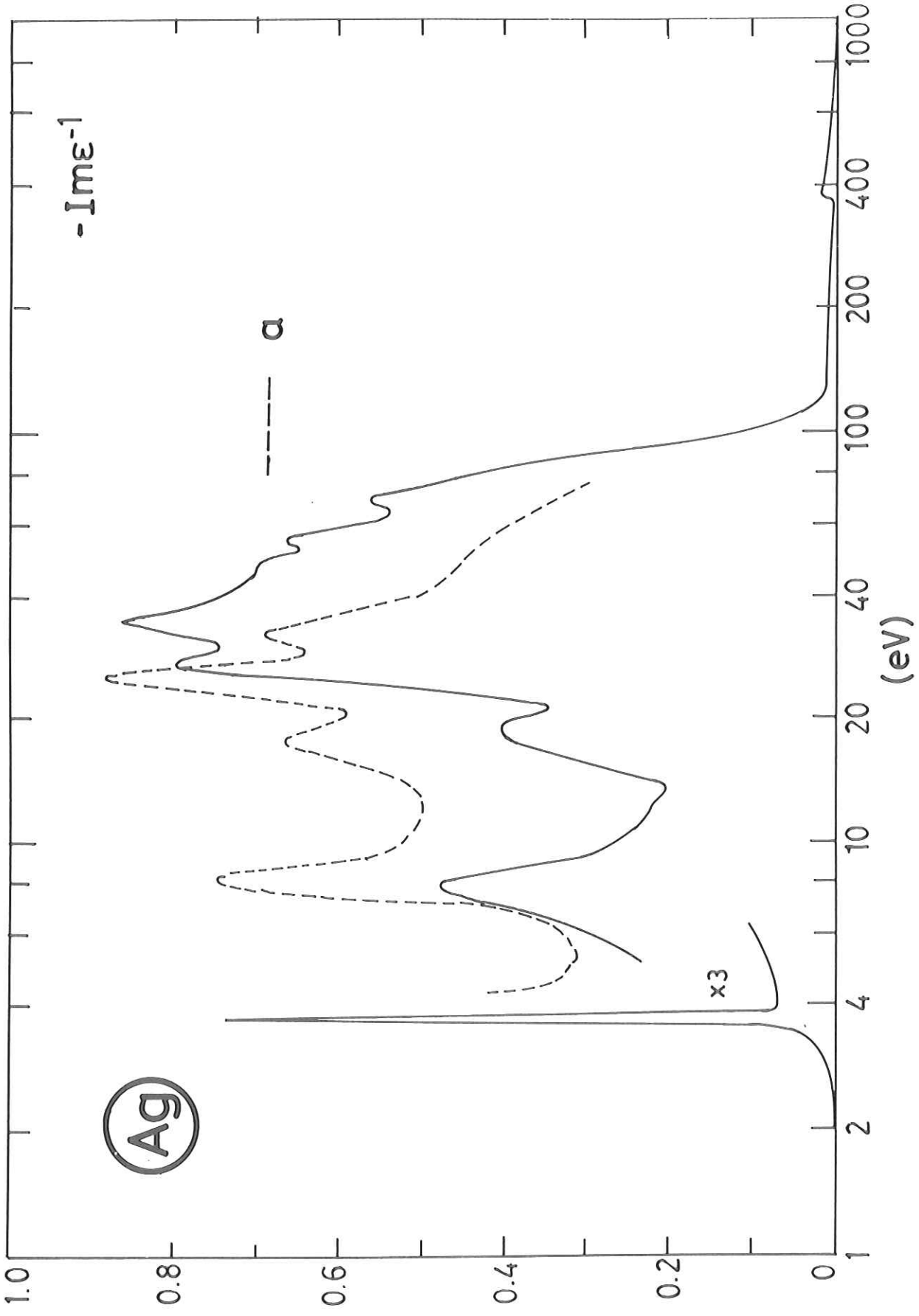

Fig. 19

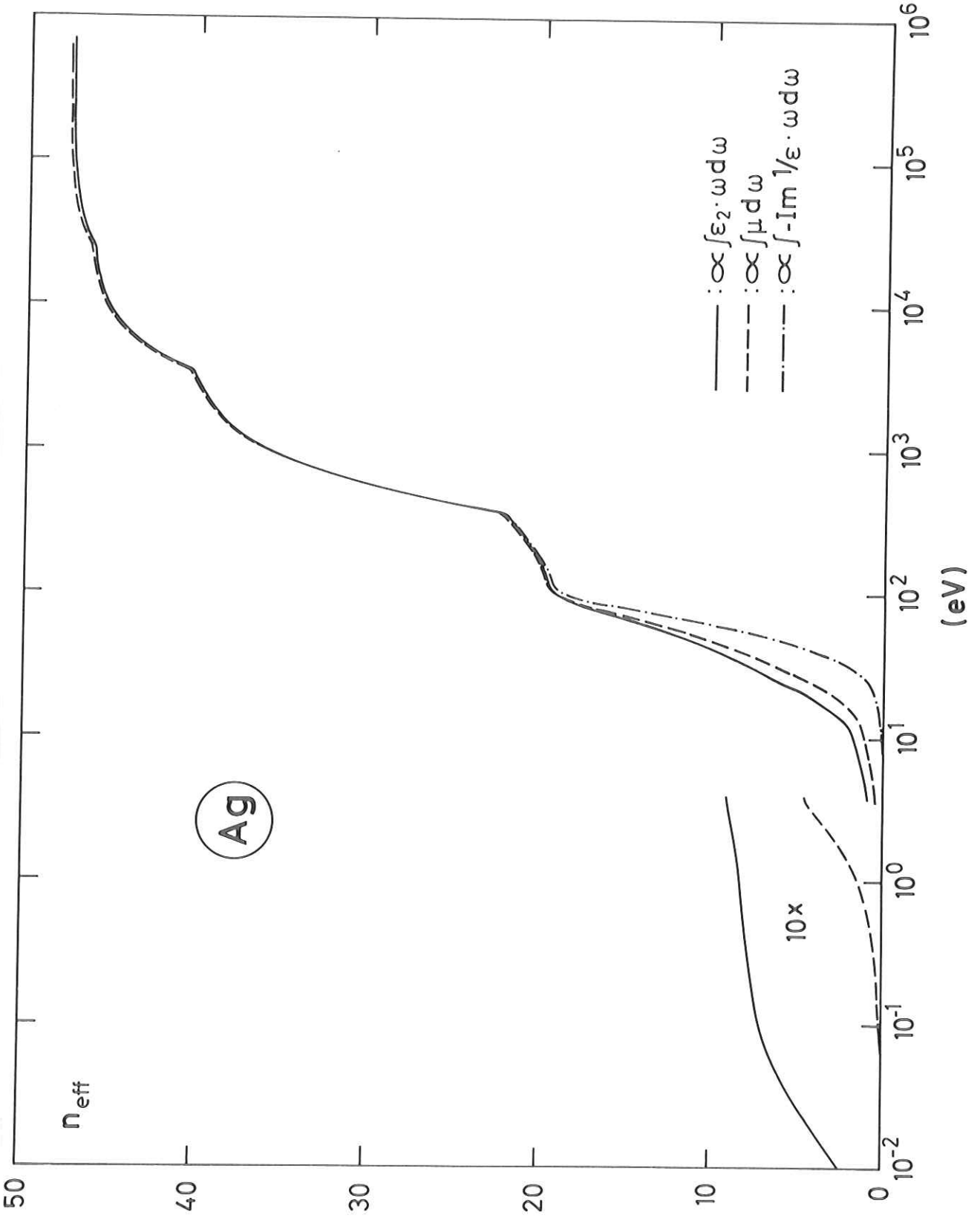
Ag
n_{eff}
$\propto \int \varepsilon_2 \cdot \omega \, d\omega$
$\propto \int \mu \, d\omega$
$\propto \int -\mathrm{Im}\, 1/\varepsilon \cdot \omega \, d\omega$
10x
(eV)
0
10
20
30
40
50
10^{-2}
10^{-1}
10^{0}
10^{1}
10^{2}
10^{3}
10^{4}
10^{5}
10^{6}

Fig. 20

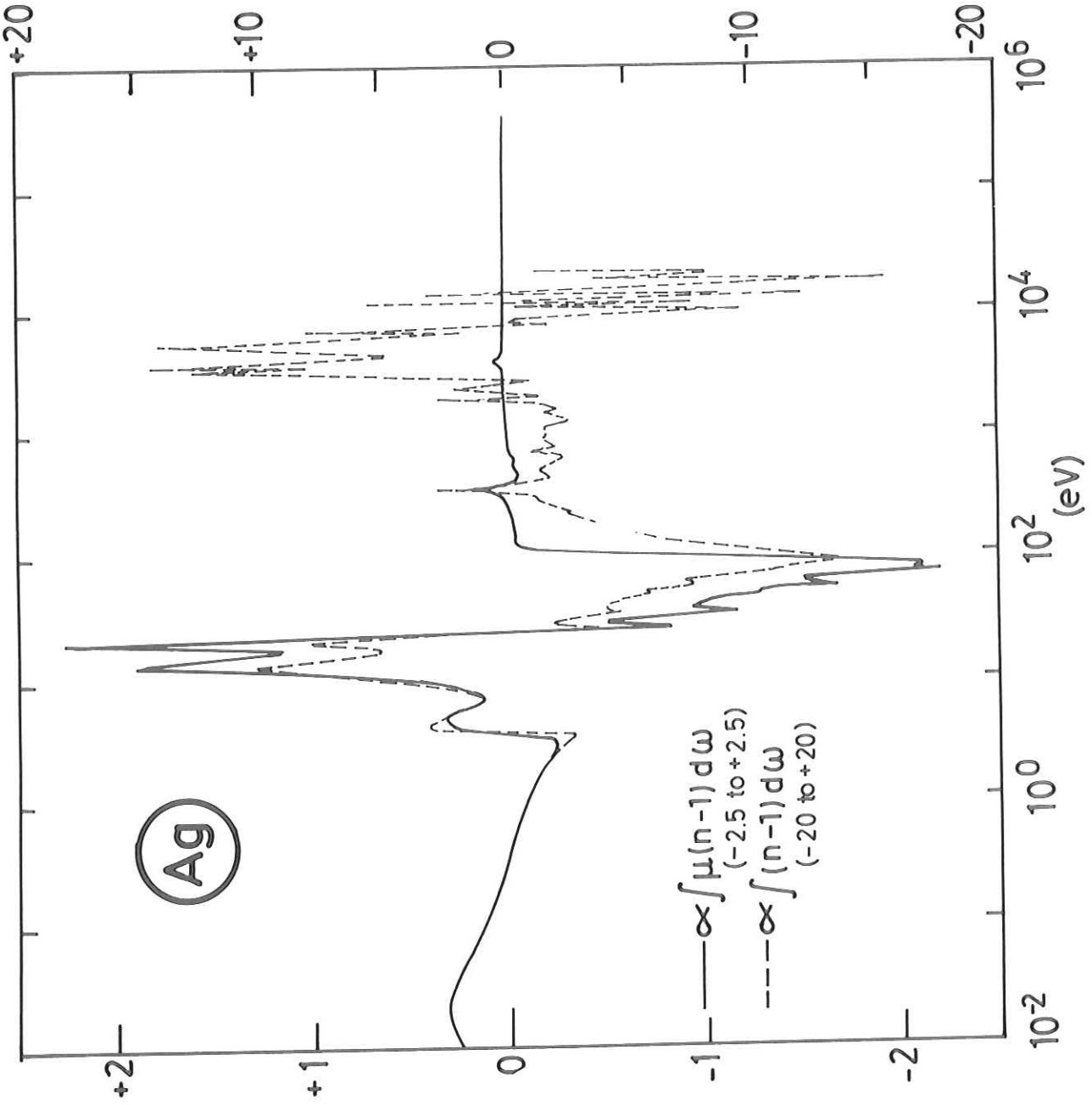
+20
+10
0
-10
-20
+2
+1
0
-1
-2
10^{-2}
10^{0}
10^{2}
10^{4}
10^{6}
(eV)
Ag
$\propto \int \mu(n-1)\,d\omega$ (-2.5 to +2.5)
$\propto \int (n-1)\,d\omega$ (-20 to +20)

Fig. 21

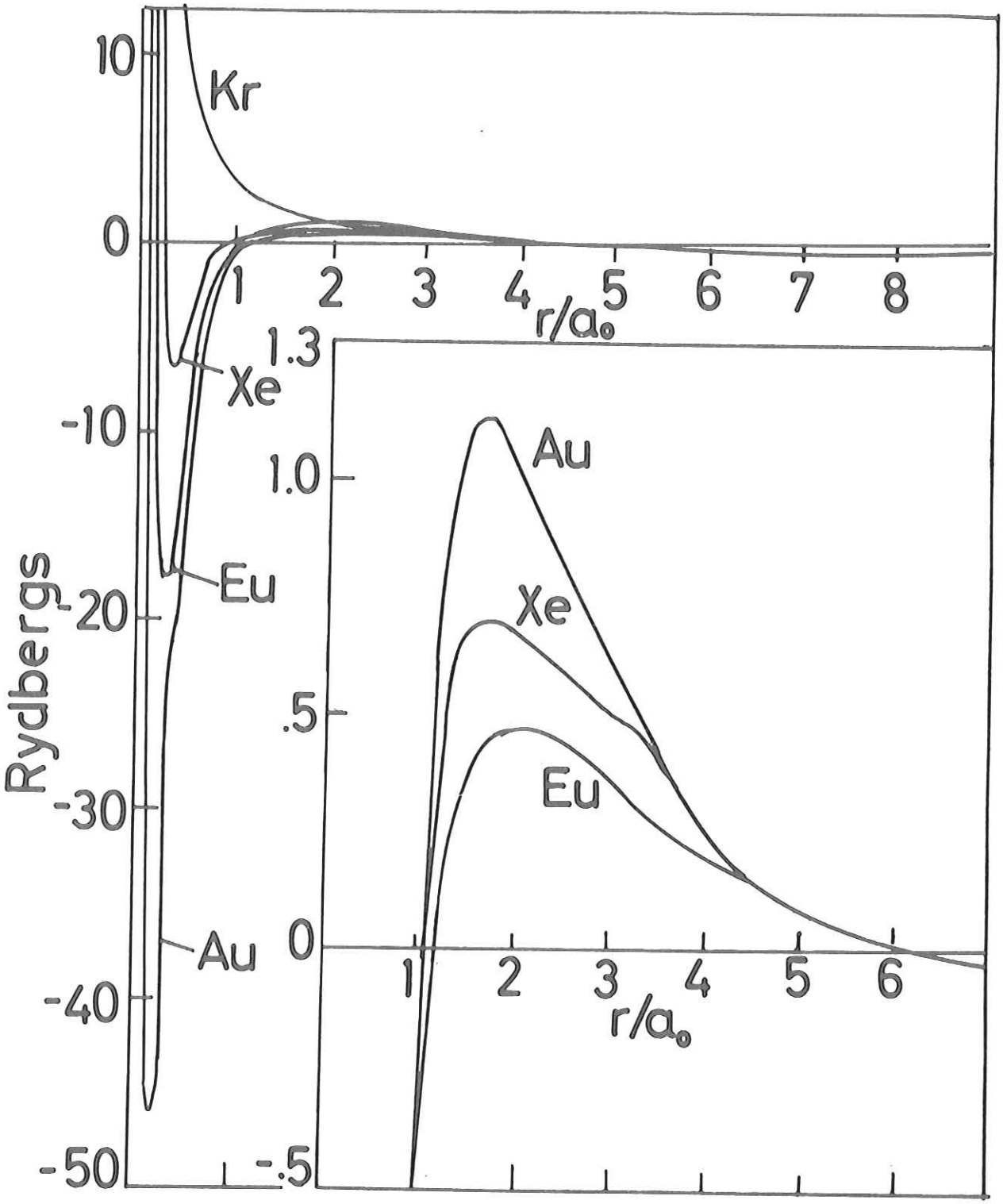
10
0
-10
-20
-30
-40
-50
Rydbergs
Kr
Xe
Eu
Au
1
2
3
4
5
6
7
8
r/a₀
1.3
1.0
.5
0
-.5
Au
Xe
Eu
1
2
3
4
5
6
r/a₀

Fig. 22

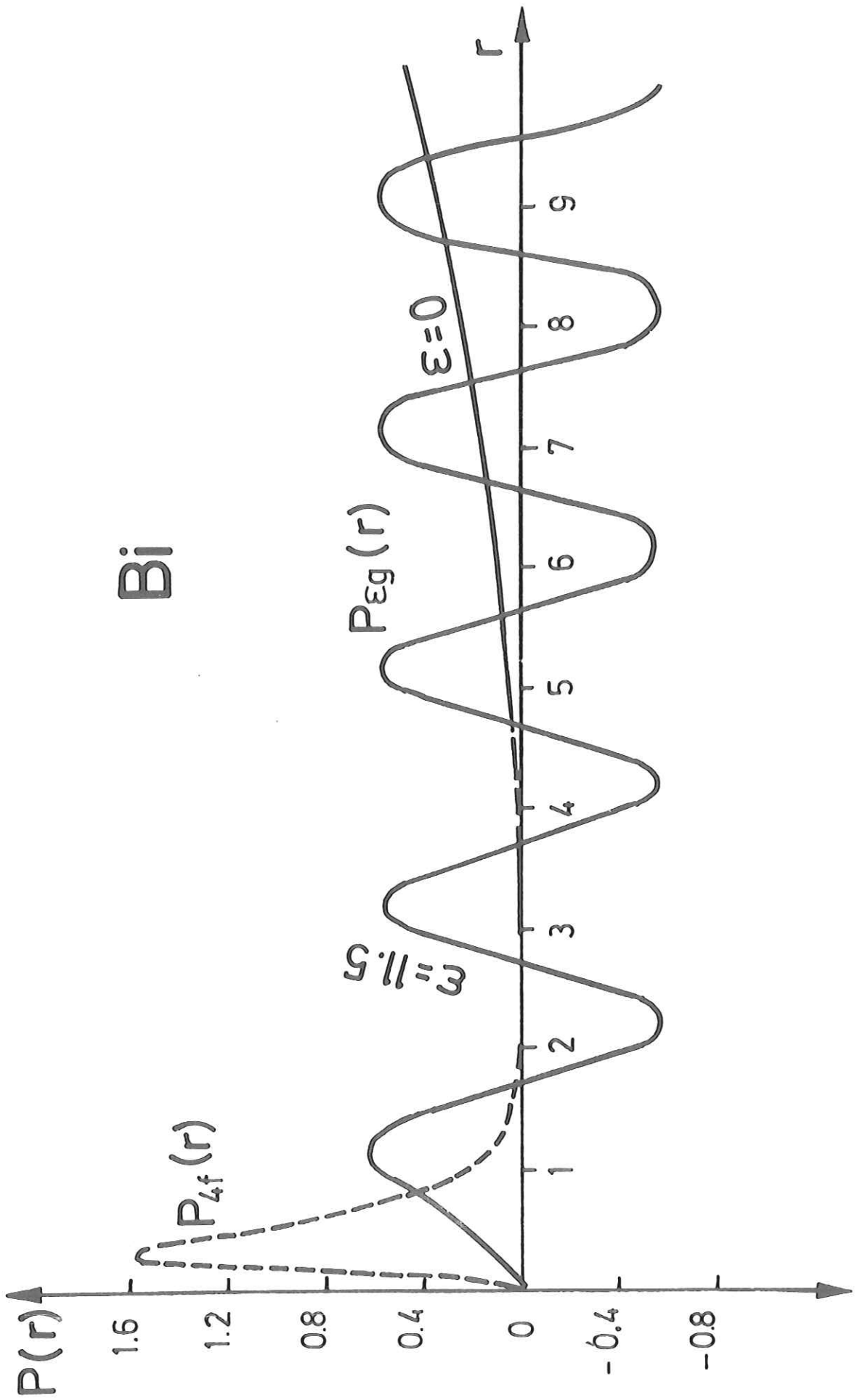
Bi
P(r)
r
1.6
1.2
0.8
0.4
0
-0.4
-0.8
1
2
3
4
5
6
7
8
9
$P_{4f}(r)$
$P_{\varepsilon g}(r)$
$\varepsilon = 11.5$
$\varepsilon = 0$

Fig. 23

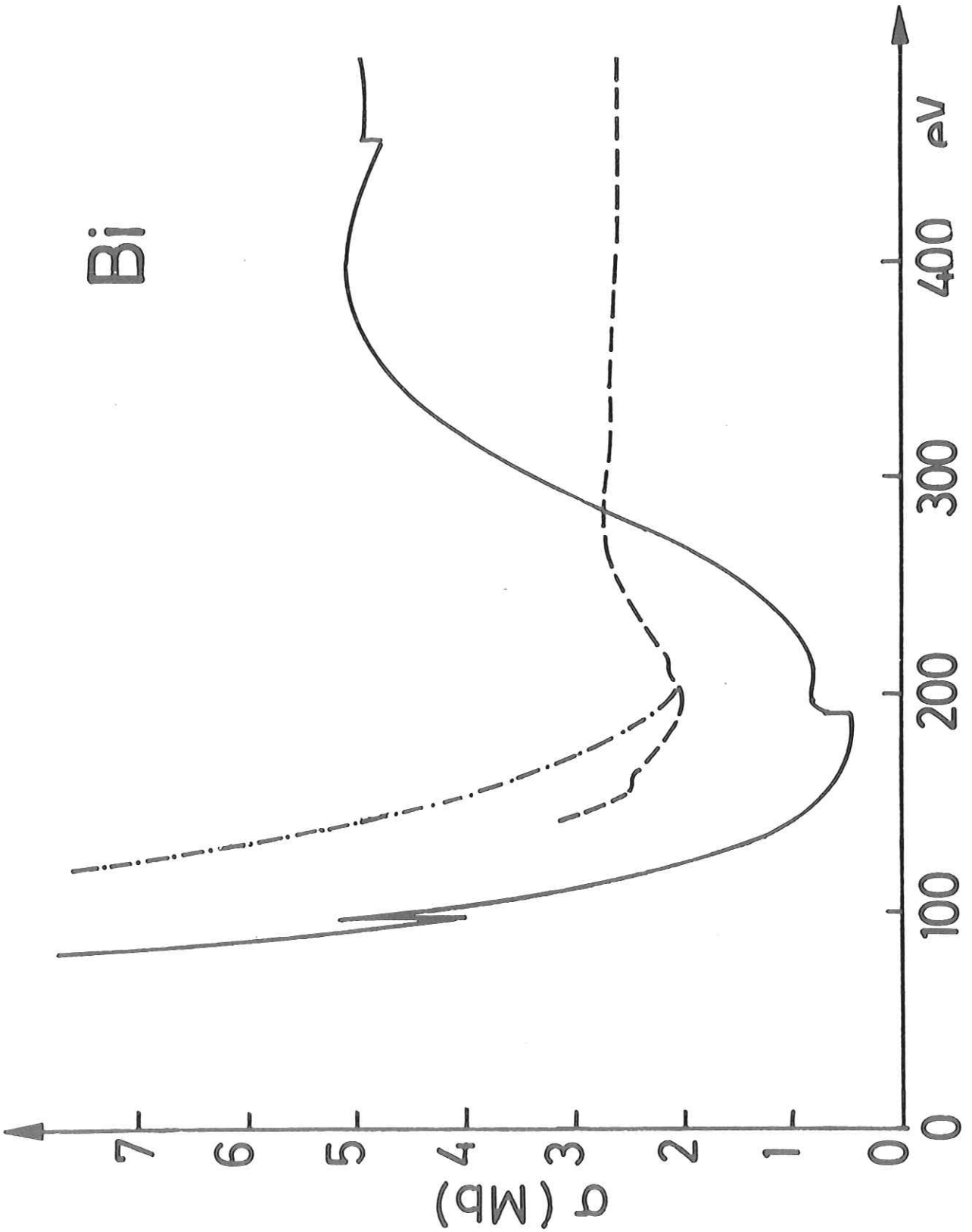

Fig. 24

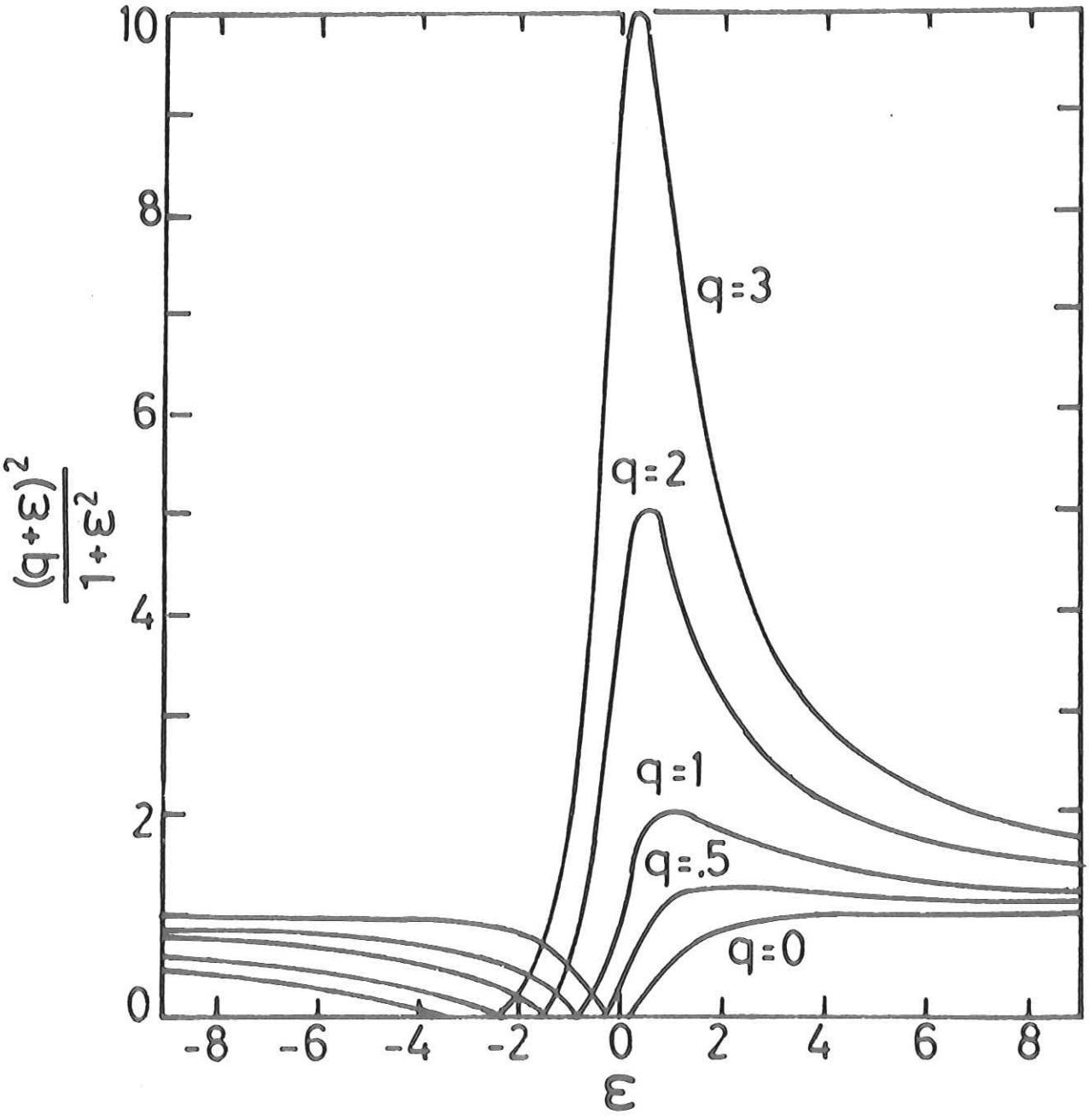
10
8
6
4
2
0
-8
-6
-4
-2
0
2
4
6
8
ε
$\frac{(q+\varepsilon)^2}{1+\varepsilon^2}$
q=3
q=2
q=1
q=.5
q=0

Fig. 25

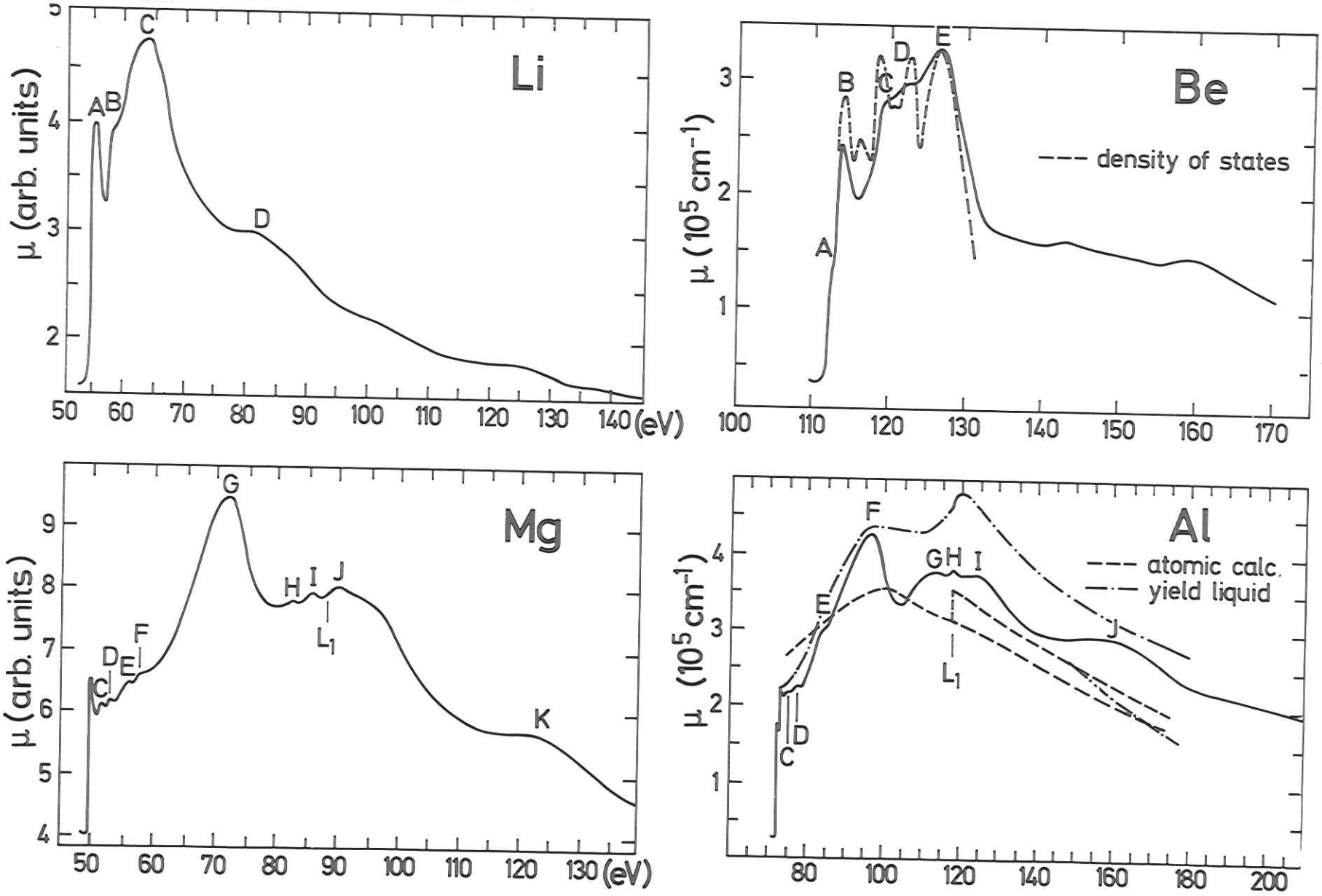
Li
μ (arb. units)
A
B
C
D
50 60 70 80 90 100 110 120 130 140 (eV)
Be
μ (10⁵ cm⁻¹)
density of states
A
B
C
D
E
100 110 120 130 140 150 160 170
Mg
μ (arb. units)
C
D
E
F
G
H
I
J
K
L1
50 60 70 80 90 100 110 120 130 (eV)
Al
μ (10⁵ cm⁻¹)
atomic calc.
yield liquid
C
D
E
F
G H I
J
L1
80 100 120 140 160 180 200

Fig. 26

Li
YIELD SOLID
YIELD LIQUID
YIELD (ARBITRARY UNITS)
1
2
3
4
50
60
70
80
(eV)

Fig. 27

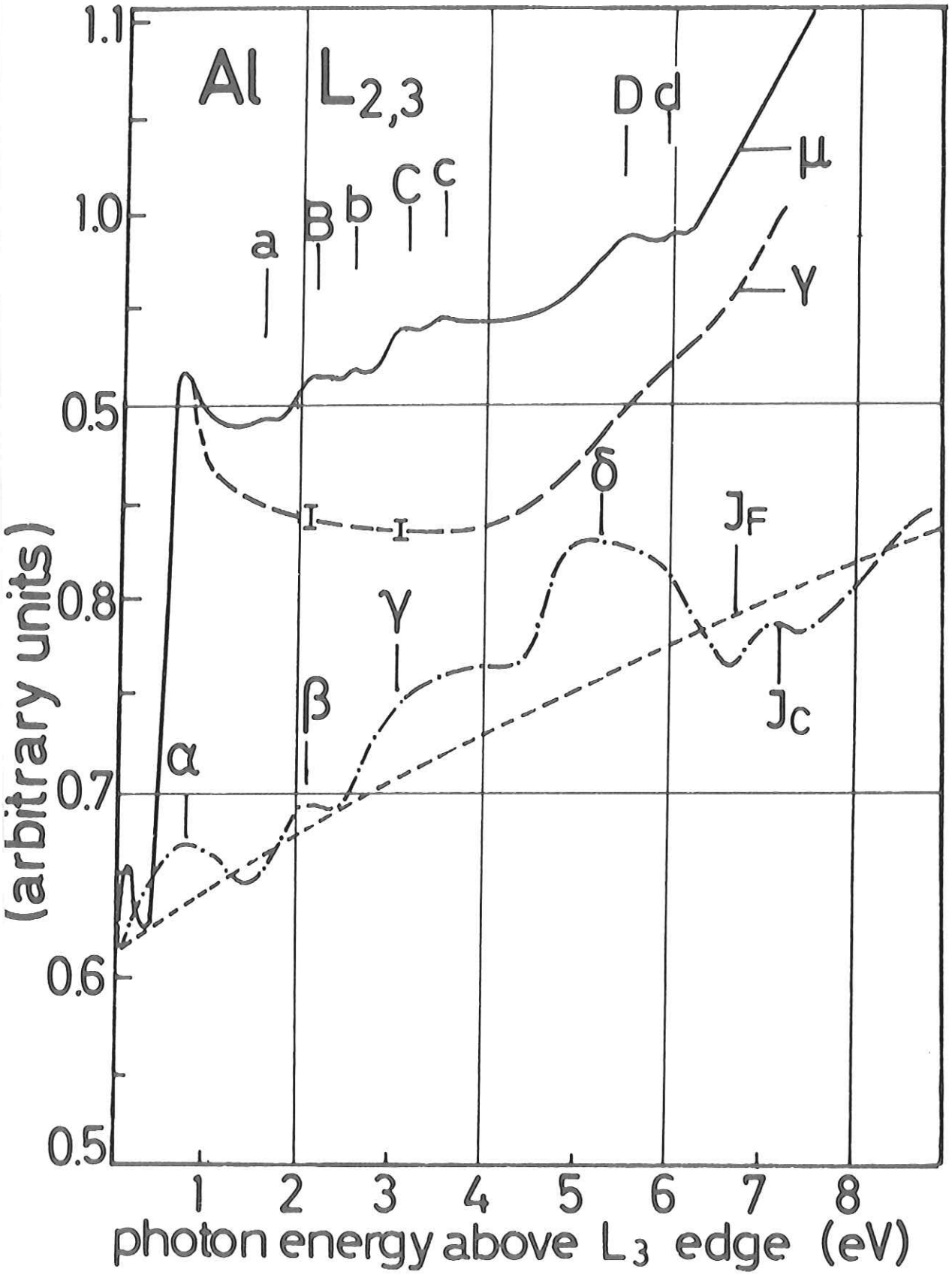
Al L2,3
D
d
μ
a
B
b
C
c
γ
δ
I
I
JF
γ
β
α
JC
1.1
1.0
0.5
0.8
0.7
0.6
0.5
(arbitrary units)
1
2
3
4
5
6
7
8
photon energy above L3 edge (eV)

Fig. 28

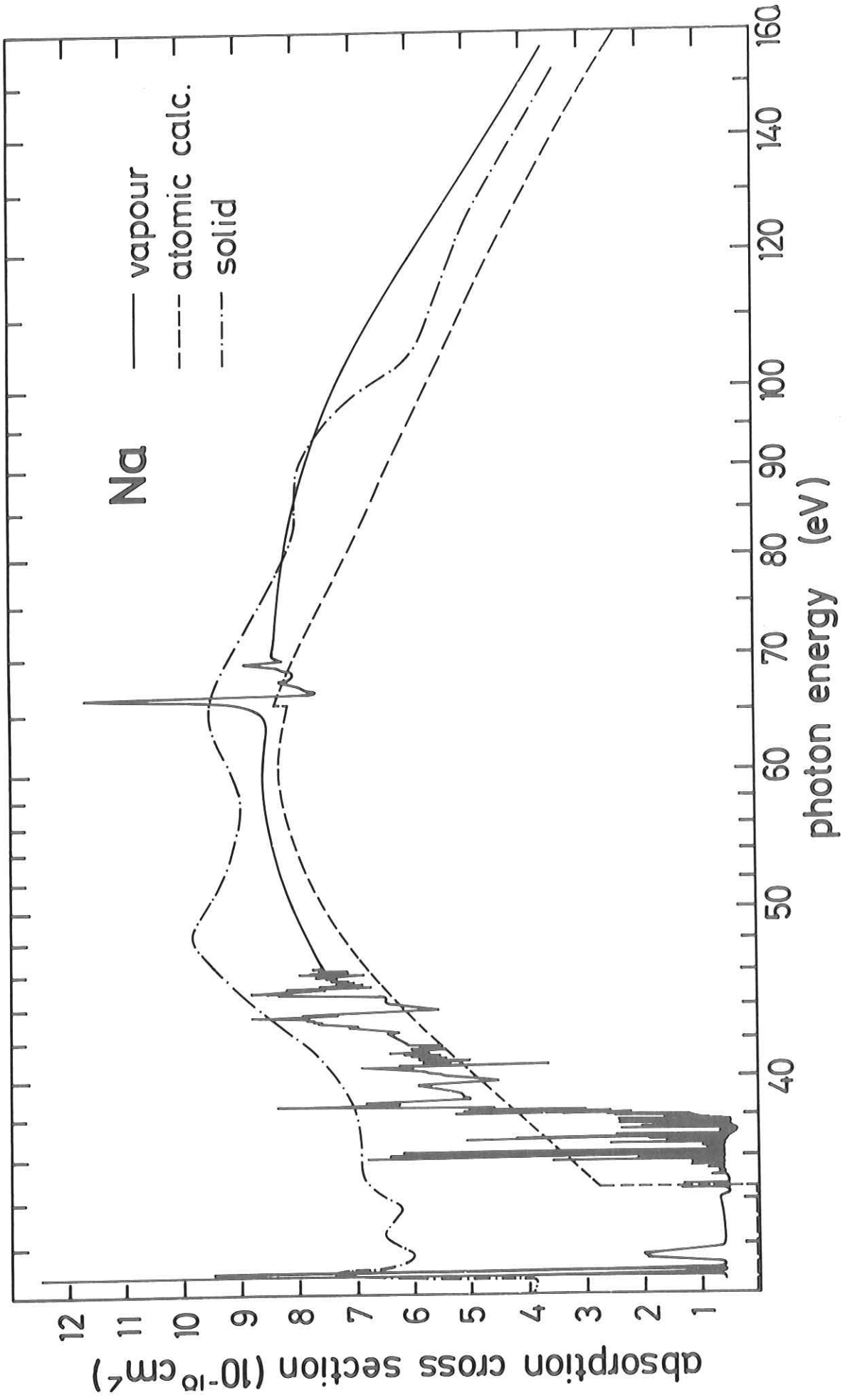
Na
vapour
atomic calc.
solid
absorption cross section (10^{-18} cm^2)
photon energy (eV)
1
2
3
4
5
6
7
8
9
10
11
12
40
50
60
70
80
90
100
120
140
160

Fig. 29

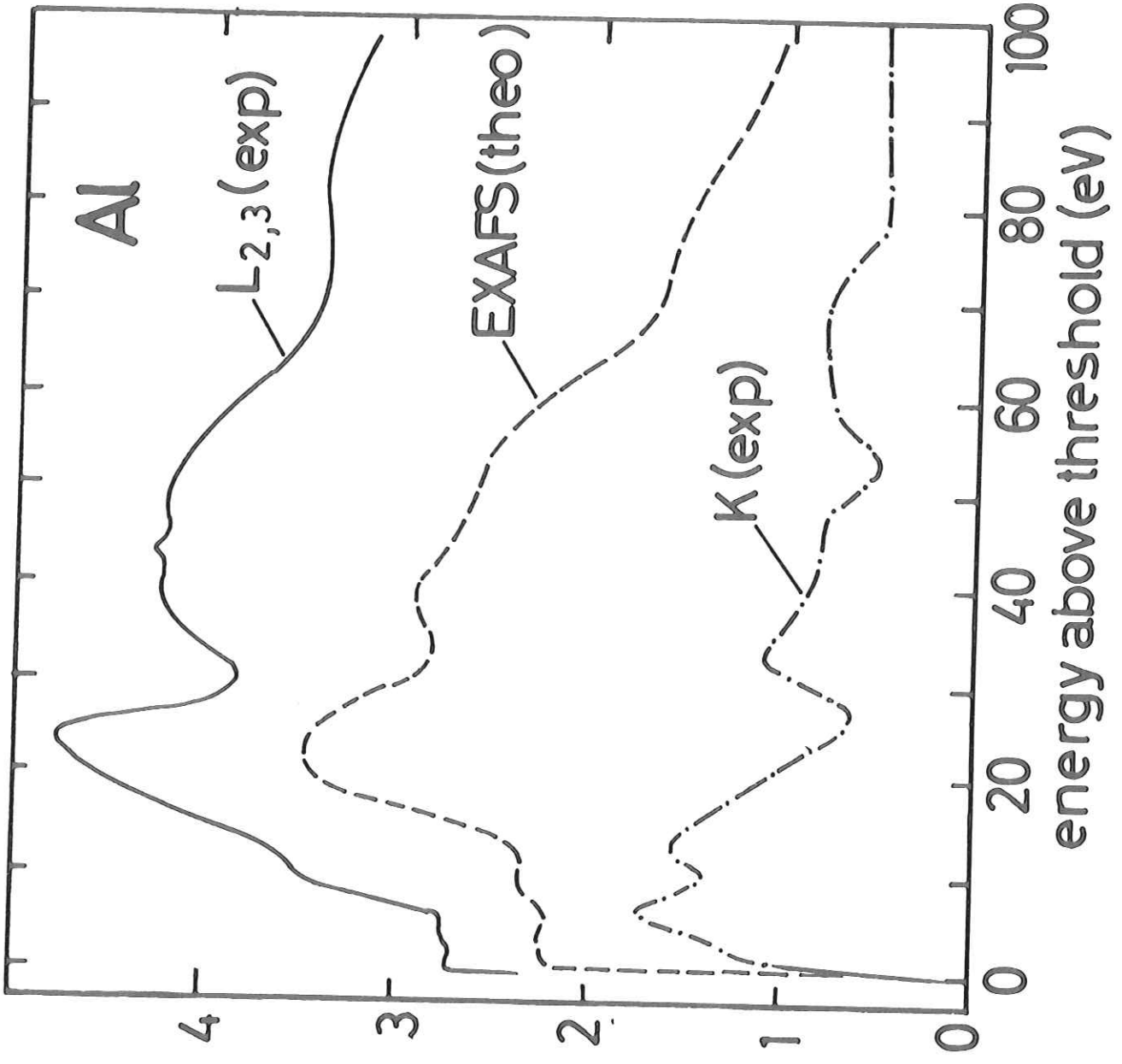
Al
$L_{2,3}$ (exp)
EXAFS (theo)
K (exp)
0
1
2
3
4
0
20
40
60
80
100
energy above threshold (eV)

Fig. 30

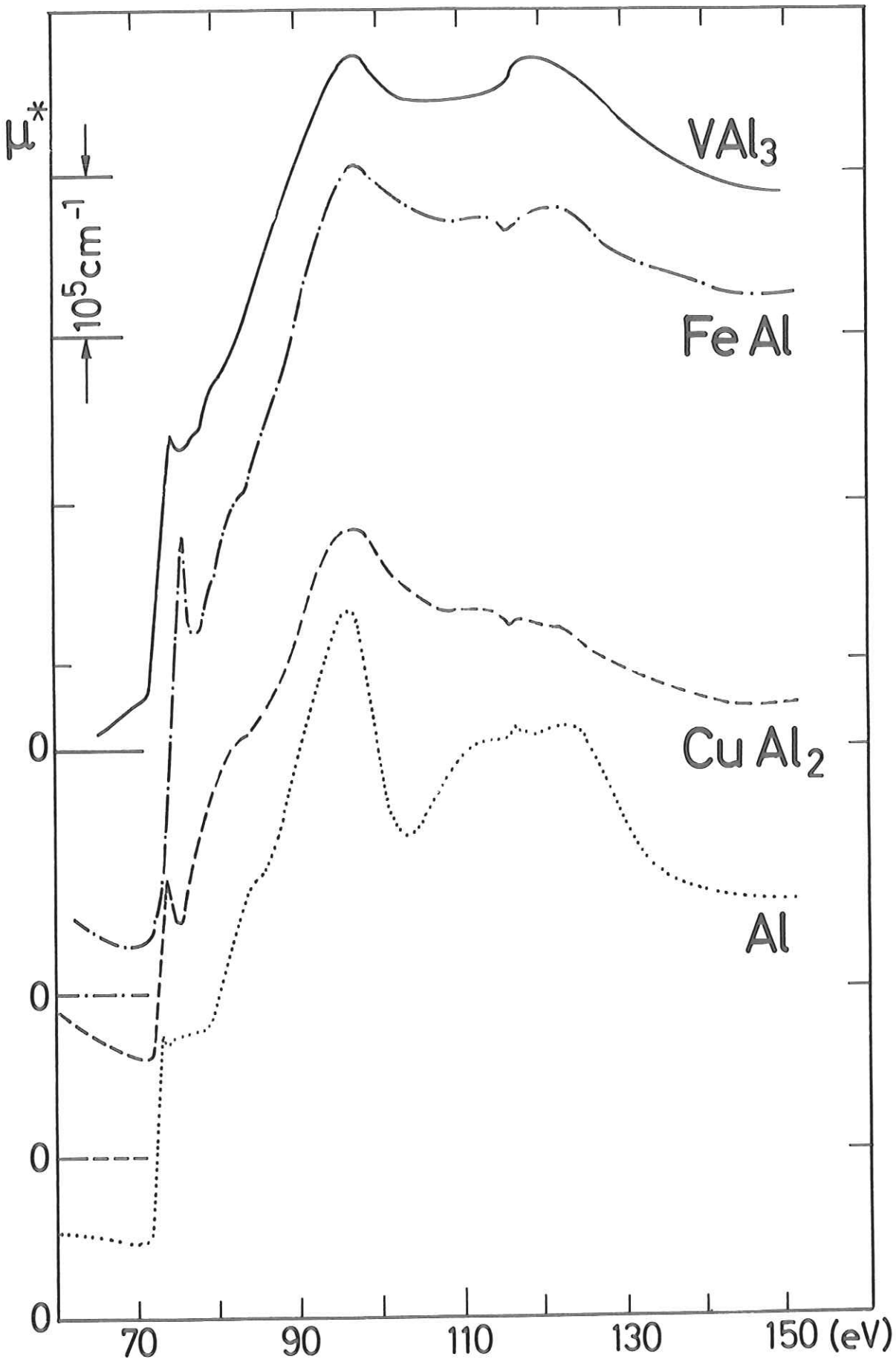

Fig. 31

ABSORPTION COEFFICIENT
ARBITRARY UNITS
Cu Al2
Ni Al3
Ni Al
Fe Al
Fe-Al, 11 %
Au Al2
72.6 eV
70
75
80
Pr Al2
VAl3
Al
V-Al, 41%
V-Al, 28%
V-Al, 16%
72.6 eV
70
75
80
(eV)

Fig. 32

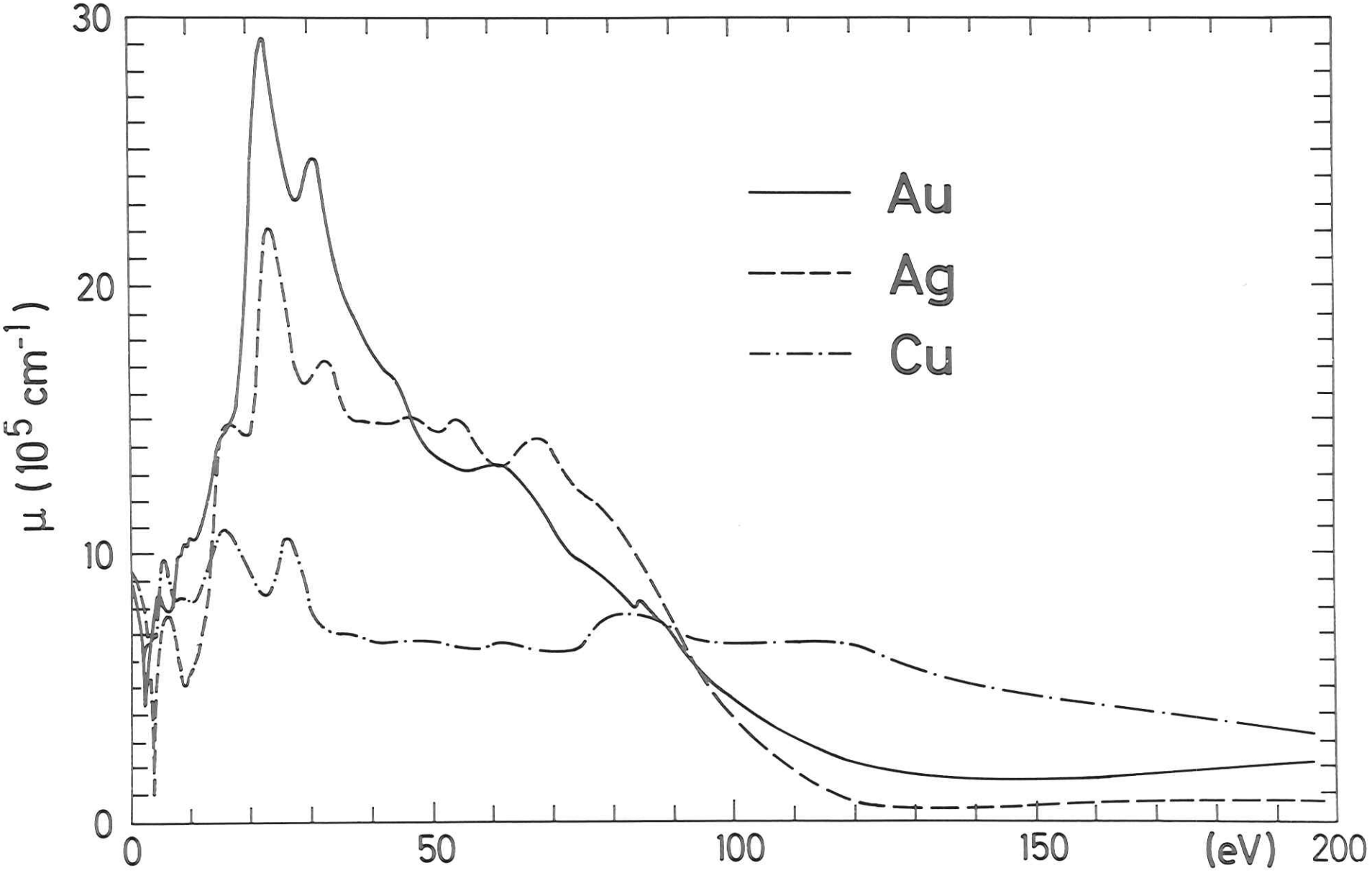

Fig. 33

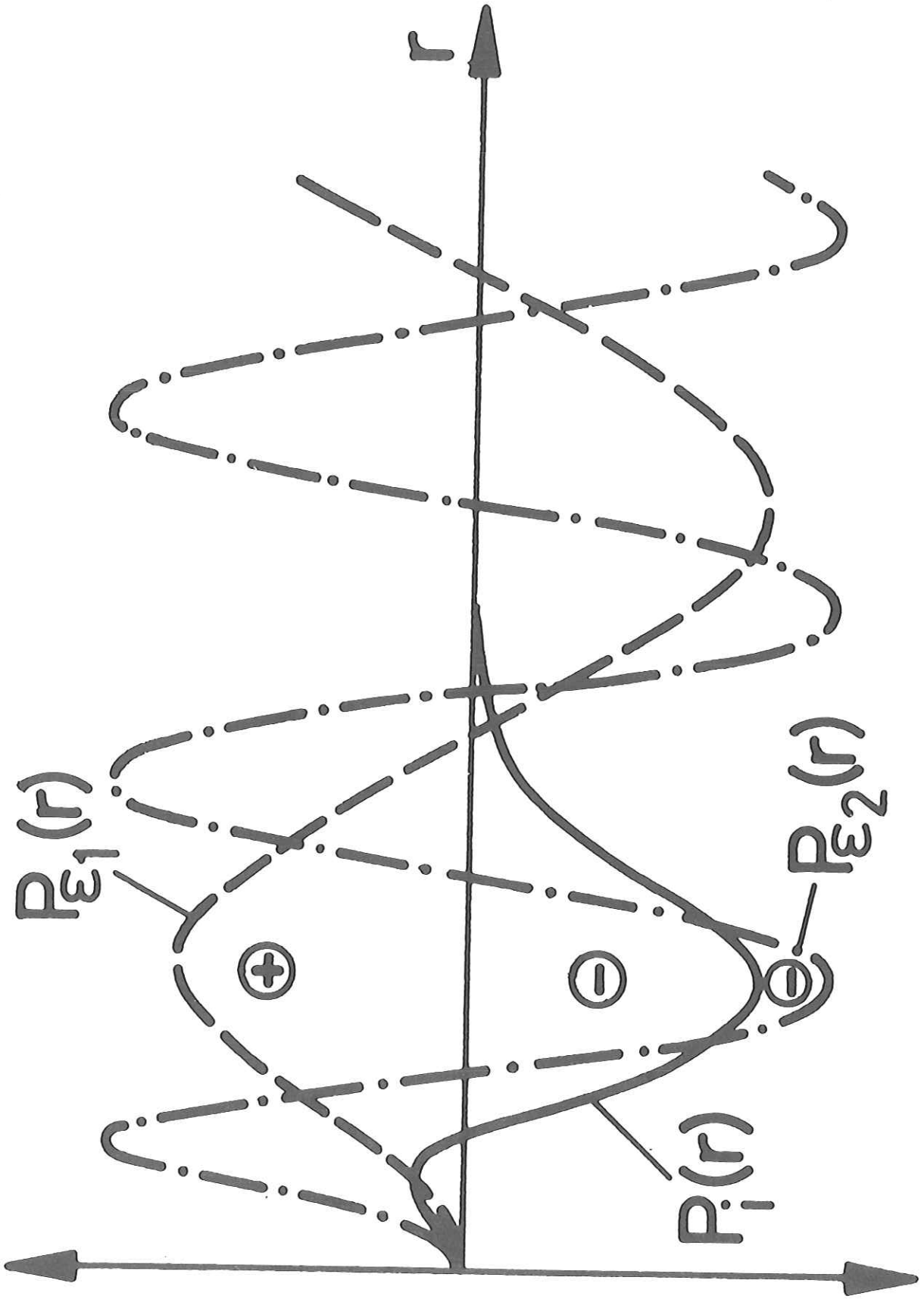

Fig. 34

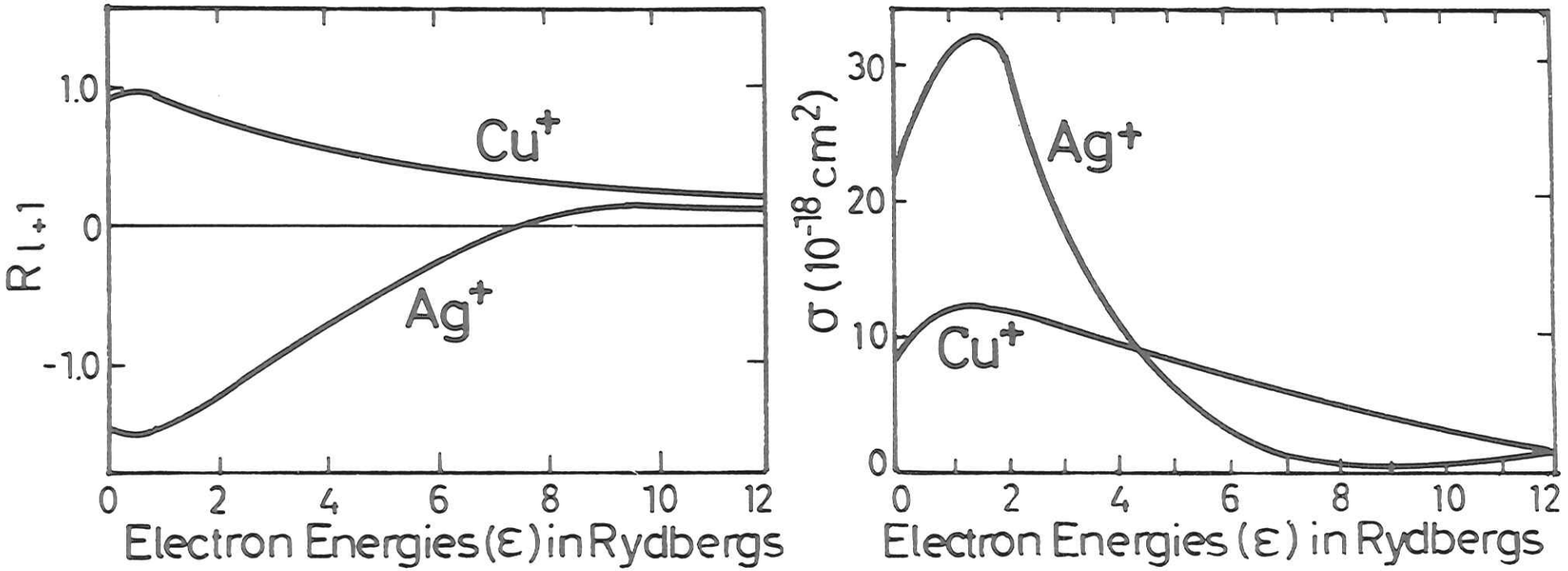
1.0
0
-1.0
R_{l+1}
Cu^+
Ag^+
0
2
4
6
8
10
12
Electron Energies (ε) in Rydbergs
30
20
10
0
$\sigma\ (10^{-18}\ cm^2)$
Ag^+
Cu^+
0
2
4
6
8
10
12
Electron Energies (ε) in Rydbergs

Fig. 35

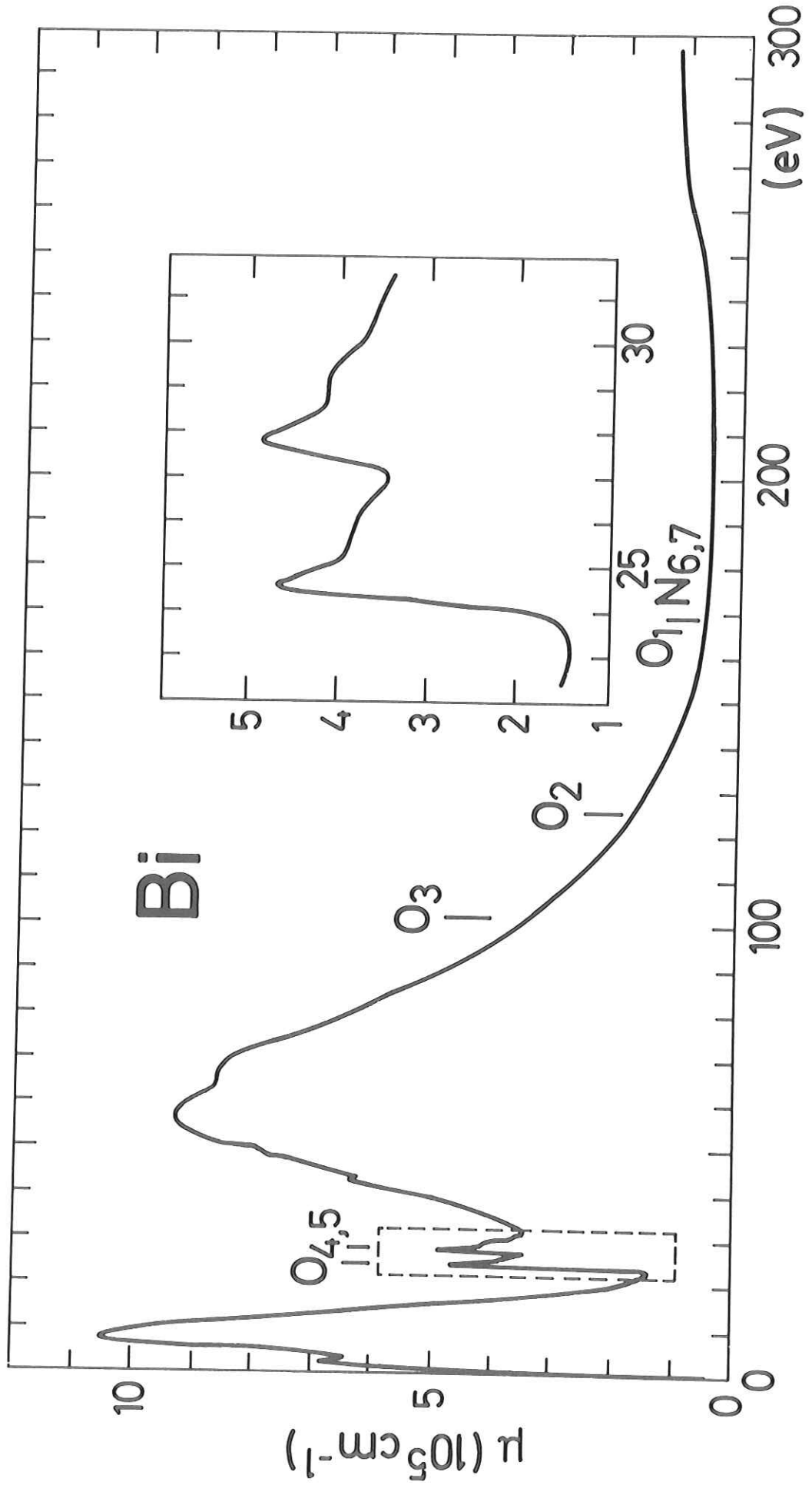

Fig. 36

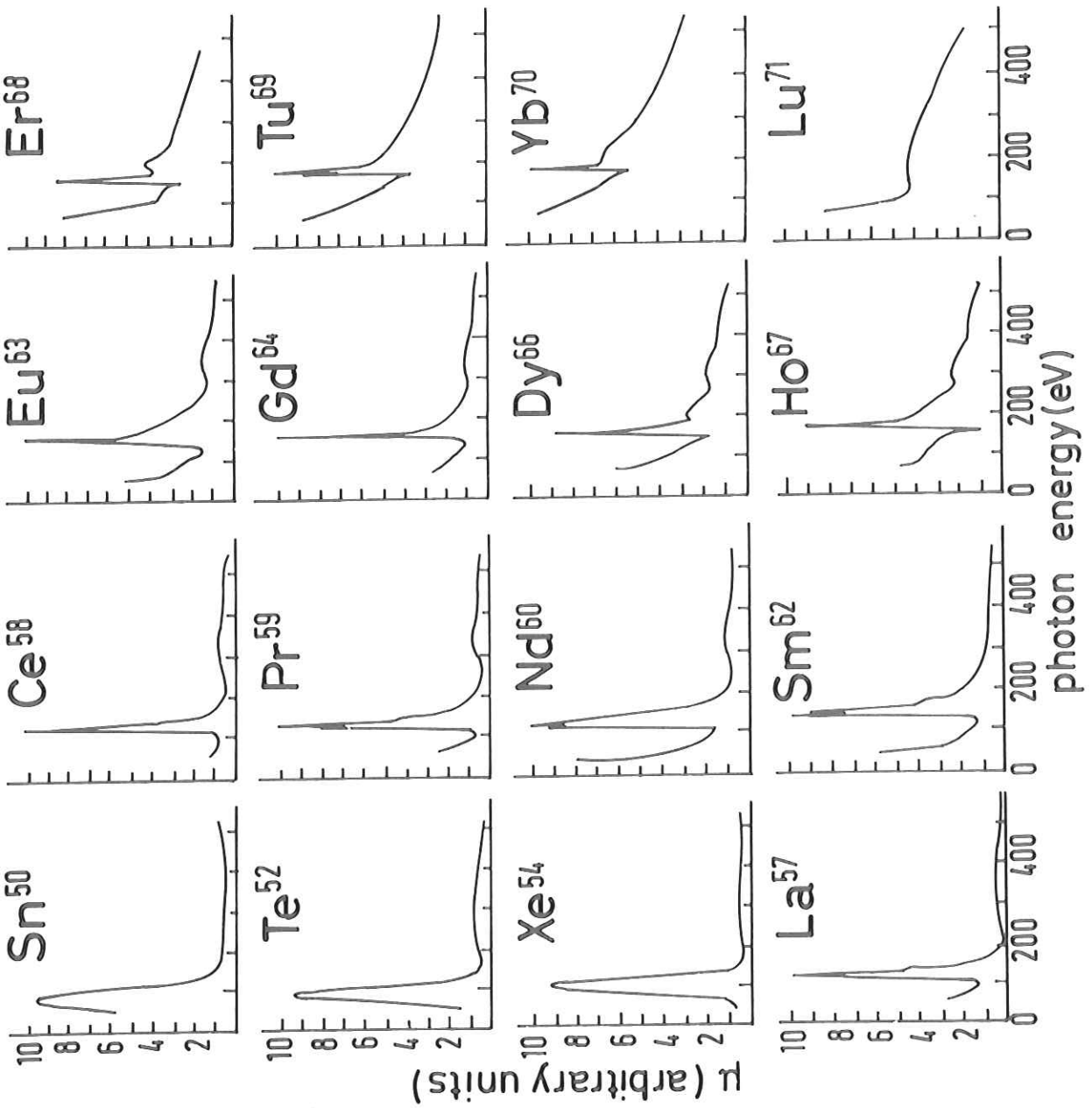
Sn50
Ce58
Eu63
Er68
Te52
Pr59
Gd64
Tu69
Xe54
Nd60
Dy66
Yb70
La57
Sm62
Ho67
Lu71
μ (arbitrary units)
photon energy (eV)
0
200
400
2
4
6
8
10

Fig. 37

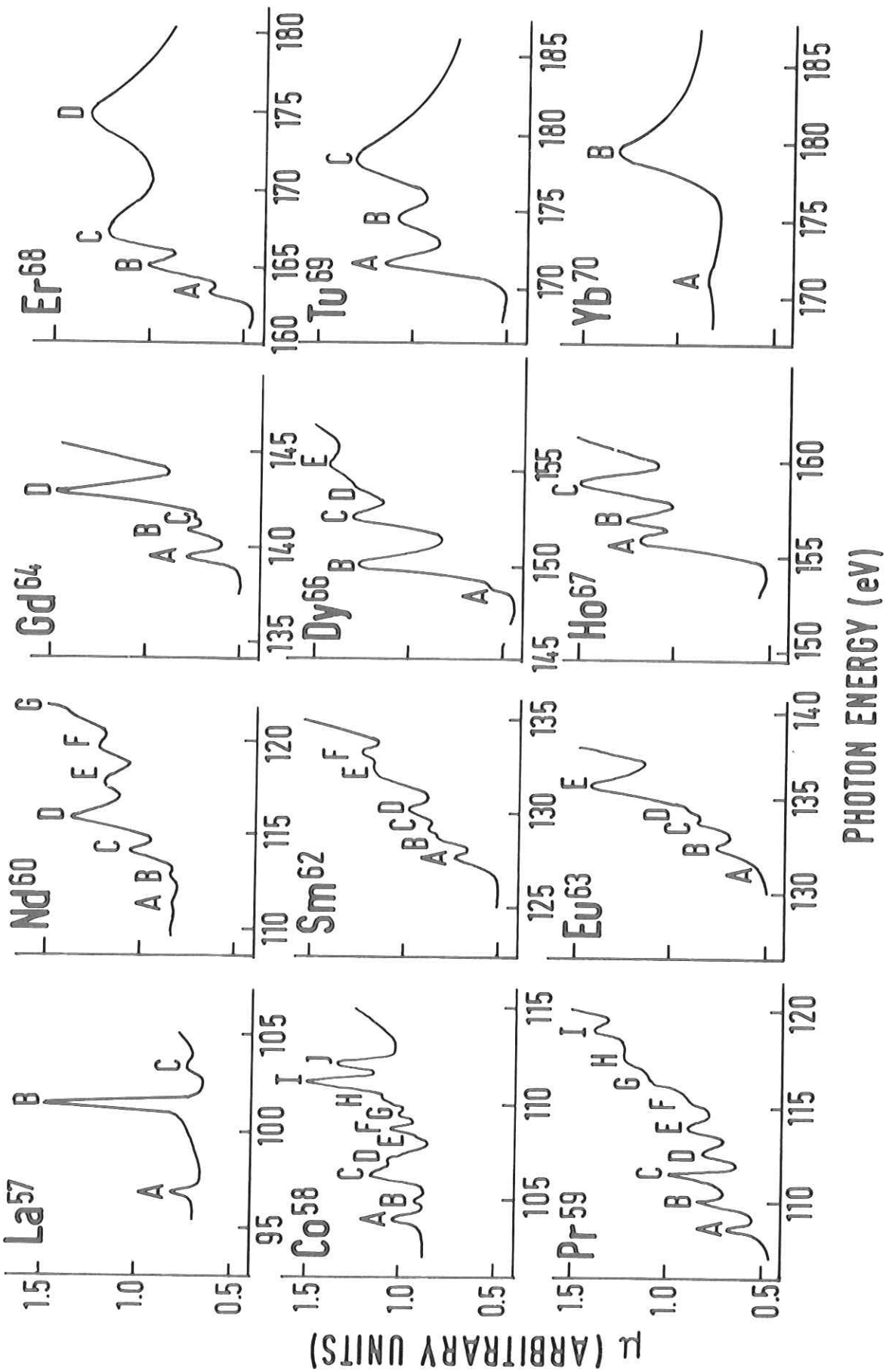
La57
Nd60
Gd64
Er68
Co58
Sm62
Dy66
Tu69
Pr59
Eu63
Ho67
Yb70
μ (ARBITRARY UNITS)
PHOTON ENERGY (eV)

Fig. 38

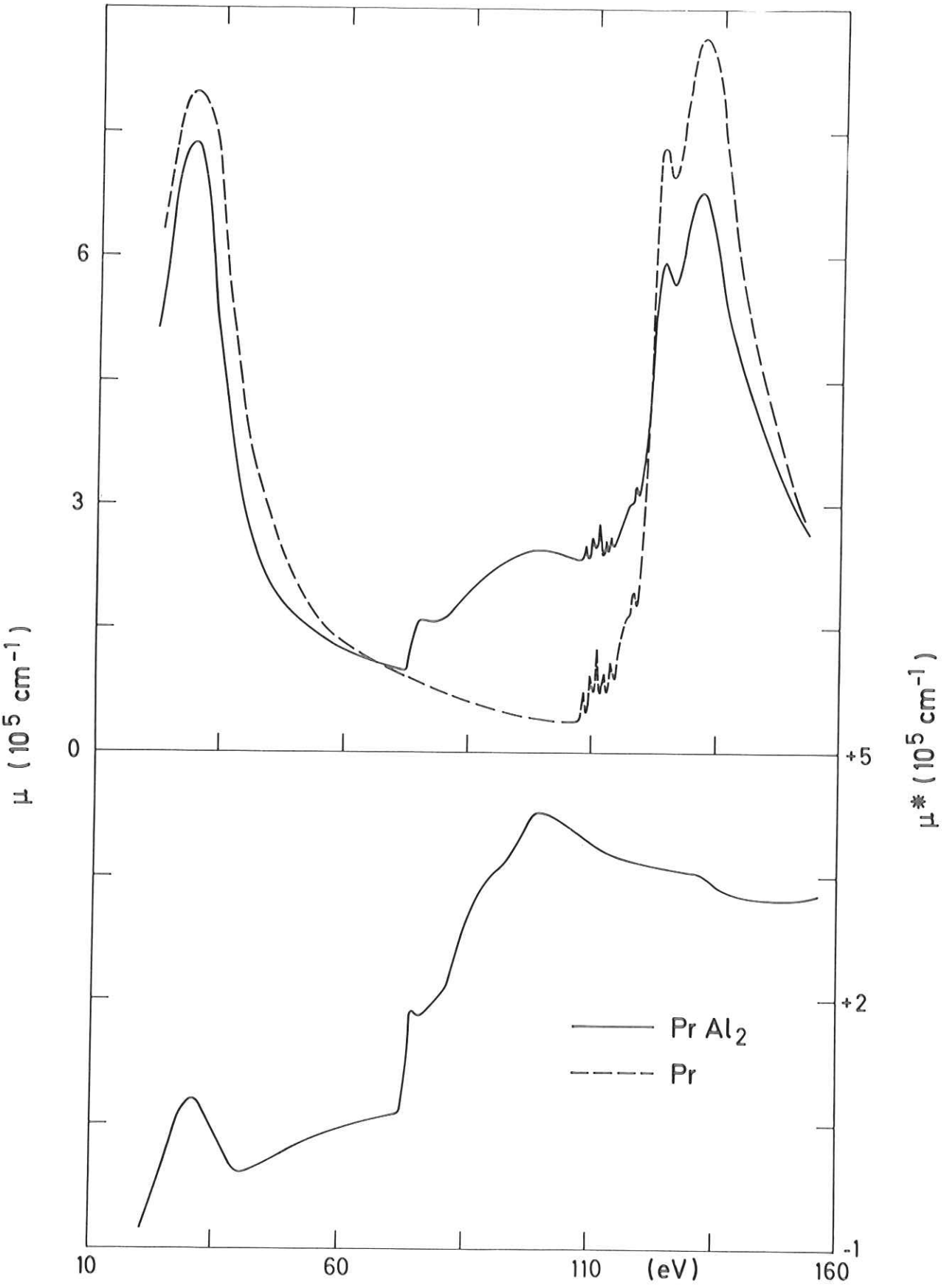

Fig. 39

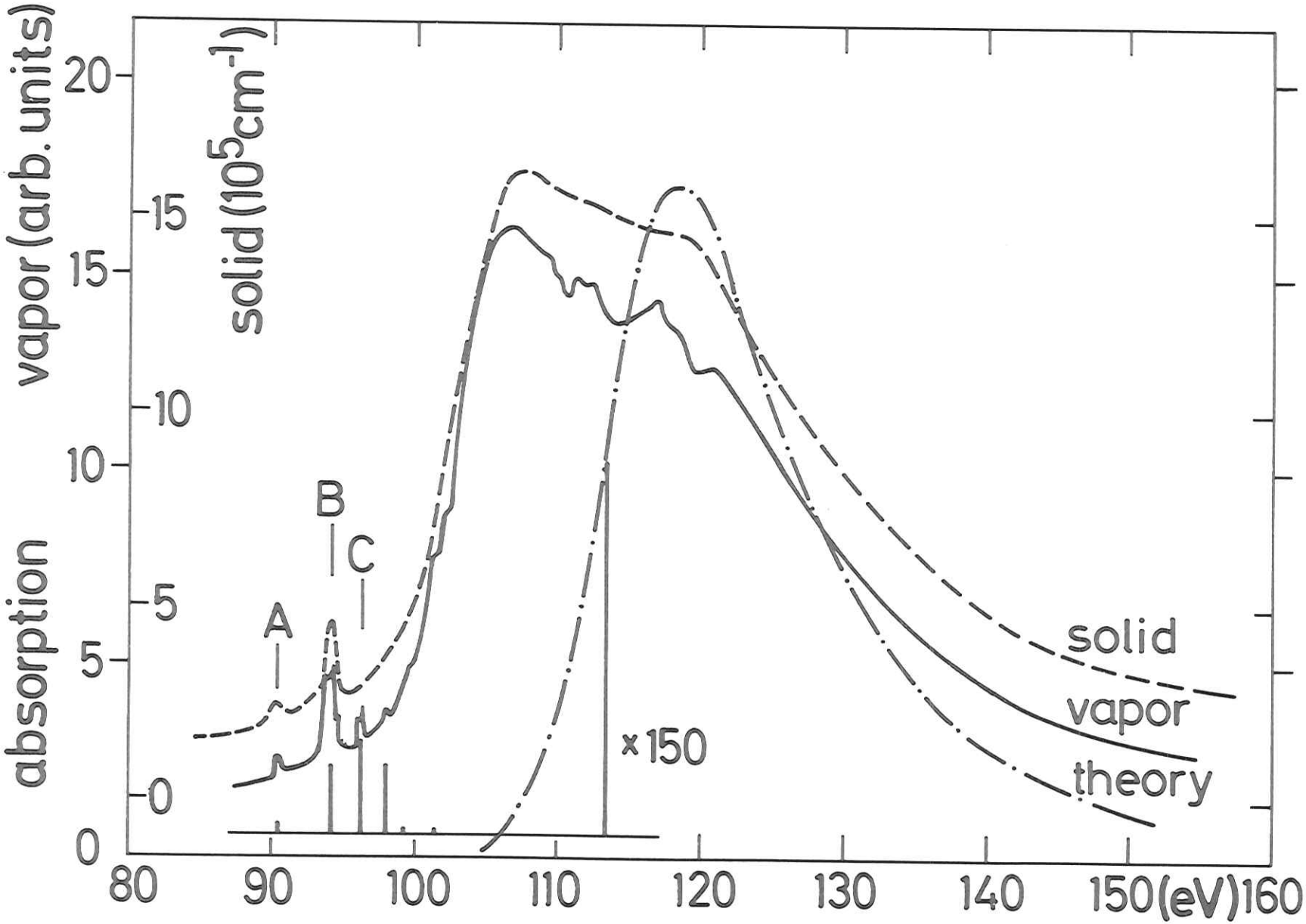
absorption
vapor (arb. units)
solid (10^5cm^{-1})
0
5
10
15
20
0
5
10
15
A
B
C
×150
solid
vapor
theory
80
90
100
110
120
130
140
150(eV)160

Fig. 40

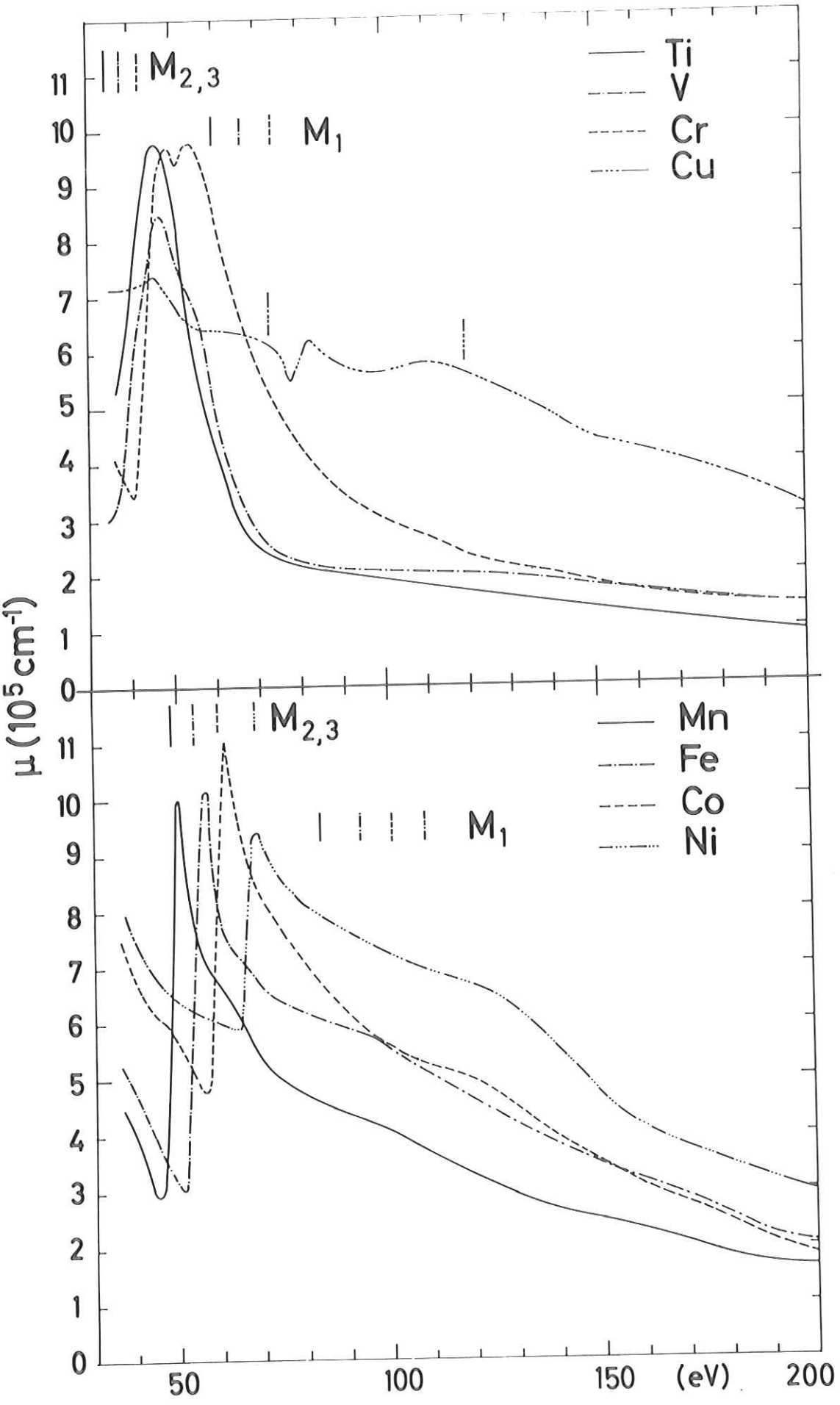
$M_{2,3}$
M_1
Ti
V
Cr
Cu
$M_{2,3}$
M_1
Mn
Fe
Co
Ni
μ (10^5 cm^{-1})
0
1
2
3
4
5
6
7
8
9
10
11
50
100
150
(eV)
200

Fig. 41

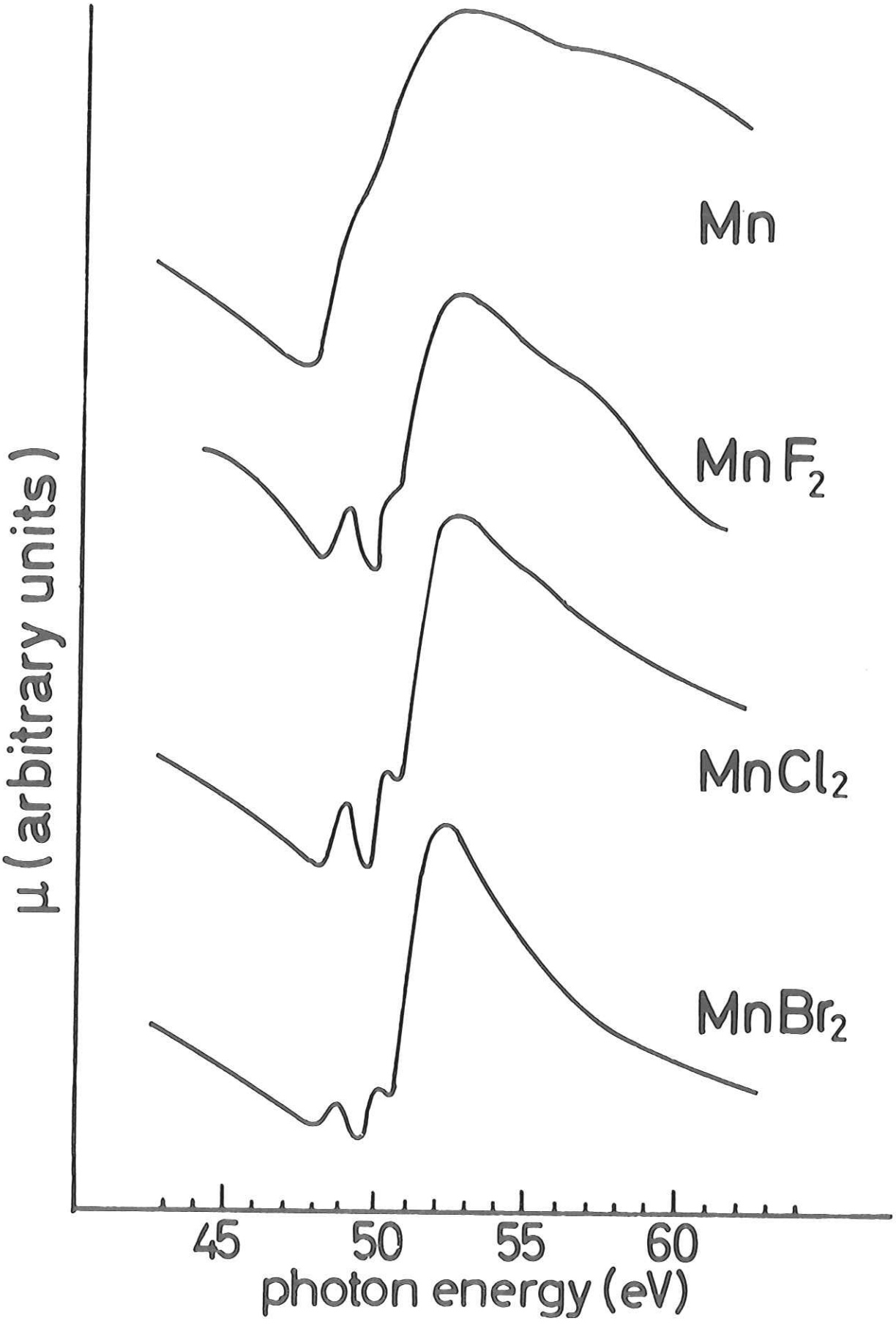
Mn
MnF2
MnCl2
MnBr2
μ (arbitrary units)
45
50
55
60
photon energy (eV)

Fig. 42

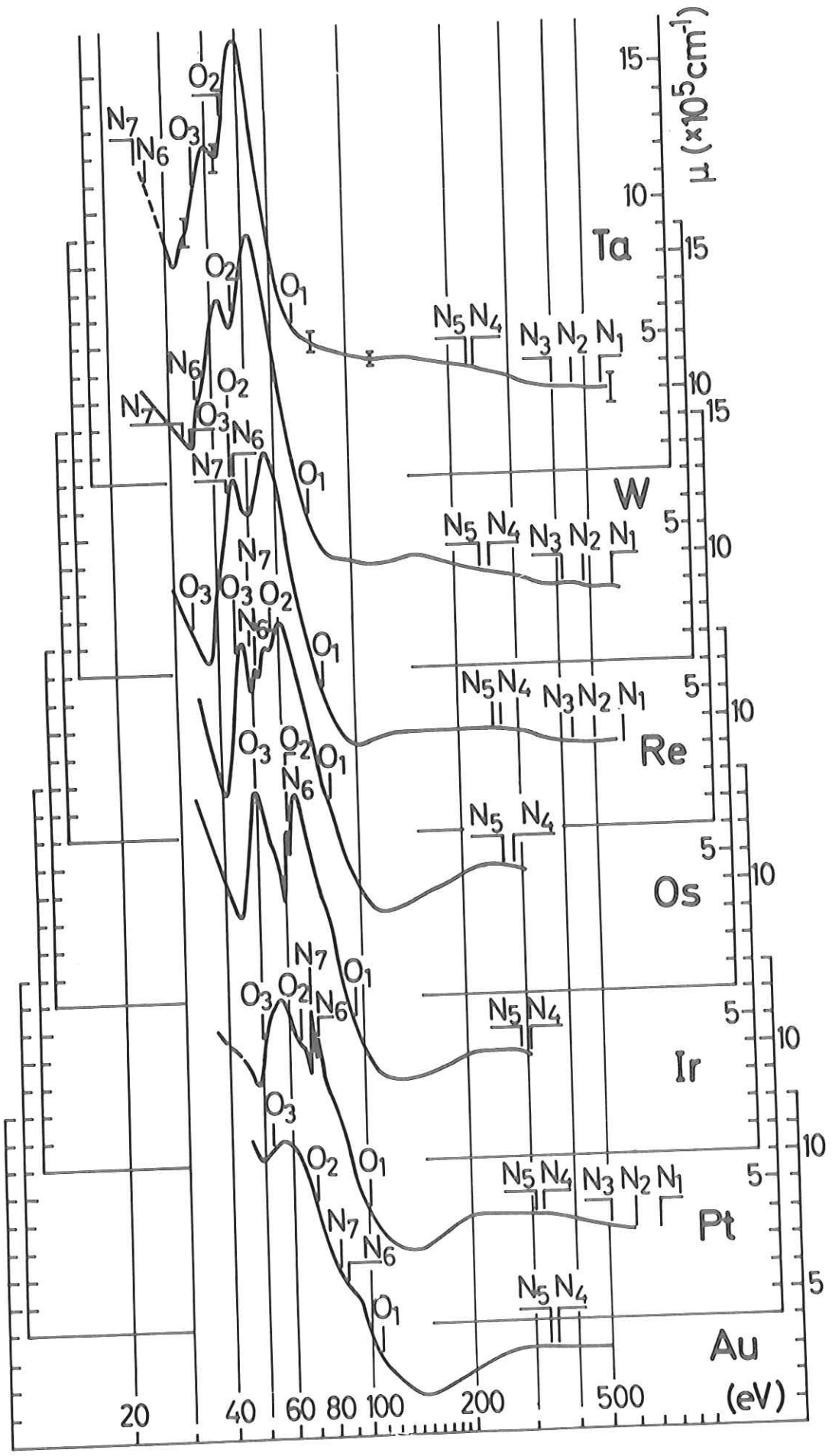

Fig. 43

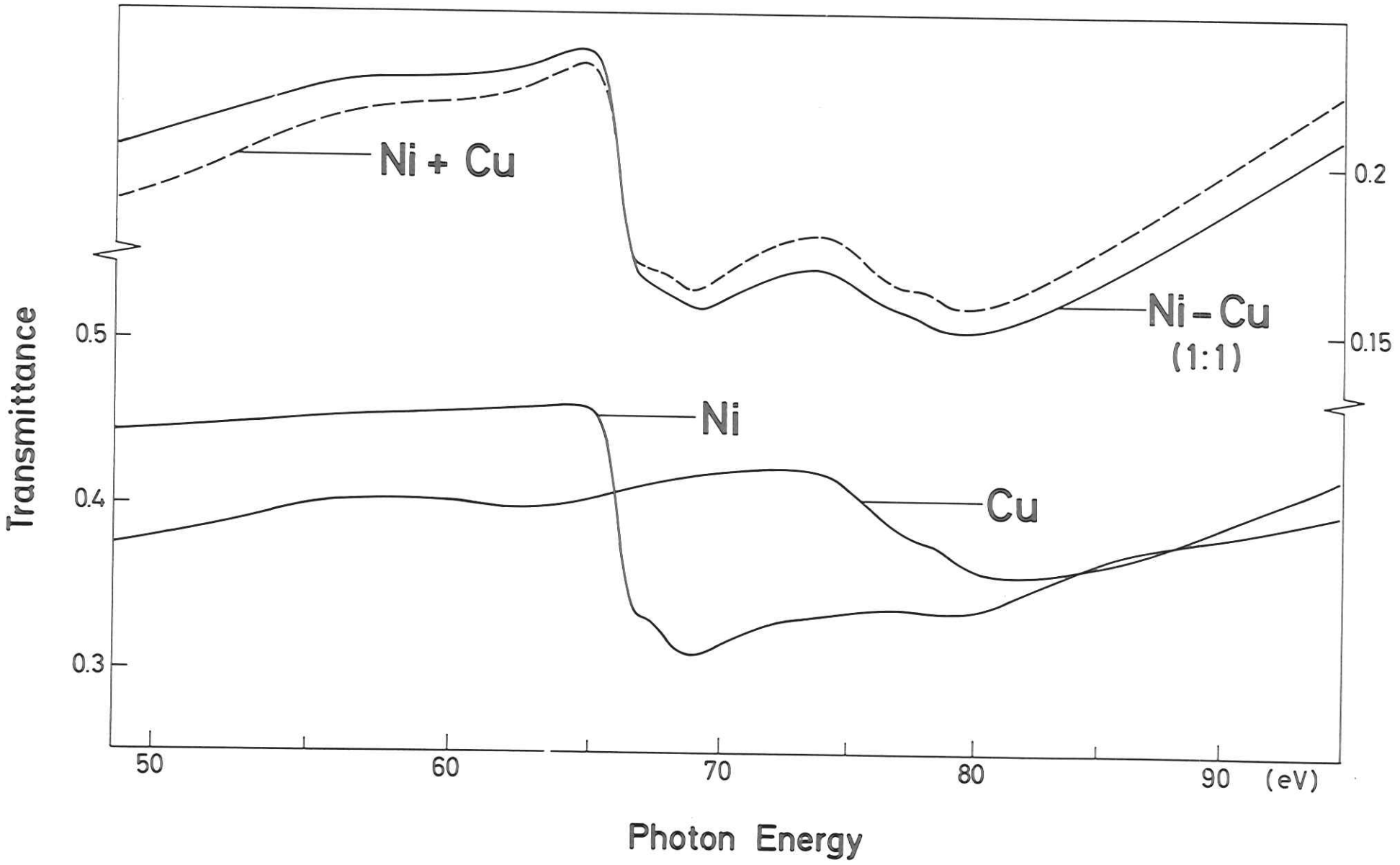
Ni + Cu
Ni – Cu
(1:1)
Ni
Cu
Transmittance
0.5
0.4
0.3
0.2
0.15
50
60
70
80
90
(eV)
Photon Energy

Fig. 44

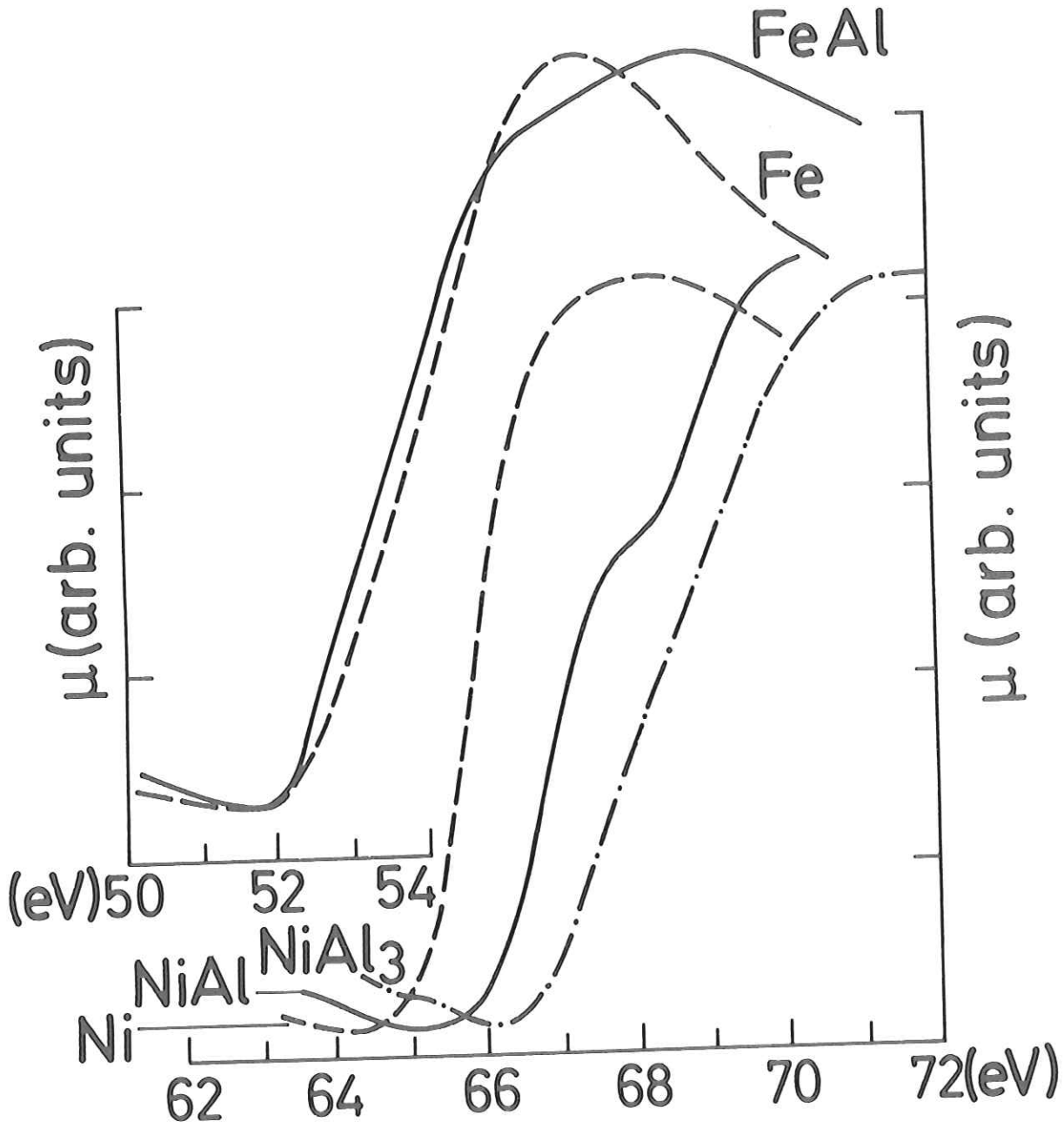
FeAl
Fe
μ(arb. units)
μ (arb. units)
(eV)50
52
54
NiAl
NiAl3
Ni
62
64
66
68
70
72(eV)

Fig. 45

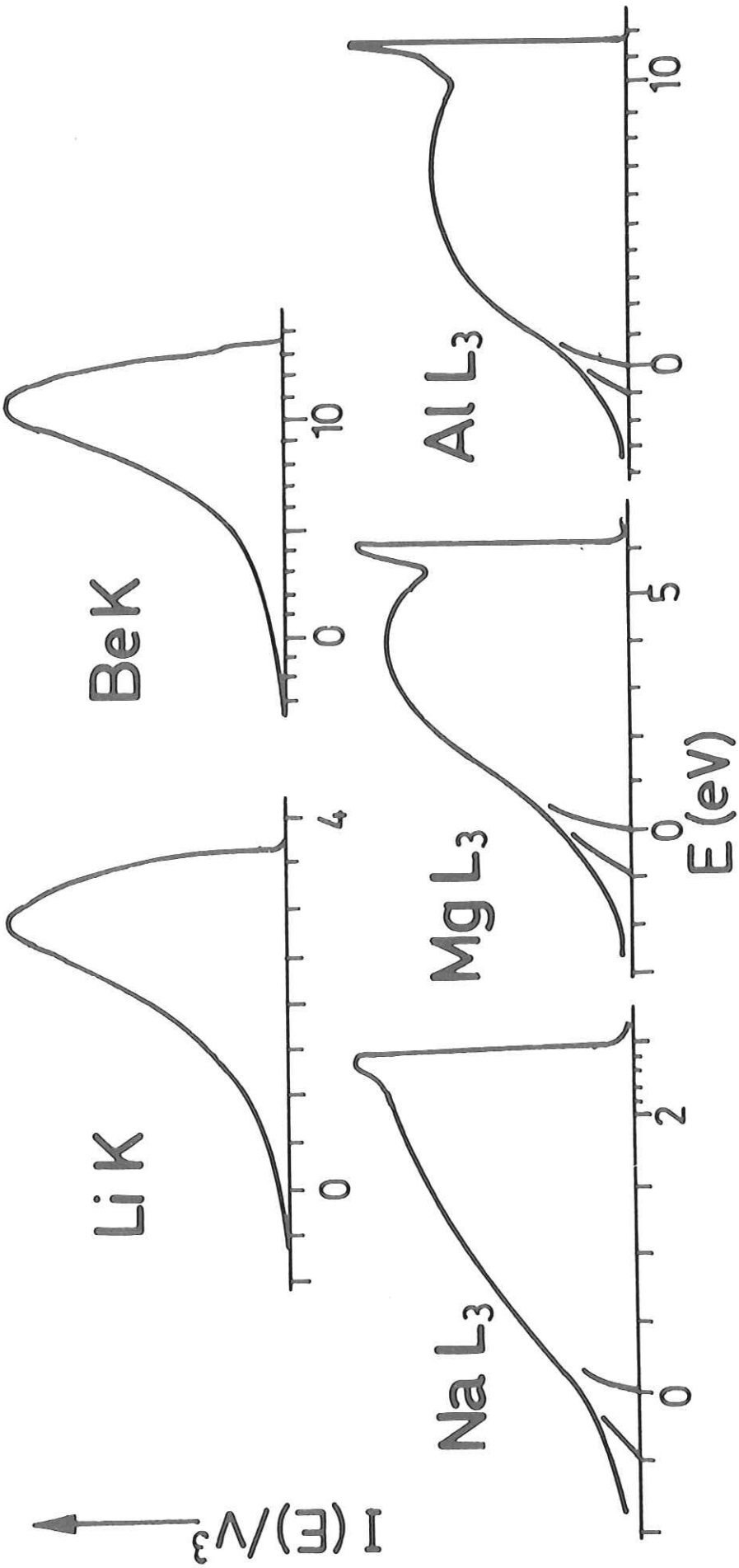

Fig. 46

Li
emission
A
μ (arb. units)
55
56
57 (eV)
Be
A
B
μ (10⁵cm⁻¹)
112
113
114
115
116(eV)
Mg
A
B
μ (arb. units)
50
51
52 (eV)
Al
A
B
μ (10⁵cm⁻¹)
72.5
73.0
73.5
74.0(eV)

Fig. 47

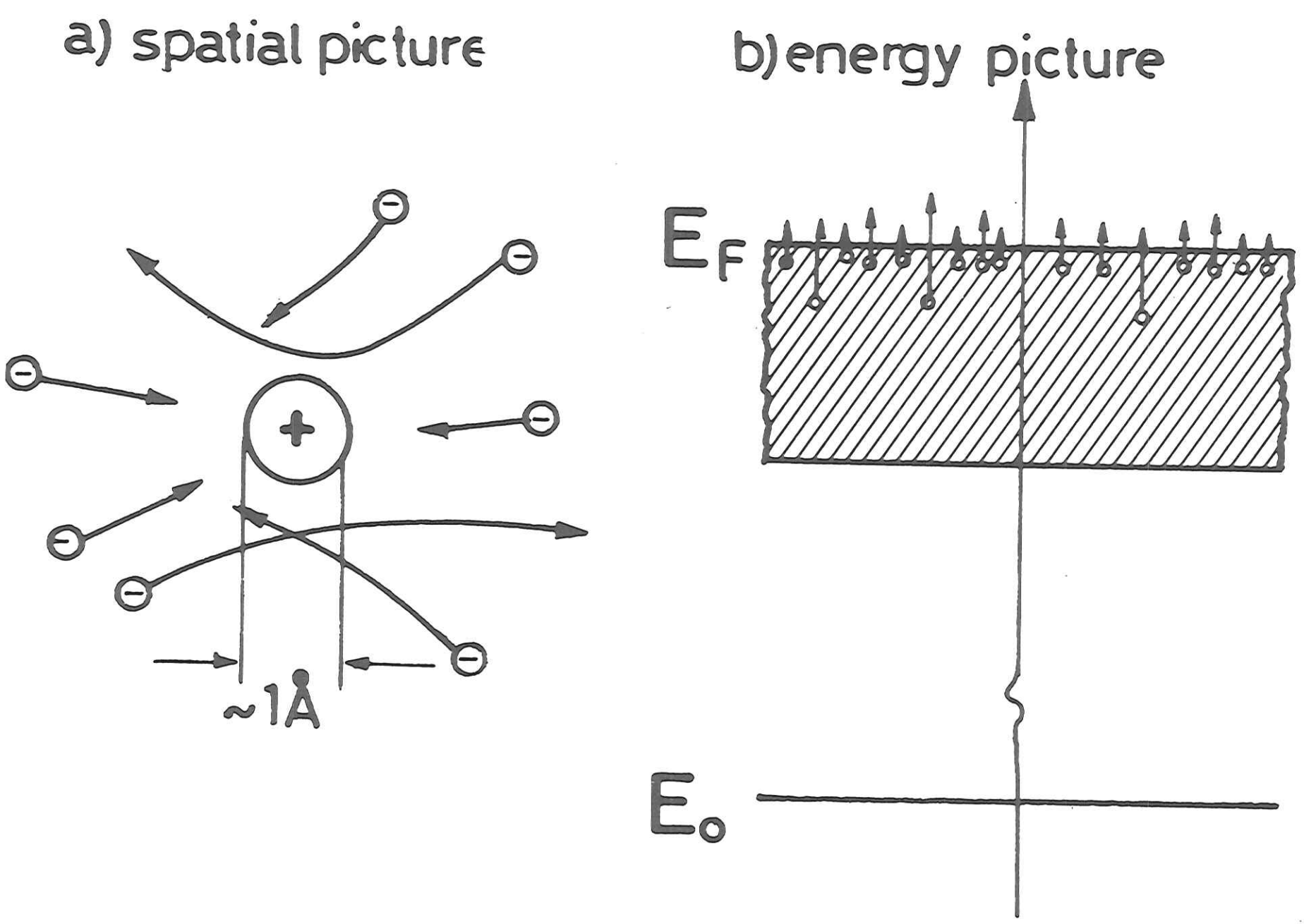

Fig. 48

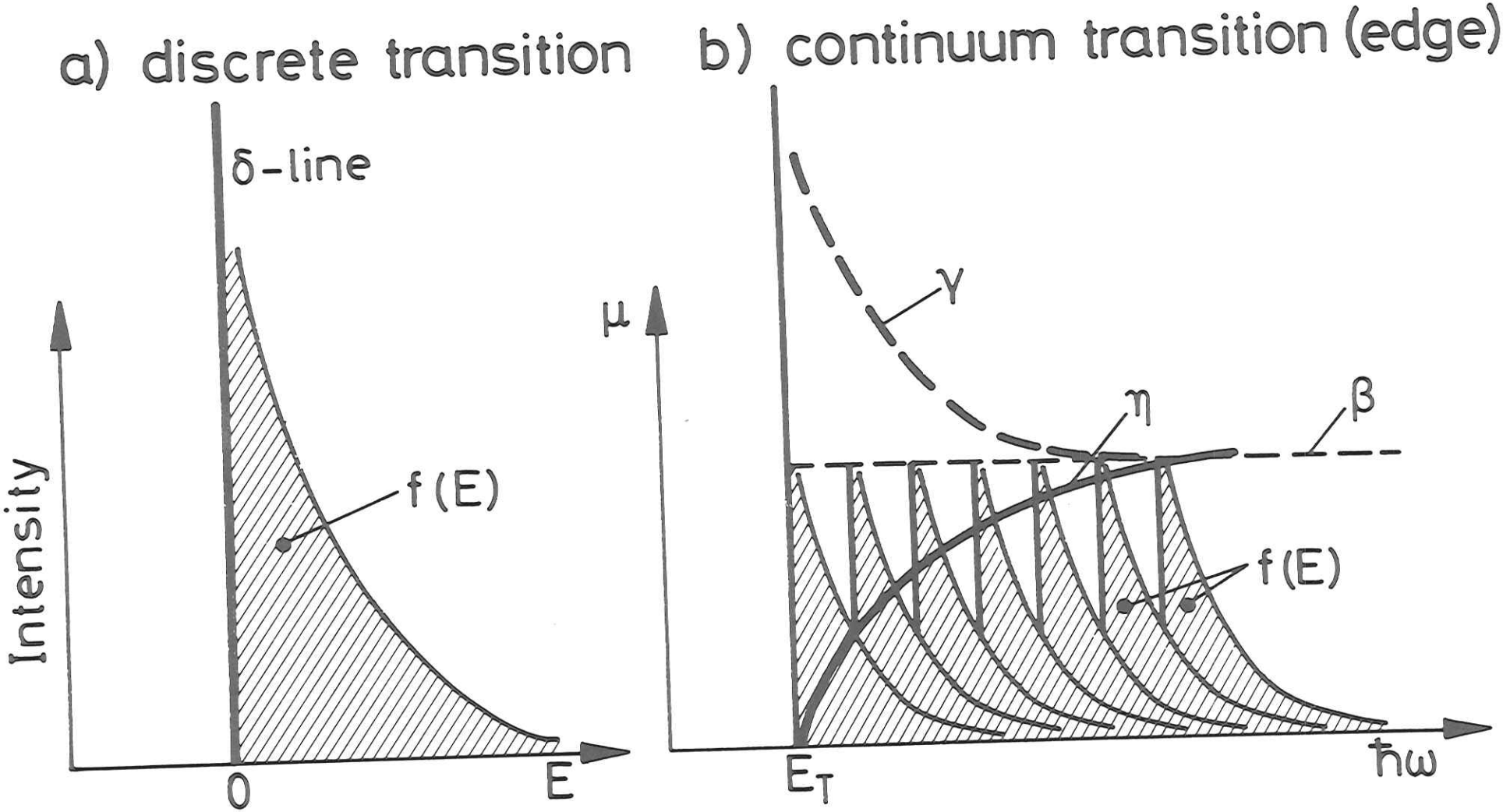
a) discrete transition
δ-line
f(E)
Intensity
0
E
b) continuum transition (edge)
μ
γ
η
β
f(E)
E_T
ħω

Fig. 49

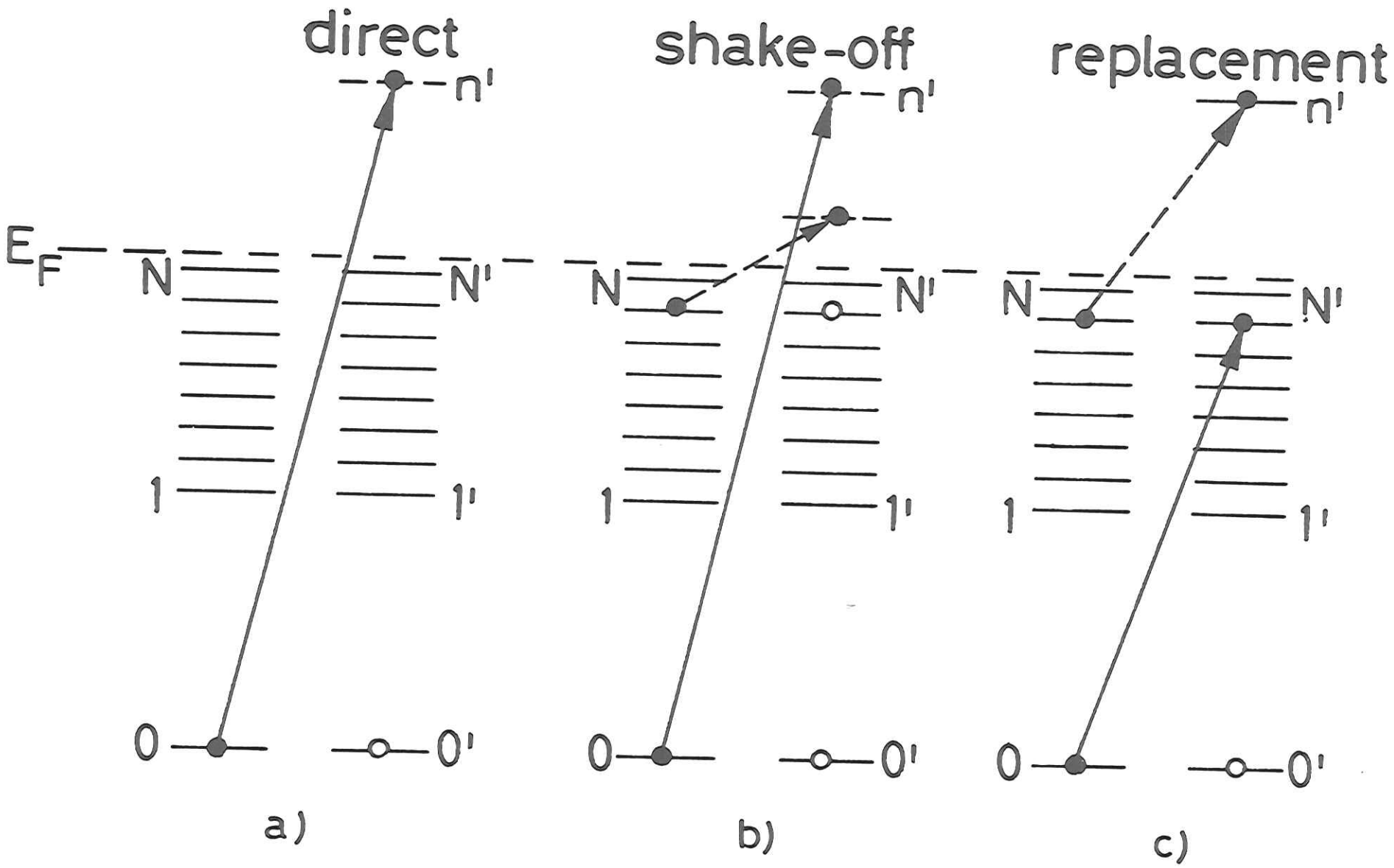

Fig. 50

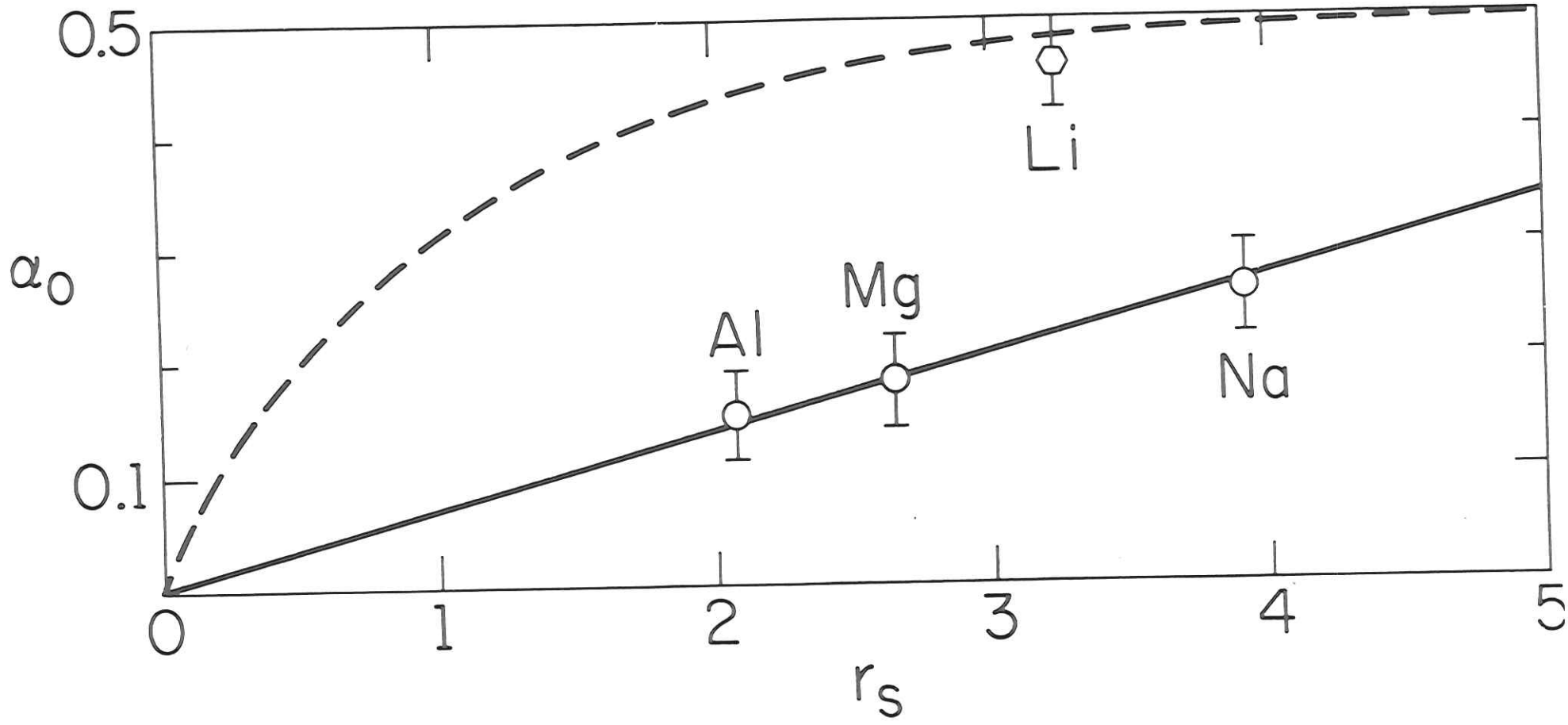

Fig. 51

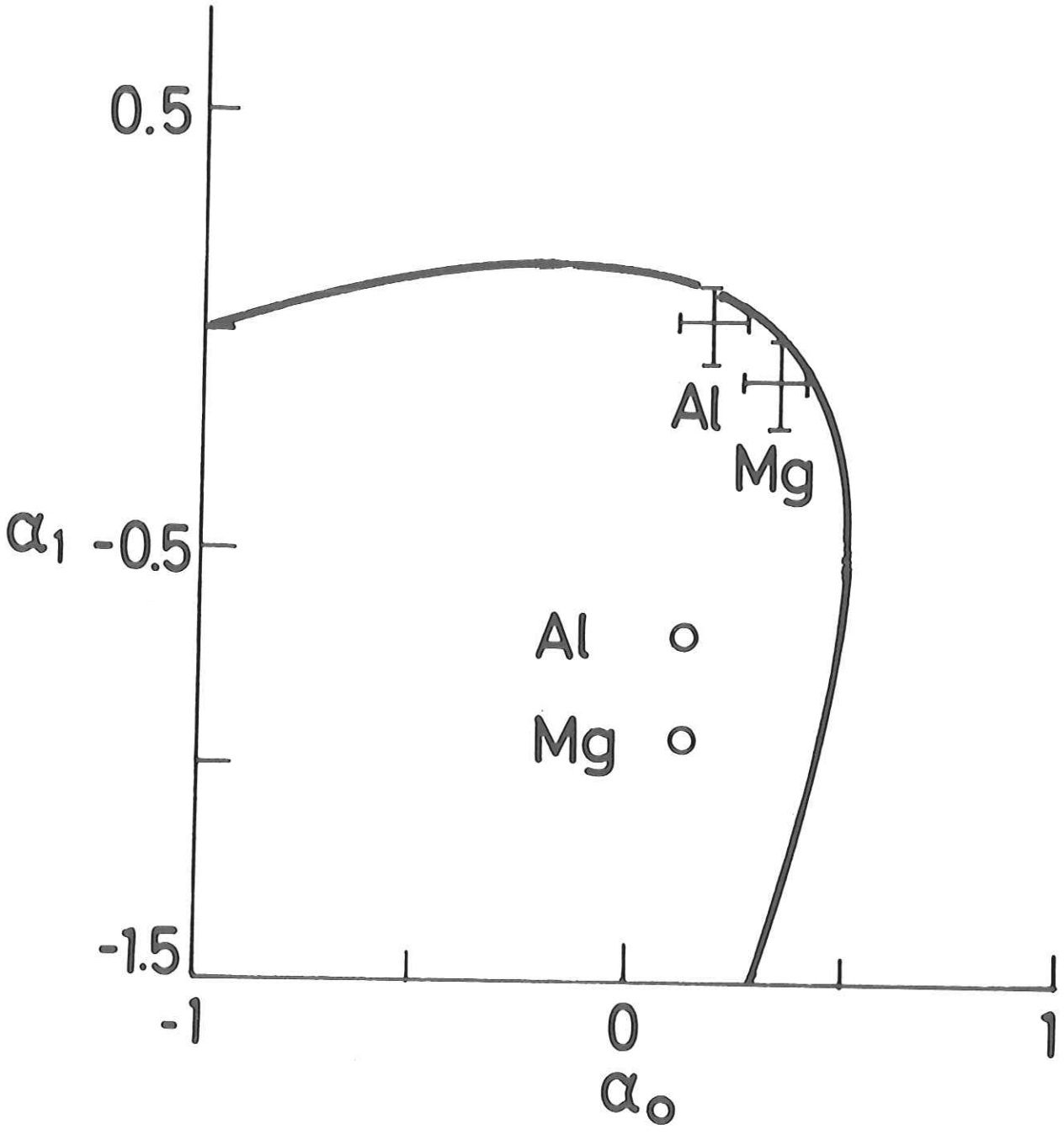

Fig. 52

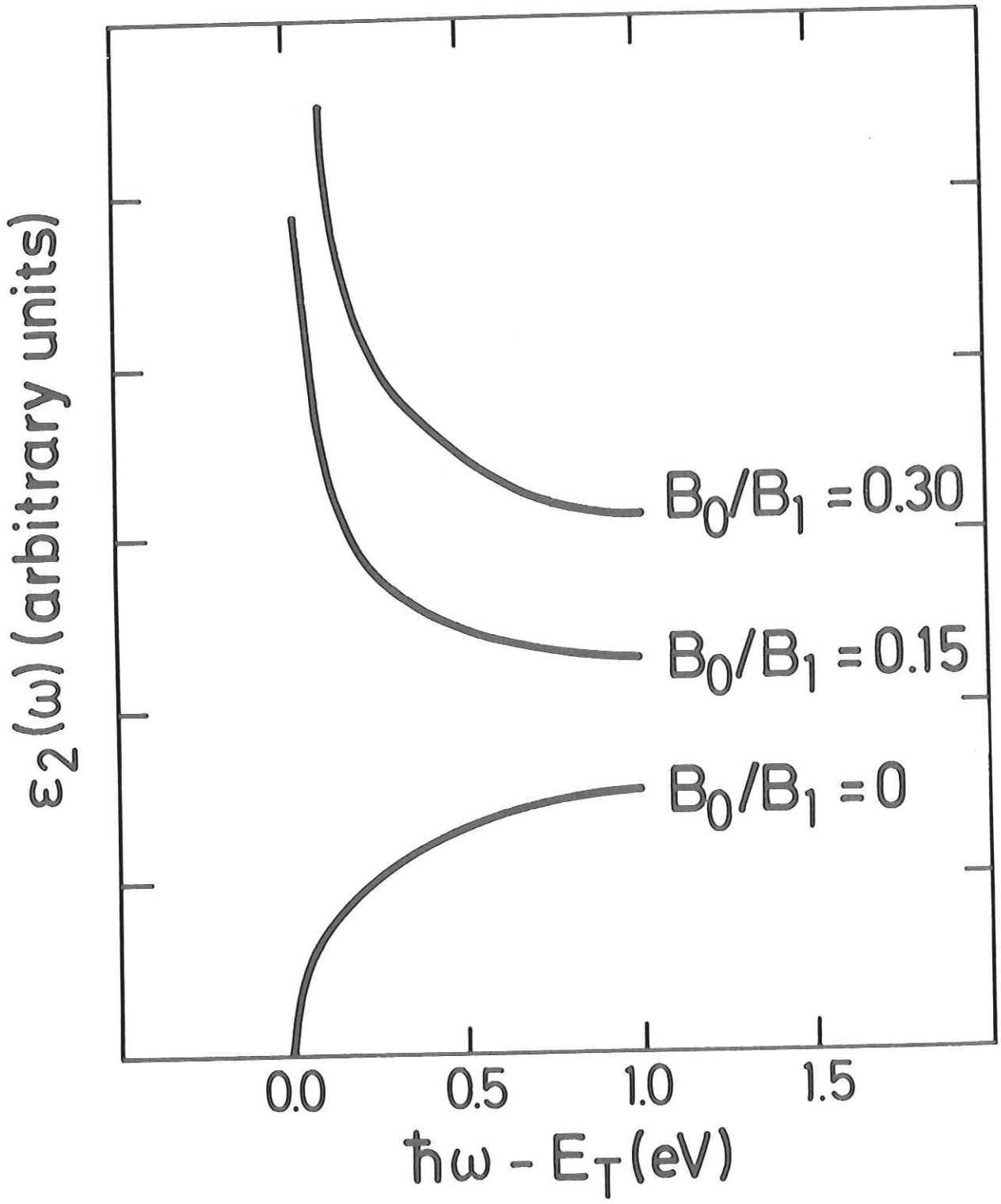
$\varepsilon_2(\omega)$ (arbitrary units)
$B_0/B_1 = 0.30$
$B_0/B_1 = 0.15$
$B_0/B_1 = 0$
0.0
0.5
1.0
1.5
$\hbar\omega - E_T$ (eV)

Fig. 53

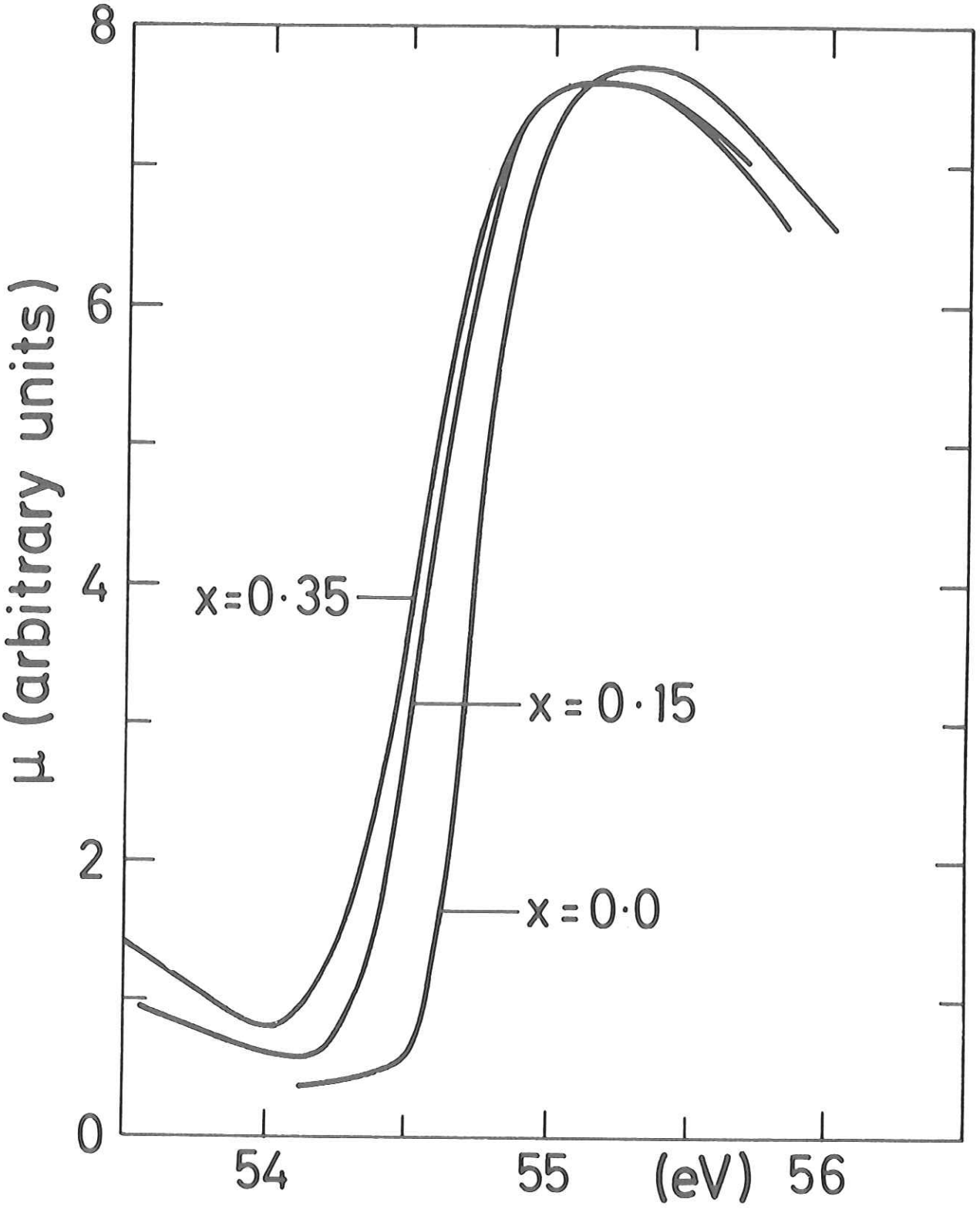

Fig. 54

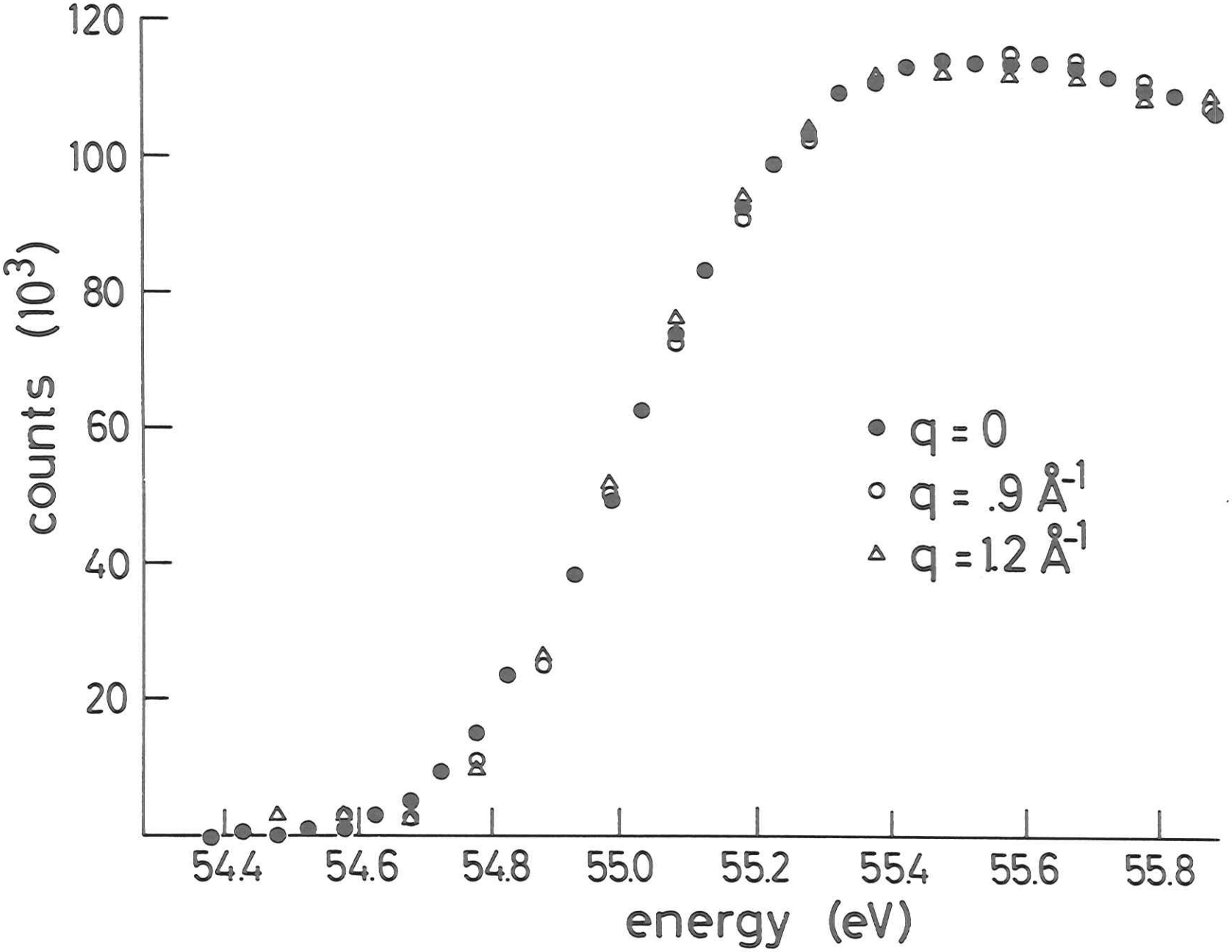
120
100
80
60
40
20
counts (10^3)
54.4
54.6
54.8
55.0
55.2
55.4
55.6
55.8
energy (eV)
q = 0
q = .9 Å^{-1}
q = 1.2 Å^{-1}

Fig. 55

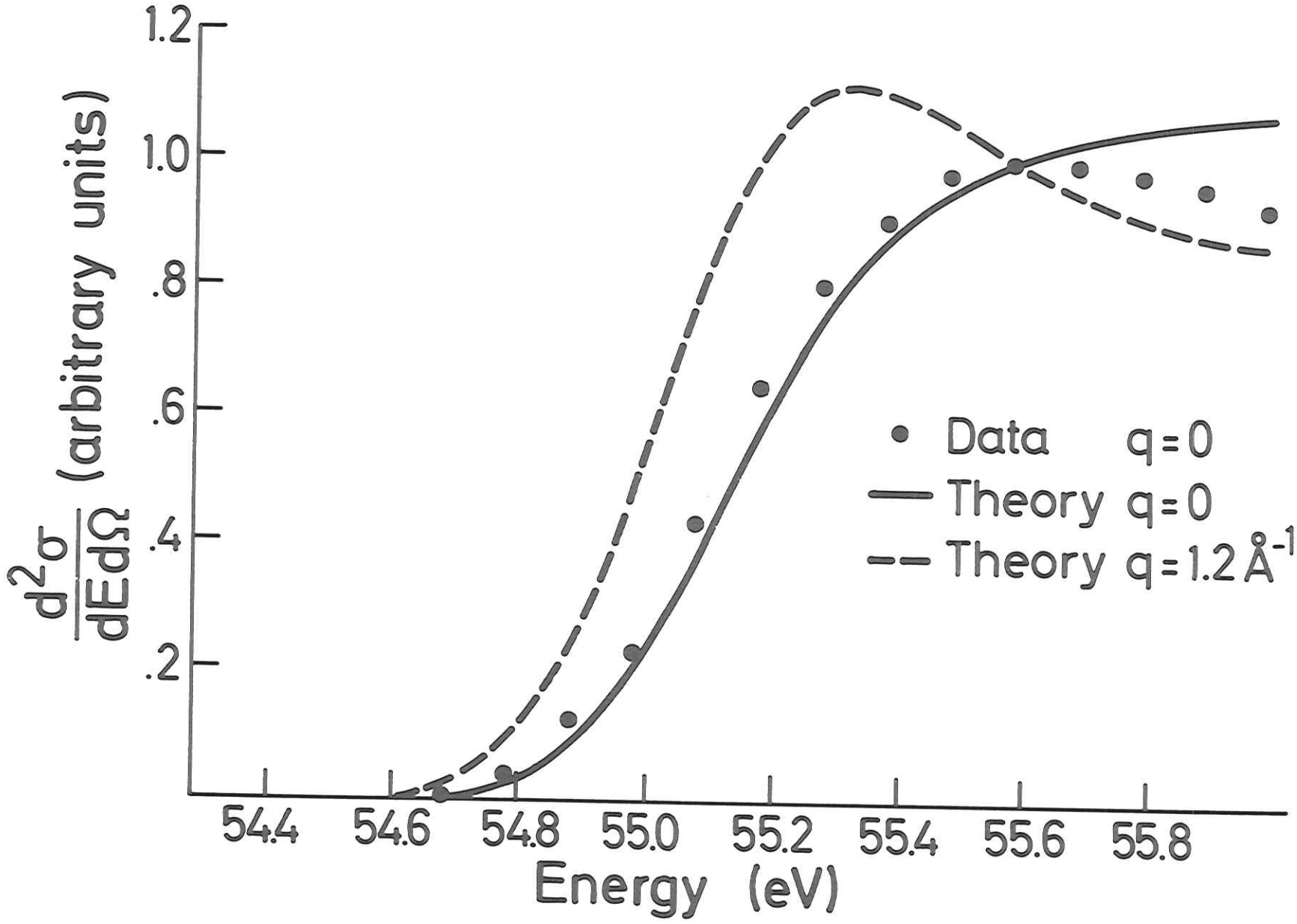
1.2
1.0
.8
.6
.4
.2
$\frac{d^2\sigma}{dEd\Omega}$ (arbitrary units)
54.4
54.6
54.8
55.0
55.2
55.4
55.6
55.8
Energy (eV)
Data q=0
Theory q=0
Theory q=1.2 Å^{-1}

Fig. 56

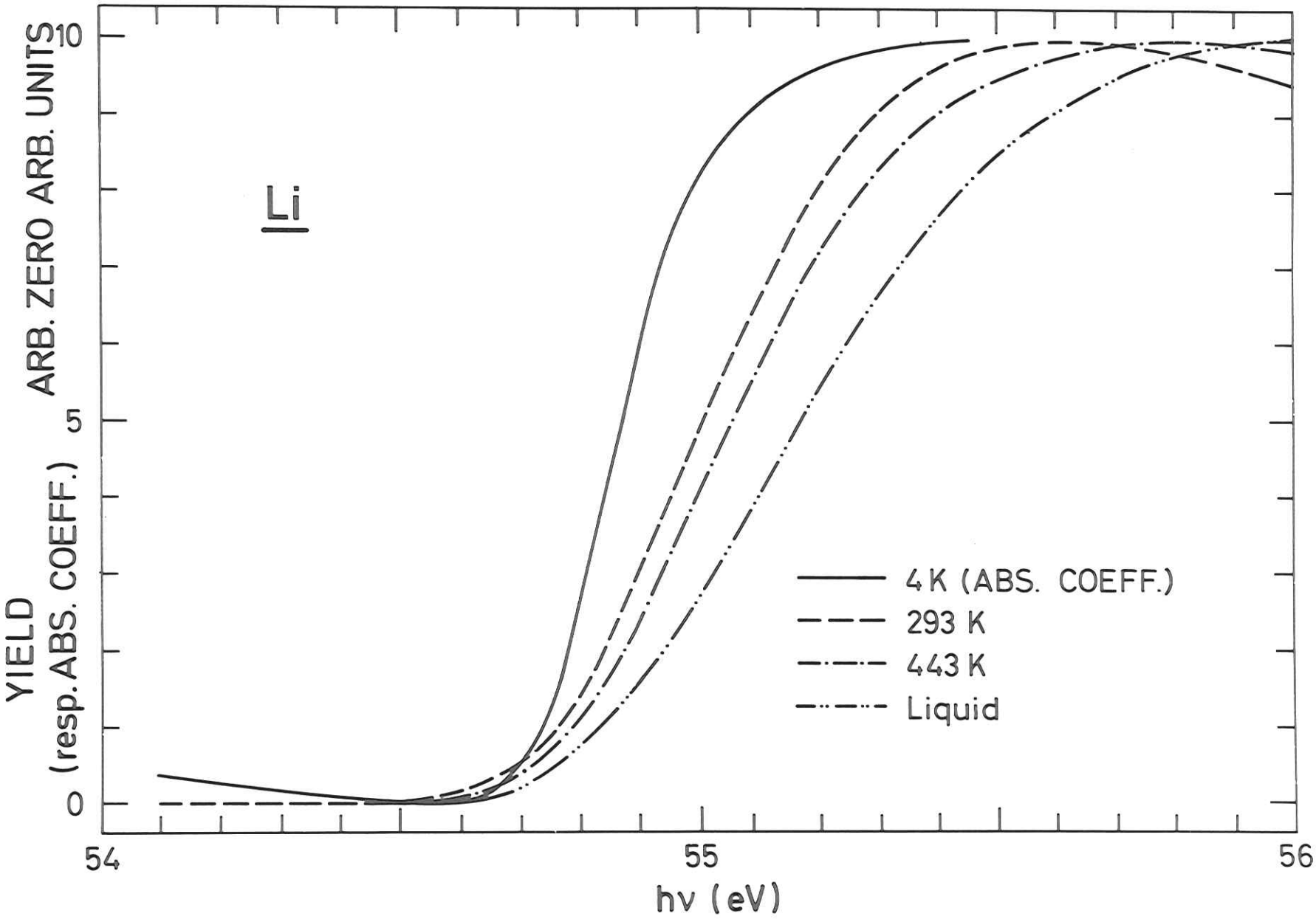
Li
YIELD
(resp. ABS. COEFF.)
ARB. ZERO ARB. UNITS
0
5
10
54
55
56
hν (eV)
4 K (ABS. COEFF.)
293 K
443 K
Liquid

Fig. 57

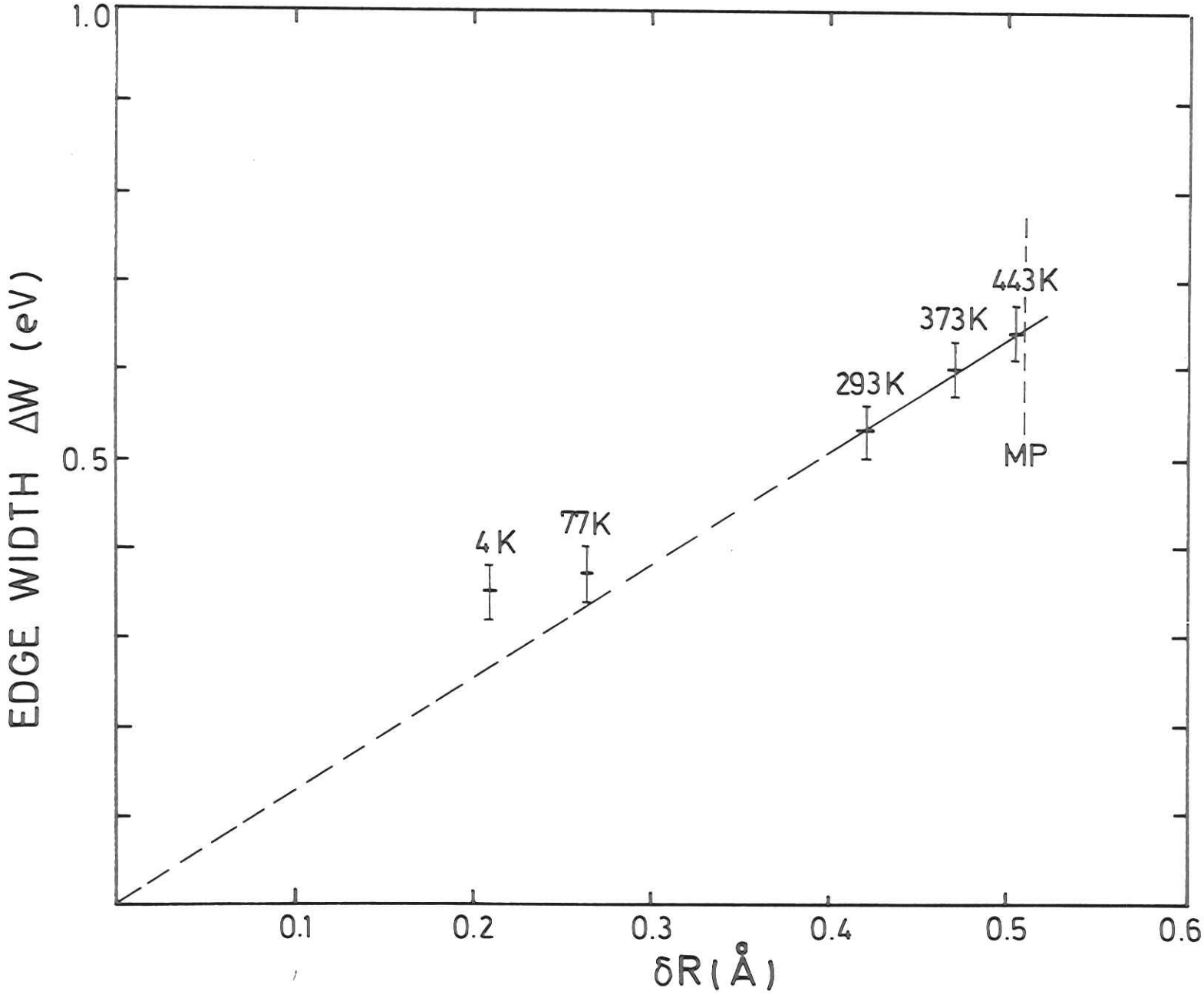
1.0
0.5
EDGE WIDTH ΔW (eV)
4K
77K
293K
373K
443K
MP
0.1
0.2
0.3
0.4
0.5
0.6
δR(Å)

Fig. 58